Defense Nuclear Agency
Alexandria, VA 22310-3398

DNA-TR-94-123

Investigation and Characterization of SEU Effects and Hardening Strategies in Avionics

Dr. Allen H. Taber
Loral Federal Systems – Owego
1801 State Route 17C
Owego, NY 13827-3998

Dr. Eugene Normand
Boeing Defense & Space Group
P.O. Box 3999
Seattle, WA 98124-2499

DTIC
ELECTE
FEB 17 1995
S G D

February 1995

Technical Report

DNA-MIPR-92-501

Approved for public release;
distribution is unlimited.

19950213 058

Destroy this report when it is no longer needed. Do not return to sender.

PLEASE NOTIFY THE DEFENSE NUCLEAR AGENCY, ATTN: CSTI, 6801 TELEGRAPH ROAD, ALEXANDRIA, VA 22310-3398, IF YOUR ADDRESS IS INCORRECT, IF YOU WISH IT DELETED FROM THE DISTRIBUTION LIST, OR IF THE ADDRESSEE IS NO LONGER EMPLOYED BY YOUR ORGANIZATION.

DNA PRINTING PLANT

REPORT DOCUMENTATION PAGE

Form Approved
OMB No. 0704-0188

Public reporting burden for this collection of information is estimated to average 1 hour per response including the time for reviewing instructions, searching existing data sources, gathering and maintaining the data needed, and completing and reviewing the collection of information. Send comments regarding this burden estimate or any other aspect of this collection of information, including suggestions for reducing this burden, to Washington Headquarters Services Directorate for information Operations and Reports, 1215 Jefferson Davis Highway, Suite 1204, Arlington, VA 22202-4302, and to the Office of Management and Budget, Paperwork Reduction Project (0704-0188), Washington, DC 20503

1. AGENCY USE ONLY (Leave blank)	2. REPORT DATE	3. REPORT TYPE AND DATES COVERED
	950201	Technical 901001 – 920930

4. TITLE AND SUBTITLE

Investigation and Characterization of SEU Effects and Hardening Strategies in Avionics

5. FUNDING NUMBERS

C - DNA-MIPR-92-501
PE - 62715H
PR - AF
TA - AG
WU - DH000060

6. AUTHOR(S)

Dr. Allen H. Taber (LFS)
Dr. Eugene Normand (Boeing)

7. PERFORMING ORGANIZATION NAME(S) AND ADDRESS(ES)

Loral Federal Systems – Owego
1801 State Route 17C
Owego, NY 13827-3998

Boeing Defense & Space Group
P.O. Box 3999
Seattle, WA 98124-2499

8. PERFORMING ORGANIZATION REPORT NUMBER

9. SPONSORING/MONITORING AGENCY NAME(S) AND ADDRESS(ES)

Defense Nuclear Agency
6801 Telegraph Road
Alexandria, VA 22310-3398
RAES/Cohn

10. SPONSORING/MONITORING AGENCY REPORT NUMBER

DNA-TR-94-123

11. SUPPLEMENTARY NOTES

This work was sponsored by the Defense Nuclear Agency under RDT&E RMC Code B4662D AF AG 00006 3400A 25904D.

12a. DISTRIBUTION/AVAILABILITY STATEMENT

Approved for public release; distribution is unlimited.

12b. DISTRIBUTION CODE

13. ABSTRACT *(Maximum 200 words)*

Data from military/experimental flights and laboratory testing indicate that typical non-radiation-hardened 64k and 256k static random access memories (SRAMs) can experience a significant soft upset rate at aircraft altitudes due to energetic neutrons created by cosmic ray interactions in the atmosphere.

It is suggested that error detection and correction (EDAC) circuitry be considered for all new avionics designs containing large amounts of semiconductor memory.

DTIC QUALITY INSPECTED 4

14. SUBJECT TERMS

Error Detection and Correction
Single-Event-Effects in Avionics
Soft-Errors
Atmospheric Radiation Environment

15. NUMBER OF PAGES

100

16. PRICE CODE

17. SECURITY CLASSIFICATION OF REPORT	18. SECURITY CLASSIFICATION OF THIS PAGE	19. SECURITY CLASSIFICATION OF ABSTRACT	20. LIMITATION OF ABSTRACT
UNCLASSIFIED	UNCLASSIFIED	UNCLASSIFIED	SAR

CLASSIFIED BY:

N/A since Unclassified.

DECLASSIFY ON:

N/A since Unclassified.

Contents

Section 1. Summary 1-1

Section 2. Introduction 2-1
2.1 Background 2-1
2.1.1 Soft Error Mechanisms 2-1
2.2 Purpose of Study 2-2

Section 3. IBM Flight Experimental Data 3-1
3.1 Flight Experimental Hardware 3-1
3.2 Ground Measurements 3-2
3.3 Low-Altitude Measurements 3-3
3.4 High-Altitude Measurements 3-3
3.4.1 Middle Latitude 3-5
3.4.2 High Latitude 3-6
3.5 Dosimetry 3-6
3.6 Data Analysis 3-7

Section 4. Military Avionics Field Data 4-1
4.1 European Area 1 Flight Upsets 4-1
4.2 European Area 2 Flight Upsets 4-1
4.3 Temporal Variation of Flight Upsets 4-2

Section 5. Space Shuttle Flight Data 5-1
5.1 Upset Rate Variation with Altitude/Latitude 5-1
5.2 Multi-Bit Upsets 5-2

Section 6. Laboratory Testing 6-1
6.1 Neutron Facilities and SEU Test Setup 6-1
6.1.1 Cyclotron Produced Neutron Beam Exposures and Dosimetry 6-1
6.1.2 Neutron Generator Produced 14 MeV Neutron Exposures and Dosimetry 6-3
6.2 Neutron Upset Cross Section Measurements 6-3
6.3 Neutron Upset Cross Sections 6-11
6.4 Adjustment Factor 6-16

Section 7. Neutron Upset Model 7-1
7.1 Radiation Environment of the Atmosphere 7-1
7.2 Model of the Atmospheric Neutron Environment 7-1
7.3 Upset Rate by Neutron Cross Section Model 7-8
7.4 Upset Rate by the Burst Generation Method 7-9
7.5 BGR Upset Rate Model for 64K SRAM 7-12
7.6 Correlation with Flight Results 7-15

Section 8. Impact on Current/Future Avionics 8-1
8.1 Effect of Memory Size 8-1
8.2 Effect of Altitude 8-2
8.3 Effect of Latitude 8-3
8.4 Effect of Multi-Bit Upsets 8-4

Section 9. Hardening Strategies 9-1
9.1 Fault Avoidance 9-1
9.1.1 Circuit Hardening 9-1

9.1.2 Component Selection 9-1
9.1.3 Shielding 9-1
9.2 Fault Tolerance 9-2
9.2.1 Single-Error Detection With No Correction 9-2
9.2.2 Double-Error Detection With Single-Error Correction 9-3
9.2.2.1 Soft Error Scrubbing 9-5
9.2.2.2 Multi-Bit Upsets 9-6
9.2.2.3 On-Chip Error Correction 9-7
9.2.3 Voting Technique 9-7

Section 10. Conclusions 10-1

Section 11. Recommendations 11-1

Section 12. References 12-1

Appendix A. Flight Data Logs A-1
A.1 European Area 1 . . . . . A-1
A.2 European Area 2 . . . . . A-2

Bibliography X-1

List of Abbreviations X-2

Accesion For
NTIS CRA&I ☒
DTIC TAB ☐
Unannounced ☐
Justification
By
Distribution /
Availability Codes
Dist | Avail and / or Special
A-1

Figures

3-1. Photograph of Flight Test Hardware 3-2
3-2. Photograph of E-3 AWACS Airplane 3-4
3-3. Photograph of NASA ER-2 Airplane 3-5
3-4. ER-2/Space Shuttle Integral LET Spectrums 3-8
4-1. Cumulative Avionics Upsets 4-2
4-2. Avionics Upset Rate vs Time 4-4
5-1. Space Shuttle SEU Rate vs Altitude/Latitude 5-2
5-2. Heavy Ion Cross Section for 1Mb SRAM 5-4
6-1. Neutron Spectra for Beams Produced at UCD 6-2
6-2. 14 MeV Upset Histogram (5V, active) 6-4
6-3. 14 MeV Upset Histogram (5V, standby) 6-5
6-4. 14 MeV Upset Histogram (2.5V, standby) 6-6
6-5. Upset Histogram (UCD, 65MeV, Dynamic) 6-7
6-6. Upset Histogram (UCD, 65MeV, Low Power Static, 1st Run) 6-8
6-7. Upset Histogram (UCD, 65MeV, Low Power Static, 2nd Run) 6-9
6-8. Upset Histogram (UCD, 40MeV, Active) 6-10
6-9. Upset Histogram (UCD, 40MeV, Low Power Static) 6-11
6-10. Bendel Model of NSEU Cross Section for 64k SRAMs (2.5V Standby Mode) 6-14
6-11. Bendel Model of NSEU Cross Section for 64k SRAMs (5V Active Mode) 6-15
6-12. Weighting Factors for Adjustment Factor Calculations 6-18
7-1. Radiation Environment in the Atmosphere 7-2
7-2. Neutron Flux vs Altitude 7-3
7-3. Neutron Flux vs Latitude 7-4
7-4. Differential Neutron Flux vs Energy 7-5
7-5. Neutron Flux vs Altitude (1-10 and 10-100 MeV Comparison) 7-7
7-6. Heavy Ion Cross Section for 64k SRAM 7-10
7-7. Integral of dN/dE × BGR(En,Er) vs. Er 7-11
7-8. Variation of Calculated/Measured Upsets with Sensitive Thickness 7-14
7-9. EDI 32kx8 SRAM Heavy Ion Upset Cross Section 7-17
8-1. Avionics MTTF Versus Memory Size 8-2
8-2. Avionics SEU Rate vs Altitude 8-3
8-3. Avionics SEU Rate vs Latitude 8-4
9-1. Example of Nine-Bit Odd-Parity Checker 9-2
9-2. Example of 32-Bit SEC-DED Configuration 9-4
9-3. Example of Memory Soft Error Protection 9-6
9-4. Example of Triple Modular Redundant Memory 9-8

Tables

3-1. Dosimetry Results 3-7
3-2. 64K SRAM Soft Error Results 3-8
5-1. IMS1601 Multi-Bit Upsets on the Space Shuttle 5-3
6-1. Summary of Neutron and Proton Cross Sections 6-12
6-2. Peak to Total Spectrum Adjustment Factors 6-17
7-1. Variation of Calculated/Measured Upsets with Sensitive Thickness 7-13
7-2. Comparison of Calculated to Actual Upset Rates 7-16
A-1. Flight Log - European Area 1 . . . . . A-1
A-2. Flight Log - European Area 2 . . . . . A-2

Preface and Acknowledgements

This work was sponsored by the Defense Nuclear Agency (DNA) and the Naval Research Laboratory (NRL) under NRL contract N00014-91-C-2177. The authors would like to thank the personnel at DNA, NRL, NASA, IBM, Boeing, Lockheed, and ERIL Research for their support of this project.

At DNA, L. Cohn and L. Palkuti provided program support; and A. Constantine (while at Rensselaer Polytechnic Institute) provided Cf^{252} tests of the 64k SRAM.

At NRL, J.C. Ritter, E.L. Petersen, W.J. Stapor, and A.B. Campbell provided technical guidance and support; and G. Belton assisted with programmatic issues.

At NASA GSFC, J.W. Adolphsen (now with Vail Research and Technology Corp.) provided the 1984 CRUX experiment which led to this work; at NASA Ames Research Center, J. Arvesen provided us with ER-2 aircraft flight time over California and Norway;

At Boeing, T.J. Baker assisted with the calculations; D.L. Oberg and J.L. Wert with all upset measurements; J.E. Sunde, B.N. Nelson, A.P. Durant, J.R. Beymer, D.A. Russell and L.T. Nirider with the preparation and conduct of the 14 MeV neutron generator tests; L.A. White, R.J. Whitbeck, D.D. Church, S.C. VanNess and D.M. O'Connell with the collection of military flight upset data; W.C. Leeper with programmatic issues, C.M. Castaneda of the University of California at Davis with the cyclotron neutron source tests; and Profs. J. Ryan, University of New Hampshire and A.D. Zych, University of California at Riverside for providing copies of their students' theses.

At IBM, T.M. Scott and J.A. Damato provided hardware, fixtures, and test software; J.F. Ziegler and T.J. O'Gorman assisted with the atmospheric radiation environment; M.Y. Hsiao and C.L. Chen with fault tolerance; C. McWilliams, Jr. and D.V. Mattson with memory programming/readout in San Francisco and Seattle; R.P. Gwara with mechanical payload design; T.M. Platt with memory programming/readout in the lab; R. Burkhardt with military aircraft data collection; R.R. Richardson and D.G. Bradt with military aircraft design information; L.D. Whitehead, M.A. Giordano and S. Saraceno with reliability calculations; and H. Sasnowitz, E.M. Nordman, L.J. Desantis, M.T. Gartman, B.A. Janosko, D.R. Wilson, D.R. Fierle, T.J. Kearney, G.J. Manzo and P.A. Pfeiffer assisted with programmatic issues.

At Lockheed/Ames, W. Ferguson helped integrate our experiment payload into the ER-2 aircraft.

At ERIL Research, Inc., E.V. Benton provided radiation dosimetry for our ER-2 and E-3 aircraft flights.

Section 1. Summary

Data from military aircraft flights at 29,000 feet, experimental flights at both 30,000 and 65,000 feet, and laboratory testing indicate that typical non radiation-hardened 64k and 256k static random access memories (SRAMs) can experience a significant soft upset rate at aircraft altitudes due to energetic neutrons created by cosmic ray interactions in the atmosphere.

Measured 64k SRAM upset rates range from 3E-8 fails/bit-day (f/bd) at 30,000 feet (5V operating mode), to 5.4E-7 f/bd at 65,000 feet (2.5 volt data retention mode). This overlaps with the range of upset rates (1.4E-7 to 8.9E-7 f/bd) measured for the same 64k SRAM devices (5V operating mode) in low earth orbit on board the Space Shuttle.

A model of the atmospheric neutron environment and two models for soft error rate prediction (Neutron Cross Section or "NCS" and Burst Generation Rate or "BGR") are presented. The models correlate with measured upset rates over altitude, latitude, device type, and operating voltage in most cases to within less than a factor of two and, with incomplete data, to within a factor of three.

It is suggested that error detection and correction (EDAC) circuitry be considered for all new avionics designs containing large amounts of semiconductor memory. Reliability equations are provided to help designers evaluate the benefits of various soft error protection schemes.

Section 2. Introduction

Inadequate experimental data exists on the reliability of integrated circuits in the natural radiation environment at aircraft altitudes. This lack of data on Single Event Upset (SEU) severely limits avionics designers' ability to incorporate appropriate reliability and availability improvement techniques in new equipment designs and operating procedures. Future avionics systems will require even higher reliability and availability while their increased memory and logic capacity make them even more susceptible to SEU. It is important to be able to understand and address this problem now.

2.1 Background

Previous studies of soft error mechanisms and hardening techniques by DoD and industry have focused primarily on nuclear weapons effects, space radiation effects, or the effects of low level radiation (alpha particles) emitted by microcircuit packaging and process materials. To date, little or no work on the effects of natural radiation on electronics at aircraft altitudes is available. Now, however, avionics systems have grown in complexity to the point where these effects become important, and perhaps critical, to their reliable operation. This study provides the DoD community with detailed laboratory and field data to publicize this problem and gain needed support for further research.

2.1.1 Soft Error Mechanisms

"Neutron-induced SEU" (NSEU) is suspected to be the predominant SEU mechanism at aircraft altitudes and is the subject of this study.

When a particle such as a neutron undergoes an elastic or non-elastic reaction with a silicon atom while passing through the chip, a nuclear recoil is created (it may be Si, Mg, Al etc., depending on the reaction). In addition to the primary reaction product, which is the nuclear recoil, charged secondaries, such as protons and alpha particles, may also be released. The recoils are the most heavily ionizing reaction product, but the charged secondary products can also ionize. The net result is bursts of charge created through the passage of the recoils and charged secondary products through the silicon. These bursts of charge can originate anywhere within the volume of a chip, causing soft fails if they occur at a sensitive node.

For example, in a static random access memory (SRAM), the storage cells rely on the potential difference between two nodes to establish a logic "one" or logic "zero", the charge collected from a recoil created by a neutron interacting with a silicon atom within a sensitive node may be enough to cause it to change its logic state and suffer a soft upset. A soft upset may be distinguished from a hard failure in that no permanent damage occurs to the microcircuit. In this case, the memory cell can be restored to its proper logic state by rewriting it.

SEUs can also be caused by the passage of heavy ions through a semiconductor. This, in fact, was how SEU was discovered, through the upsets caused by the heavy ion portion of the galactic cosmic rays in semiconductor devices in space [Ref. 1]. Most microelectronics tested for susceptibility to SEU are tested with heavy ions for space applications. As shown in 7.4, "Upset Rate by the Burst Generation Method" on page 7-9, this heavy ion SEU data can also be utilized to obtain estimates of neutron induced SEU by use of the BGR methods.

With a heavy ion beam, the positively charged ion enters the silicon lattice of a microelectronic circuit and begins to lose energy by ionizing the atoms along its path. The electron-hole pairs that are created form a cylindrical column with a net neutral charge. The column then decays into a cascade of carriers, resulting in one electron-hole pair for every 3.6 electron volts (eV) of energy lost by the ion. This process occurs within a time of the order of picoseconds, and a radius of about 0.1 micrometer (μm).

When an ion track penetrates an electric field, such as the depletion region of a P-N junction, the column of carriers drastically disturbs the depletion layer. Inside the depletion region, the generated electrons drift to a more positive potential side, while the generated holes drift to a more negative potential side. The carrier drift process reduces the net charge in the original depletion region and causes the potential across it to change [Ref. 2]. Additional carriers may also reach the depletion region by diffusion and contribute to this effect.

2.2 Purpose of Study

The overall objective of this project was to improve the reliability and availability of avionics hardware with respect to their sensitivity to SEU caused by the natural radiation environment of the earth's atmosphere.

Avionics systems containing up to several megawords of semiconductor memory have now reached the field and, at aircraft altitudes, are experiencing on the order of one single event upset (SEU) per flight. Existing data suggested that these SEUs were caused either directly or indirectly by cosmic rays, in particular by the atmospheric neutrons generated by the cosmic rays. This was a relatively new finding and little work had been done to understand/quantify the problem and develop appropriate hardening strategies.

Therefore, the purpose of this study was to investigate and characterize SEU effects and hardware strategies for avionics systems. To achieve this, the study was divided into five separate tasks defined as follows:

1. Review IBM and Boeing collected avionics field upset data to demonstrate/quantify the problem;
2. Perform laboratory SEU testing of the same microelectronics that exhibited flight upsets;
3. Develop models to correlate laboratory test results with existing data;
4. Predict the impact on current/future avionics designs; and
5. Determine and recommend hardening strategies.

Section 3 through Section 9 document the manner in which these tasks were accomplished.

The flight upset data are described in Section 3, "IBM Flight Experimental Data" on page 3-1 and Section 4, "Military Avionics Field Data" on page 4-1. Most of the flight upsets recorded are for a 64k×1 SRAM, although there is also a limited amount of data for a 256k×1 SRAM. As part of this study, the same 64k SRAM was tested in the laboratory with neutron beams of three different energies, as described in Section 6, "Laboratory Testing" on page 6-1, to obtain neutron upset cross sections. Heavy ion SEU testing had been performed on this 64k SRAM previously, and the heavy ion SEU cross section curve was available.

Three models are described in Section 7, "Neutron Upset Model" on page 7-1, one to calculate the atmospheric neutron flux and two different models to calculate the upset rate at aircraft altitudes. One of these upset models uses the neutron upset cross section data and the other uses the heavy ion SEU cross section curve via the burst generation rate (BGR) method. Section 8, "Impact on Current/Future Avionics" on page 8-1 uses the measured flight upset data to assess the effect of upsets on current and future avionics. Strategies to minimize SEU occurrences are discussed in Section 9, "Hardening Strategies" on page 9-1.

Section 3. IBM Flight Experimental Data

A portion of this study involved flying an experimental soft error measurement package on board two types of aircraft to record flight upsets. For these measurements, we used an approach that had worked successfully in 1984 on the Cosmic Ray Upset Experiment (CRUX III) flown on the Space Shuttle (IBM project 5V25) [Ref. 3]. This consisted of flying a large quantity of complementary metal oxide semiconductor (CMOS) static RAM memory devices. The devices were programmed on the ground, flown in the data retention mode (battery power), and read out on return. The actual flight upset data is summarized in 3.6, "Data Analysis" on page 3-7.

All flights of the experimental package contained a large number of 64k SRAMs. The same 64k SRAM is used in the CC-2E Digital Computer flown on the military aircraft that provides the avionics field upset data described in Section 4, "Military Avionics Field Data" on page 4-1. This same 64k SRAM was tested for upset in the laboratory by exposing a number of these SRAMs to neutron beams of various energies, as described in Section 6, "Laboratory Testing" on page 6-1.

3.1 Flight Experimental Hardware

The test hardware consisted of the following:

- 11 64K×1 SRAM boards;
- Three 256K×1 SRAM boards;
- Two aluminum flight containers;
- Six film pack holders;
- One tester interface card and cables; and
- IBM PC RS-232 controller software.

A photograph showing examples of this hardware appears in Figure 3-1.

The SRAM boards were adapted from the original 1984 CRUX III design by T. Scott of IBM Manassas, VA (IR&D co-investigator during 1988). The modifications included changing from hand-wired circuitry to a printed circuit approach for higher reliability and more devices per board.

Both the 64K and 256K board types were laid out identically, with 28 SRAMs, seven 3.0-V alkaline batteries, and one edge connector. The SRAMs were wired so that the batteries would keep data "alive" for several months, using the vendor's data retention mode. All SRAM I/O signals were routed to the edge connector so that programming and readout could be done simply by connecting a ribbon cable to the external tester, without removing the board from the flight container. When the tester was disconnected, all signal lines were pulled to ground or 3V with on-board resistors and a termination connector to prevent electrical noise from disturbing the stored data. Fuses also provided protection if CMOS latchup were to occur, while diodes isolated the batteries from the external 5V tester supply.

The 11 64K boards were built using the same 64K×1 CMOS static RAM device type that was flown in the 1984 CRUX III experiment [Ref. 3]. This IMS1601S70LM 64K×1 SRAM was manufactured by Inmos Corporation using 1.3μm effective channel lengths on a 25.4mm^2 N-type substrate. It has four-transistor N-channel MOS (NMOS) cells with a CMOS periphery. Each cell has a total area of 220μm^2. Total memory density for all 64K boards combined was 11×28×64K, or 19.25 megabits.

The three 256K boards contained 256K×1 static RAMs of construction similar to the 64K. These parts were manufactured by Electronic Designs, Inc., having a part number of EDI81256P55Q1 and package lot/date codes of "PTS178S 8832." The 256K devices had smaller 1.1μm ground rules, however, and a twin-

well CMOS process. Total memory density was 3×28×256K, or 21 megabits. Both the 64K and 256K SRAMs had a low power data retention mode suitable for battery backup.

Programming and readout was accomplished with a portable memory tester and adapter card/cable. The tester was interfaced to an IBM PC through an RS-232 cable. Using IBM BASIC controller software developed by T. Scott, we were able to program half the boards with a checkerboard pattern and the other half with checkerboard complement. At the end of exposure, the tester was again used to determine which chips had failed. The software was able to determine the failed cell's physical locations on each chip, using topological descrambling, so that we could look for symptoms such as multiple-bit errors.

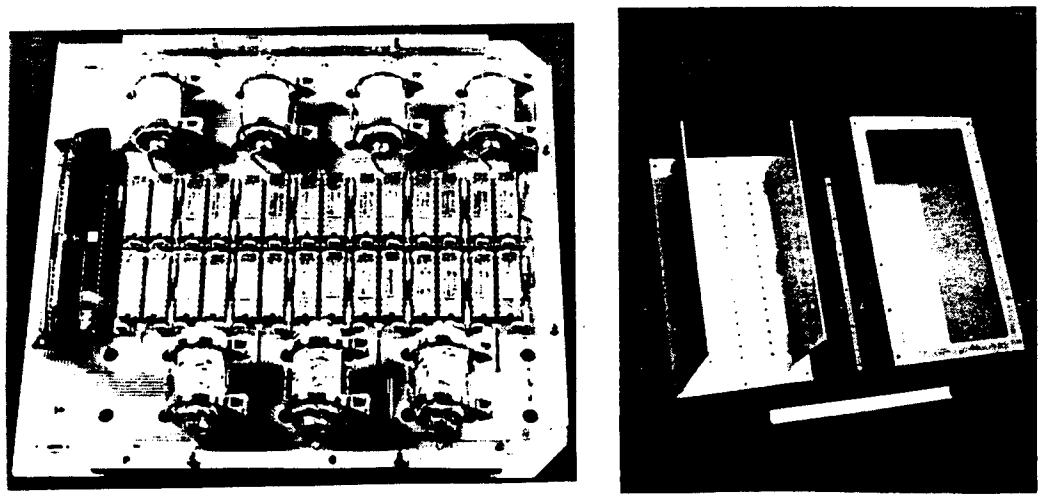

Figure 3-1. Photograph of Flight Test Hardware. Alkaline batteries were mounted directly on each static RAM memory board to provide up to several months of data retention. The memory boards were then mounted in an aluminum container for the test flights.

3.2 Ground Measurements

In order to determine the sea level (or reference) soft upset rate, 21 64K×1 SRAM boards were used, including ten that had been built for future CRUX experiments. Between April, 1988 and January 1989, periodic programming and readouts were performed on the ground, with 11 soft upsets observed in 1,100,736 device hours, or a soft fail rate of 3.7×10^{-9} fails/bit-day (f/bd).

This upset rate was later used to estimate the proportion of soft fails occurring on the ground between flight tests. It should be noted that a significant percentage of this ground upset rate may have been due to alpha particle emissions from internal package and process materials, rather than from cosmic rays. Upset caused by alpha particles from microelectronics packaging materials is a well known phenomenon [Ref. 4].

Also, in cooperation with the Nuclear Engineering department of Rensselaer Polytechnic Institute, we obtained Californium-252 soft error cross-section measurements of the 64K×1 SRAM. This soft error testing was done by graduate student A. Constantine in 1988 using a 0.75 microcurie source at a distance of 0.5cm in air [Ref. 5]. At 5V, the soft error cross-section was found to be about $29\mu m^2$ per bit, which compares very well with a $36\mu m^2$ sensitive region calculated in 1984 from cell photomicrographs [Ref. 6].

3.3 Low-Altitude Measurements

In the summer of 1988, ten 64K×1 SRAM boards were flown on board an E-3 Airborne Warning and Control System (AWACS) model JE-3C aircraft in cooperation with the Boeing Aerospace Company in Seattle, Washington. A photograph of the E-3/AWACS is shown in Figure 3-2. Our test equipment was shipped to D. Mattson at the IBM Field Service office near Boeing airfield so that he could perform the readout and programming on-location between flights. Support was also provided by T. Scott of IBM Manassas.

The low altitude tests began on June 27th and ended on July 22nd, 1988. During this time, the boards were exposed to a round trip commercial shipping flight between Manassas and Seattle (5.8 hours), 13 E-3 test flights out of Seattle (59.6 hours), a round trip E-3 flight between Seattle and Tampa, Florida (10.7 hours), and five E-3 test flights out of Tampa (25.3 hours). This represented a total of about 106 hours of flight time at an altitude of from 26 kft to 40 kft. The Boeing Co. provided a record of the E-3 aircraft's altitude, latitude, and longitude approximately every 12 minutes during flight. Seattle was considered to be at a middle latitude (47°N).

During this time, there were a total of 11 soft fails. None of these were in adjacent memory locations (multiple-bit). The ground time of 561 hours was assumed to have caused about one of these 11 failures, leaving a flight upset rate of about 1.2E-7 f/bd. This is about 30 times higher than the rate we observed at sea level.

3.4 High-Altitude Measurements

Soft fail rates were also measured at high altitudes (19.8km or 65 kft) on board an ER-2 research plane in cooperation with the National Aeronautics and Space Administration's (NASA's) Ames Research Facility at Moffett Field, California. A photograph of the ER-2 is shown in Figure 3-3.

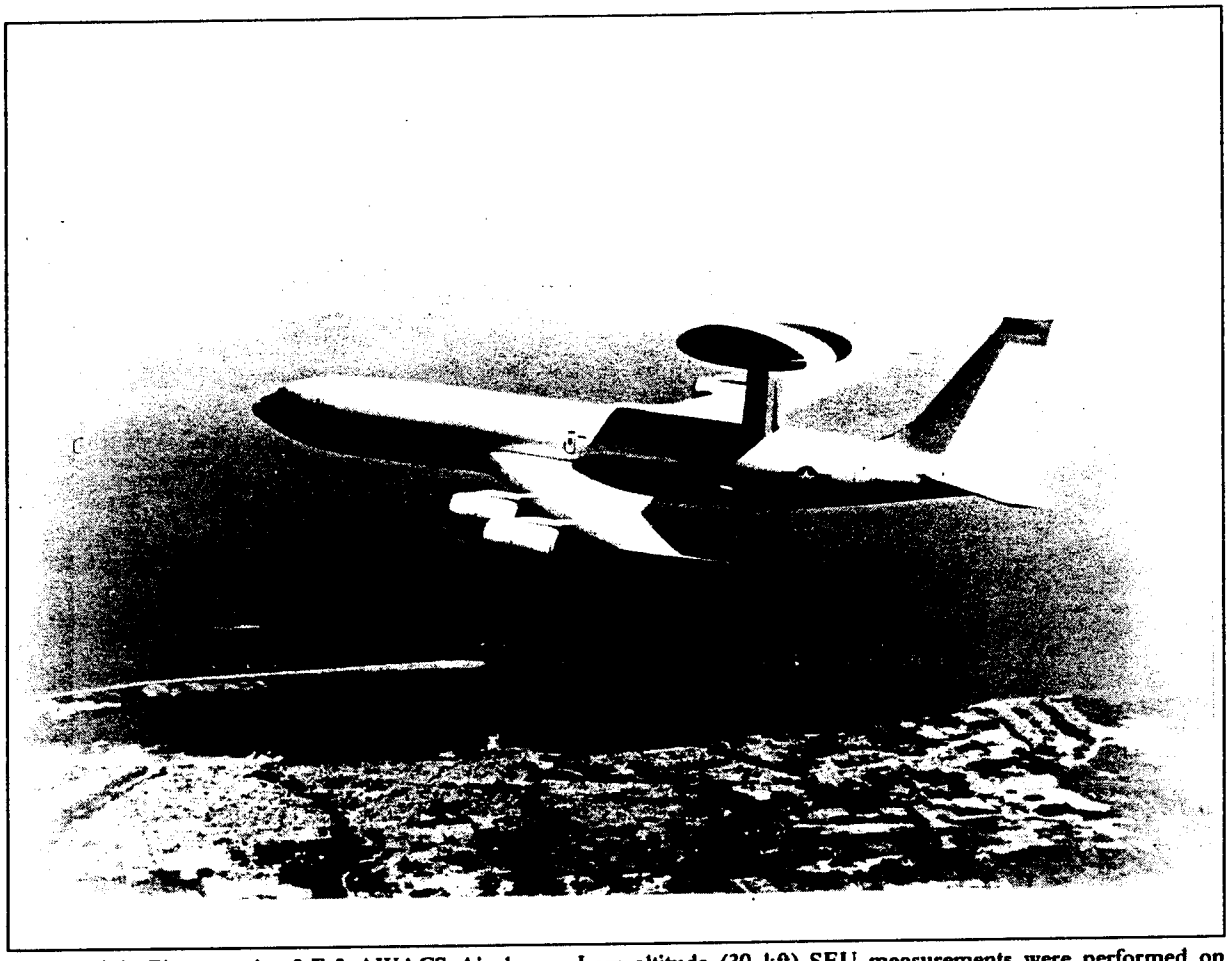

Figure 3-2. Photograph of E-3 AWACS Airplane. Low altitude (30 kft) SEU measurements were performed on board a Boeing Aerospace E-3 AWACS aircraft.

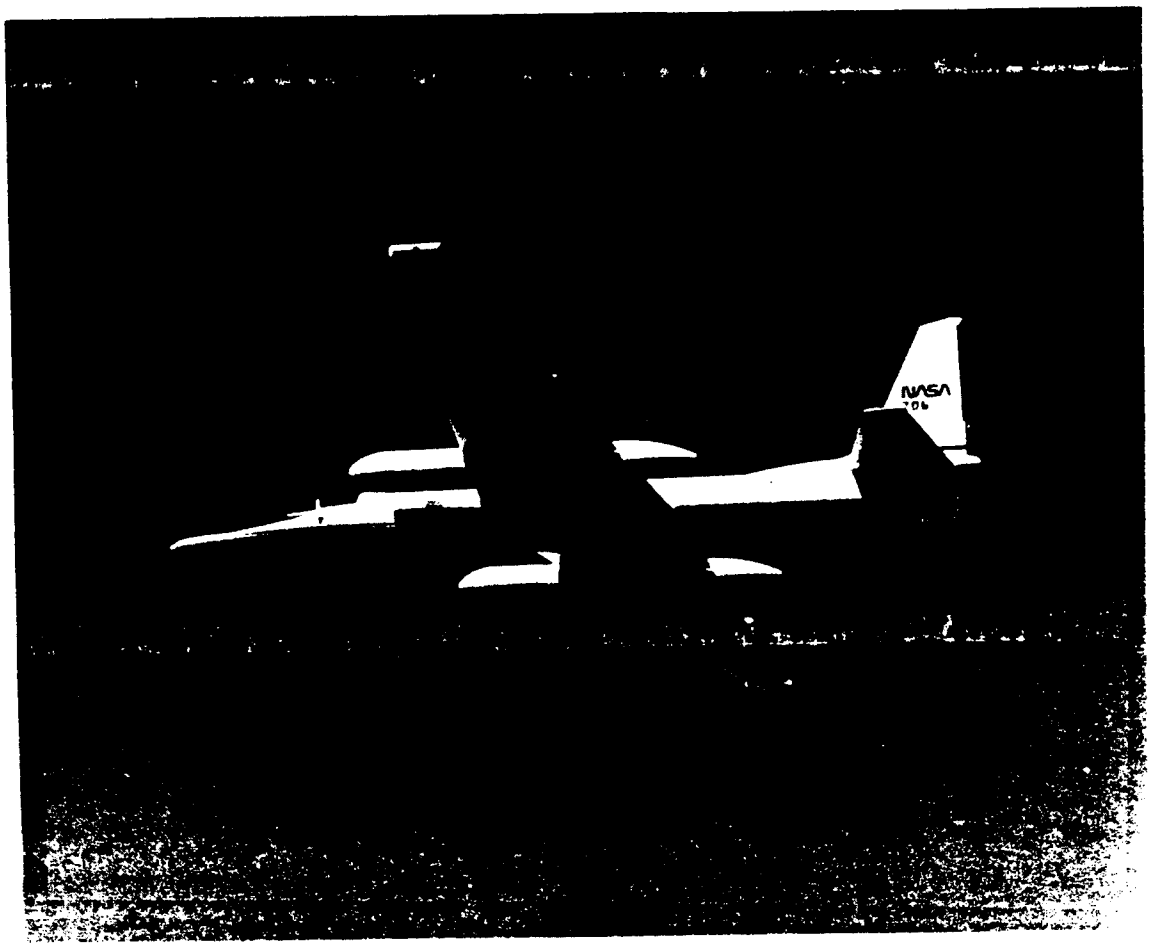

Figure 3-3. Photograph of NASA ER-2 Airplane. The FLUX experiment payload was mounted inside the rear cargo door during flights at 65,000 feet.

For these tests, the FLUX flight container was mounted inside the rear compartment door. NASA provided a record of the ER-2's altitude, latitude, longitude, and heading for each minute of flight. Many of the data readouts were performed on location by C. McWilliams, Jr. of IBM San Jose, with support from T. Scott of IBM Manassas.

3.4.1 Middle Latitude

A total of 20 ER-2 flights were performed at 65,000 feet over California, using the 64K SRAM boards. During these flights, the 64K×1 SRAMs experienced 20 soft fails in 16,875 device hours. None of these were multiple-bit fails. If we assume 7.9 of the 20 soft fails occurred during the ground hours and cross country commercial shipping flights, then the 65,000 foot upset rate at this middle latitude (37°N) would be about 2.6E-7 f/bd for the 64K×1 SRAM, or about 70 times the sea level upset rate.

3.4.2 High Latitude

We also had the opportunity to fly the experiment at high latitudes when the ER-2 was sent to Norway in Jan/Feb 1989 for the NASA Arctic Ozone Expedition. The soft fail rates at such high latitudes were expected to be significantly higher, since the Earth's magnetic field provides less shielding of the charged particle cosmic rays. The 256K boards were ready then and were included with the 64K boards for the first and only time on these flights.

A total of 14 flights were performed out of Stavenger Air Force Base, Norway, flying as far north as 82°N latitude at 65,000 feet. When the hardware was returned, we found a total of 57 upsets in the 64K SRAMs and six upsets in the 256K SRAMs. Two of the 64K upsets were in physically adjacent memory cells, indicating a possible multiple-bit fail from a single cosmic ray. If we assume 5.4 of the 57 upsets occurred in the 64K SRAMs during ground time and commercial shipping flights, then the 64K upset rate at 65,000 feet at high latitude would be 51.6 fails per 34,907 device hours, or 5.4E-7 f/bd. This is about 150 times higher than the middle latitude sea level rate.

There was no ground test data available for the 256K SRAMs that could be used to subtract out the background upsets. However, if we assume that *all* fails occurred in the air over Norway, then the *upper bound* for the 256K soft fail rate at high latitude would be 6 fails per 3,647 device hours, or 1.1E-7 f/bd. This upper bound is still lower than the 64K upset rate.

3.5 Dosimetry

Sets of passive radiation detectors were also flown along with the memory devices [Ref. 7]. The purpose of the detectors was to provide a record of the radiation environment for input to our soft error modeling.

The flight detectors were configured as stacks in three identical packages. Since some of the detectors had directionality of response to incoming radiation, the three stacks were mounted in an orthogonal array. A fourth stack remained on the ground as a control. Each detector stack consisted of four components. These were:

1. Nuclear emulsions;
2. Thermoluminescent detectors (TLD-200, CaF_2 and TLD-700, ^7LiF);
3. Thermal and epithermal neutron detectors (^6LiF radiators with CR-39 PNTD alpha particle detectors with and without gadolinium covers); and
4. CR-39 PNTD film, in pairs.

The nuclear emulsions recorded the tracks of protons down to minimum ionizing energies. The TLDs gave a measurement of total radiation dose, while the ^6LiF/CR-39 detectors used the ^6Li(n,alpha)T reaction to measure low energy neutron fluence. The gadolinium foils (25μm thick) had an effective neutron absorption cutoff of about 0.2eV. This allowed a separation of neutron response into thermal (<0.2eV) and epithermal (0.2eV to 1MeV) regions. Thus, this dosimetry package did not measure the energetic neutrons (1<E<1000MeV) in the atmosphere that are discussed in detail in Section 7, "Neutron Upset Model" on page 7-1 and are considered as the major cause of flight upsets. The CR-39 PNTD pairs recorded heavy ions (protons of $E \leq 10$ MeV and ions of $Z \geq 2$ up to higher energies).

The film packs were attached to the FLUX flight container on the E-3/AWACS flights, but carried near the nose of the plane for the ER-2 flights. They were separated from the flight container because the ER-2's interior temperature near the engine was found to be too high for the emulsions during runway taxiing.

All detectors have been processed, and all but the nuclear emulsions have been analyzed.

Table 3-1. Dosimetry Results. There was a factor of four increase in total dose equivalent going from 30,000 to 65,000 feet, and a further 60% increase at polar latitudes.

Altitude	30 kft	65 kft	65 kft
North Latitude	39-48°	32-40°	59-82°
Aircraft Type	E-3	ER-2	ER-2
TLD Dose *(mrem/day for LET < 5keV/μm in H_2O)*	1.5	8.9	12.0
PNTD Dose *(mrem/day for LET > 5keV/μm in H_2O)*	Negligible	Negligible	2.1
Neutron Dose *(mrem/day for E < 1 MeV)*	0.83	0.46	0.67
Total Radiation Dose *(mrem/day)*	2.3	9.4	14.8

The TLD doses were seen to increase with both altitude and latitude, as shown in Table 3-1. However, it is not certain that there would be a significant latitude difference outside the polar regions. There was a factor of four increase in total dose equivalent in going from 30,000 to 65,000 feet, and a further 60% increase at polar latitudes. In Norway, 81% of the measured dose came from radiation having a Linear Energy Transfer (LET) of less than 5keV/μm (H_2O), which would be high energy protons, electrons, gamma rays, and any other lightly ionizing particles. This fraction would increase to about 95% for flights in more southern latitudes, where heavy particle fluxes are insignificant [Ref. 7].

The measured LET total flux spectrum is compared with three space shuttle measurements in Figure 3-4. The three shuttle missions, STS 51F, -51J, and -61C, have different orbits and encounter different heavy charged particle fluxes, but none of the orbits extend over the polar regions [Ref. 7].

Cyclotron tests [Ref. 8] have shown the 64K×1 SRAM to have a heavy ion LET upset threshold of approximately 2 MeVcm^2/mg (200 keV/μm in H_2O) at 5V. Figure 3-4 shows that there are about 5E-8 particles/cm^2 sec-steradian with this LET or greater over Norway. Using a sensitive area per bit of 29μm^2 [Ref. 5], the predicted upset rate would be:

$$\begin{aligned} &5\text{E-8 particles/cm}^2\text{-sec-steradian} \\ &\times 1\text{E-8cm}^2/\mu\text{m}^2 \times 29\mu\text{m}^2\text{/bit} \\ &\times 3600\text{sec/hr} \times 24\text{hr/day} \times 4\pi \text{ steradians} \\ &= 1.6\text{E-8 particles/bit-day.} \end{aligned}$$

If we then use a scaling factor of 3.5× [Ref. 3] to estimate the increased upset rate at battery voltage, we would have a predicted upset rate of 5.5E-8 f/bd. This is about one-tenth the observed rate of 5.4E-7 f/bd. As discussed in Section 7, "Neutron Upset Model" on page 7-1, the remaining portion of the soft error rate is likely to be attributed to NSEU.

3.6 Data Analysis

In order to use the flight data, its statistical significance must be considered. Several aspects of the experiment may have affected the observed error rates:

1. The measurement of the number of soft fails at time of readout was considered exact (no inaccuracy);
2. The chance of the same memory cell locations having changed state more than once was considered negligible because of the small number of fails;
3. The recording of flight times was expected to be accurate to within a few minutes per flight, or about 1-2%; and
4. The recording of altitude measurements was assumed to be accurate to within about 1000 feet.

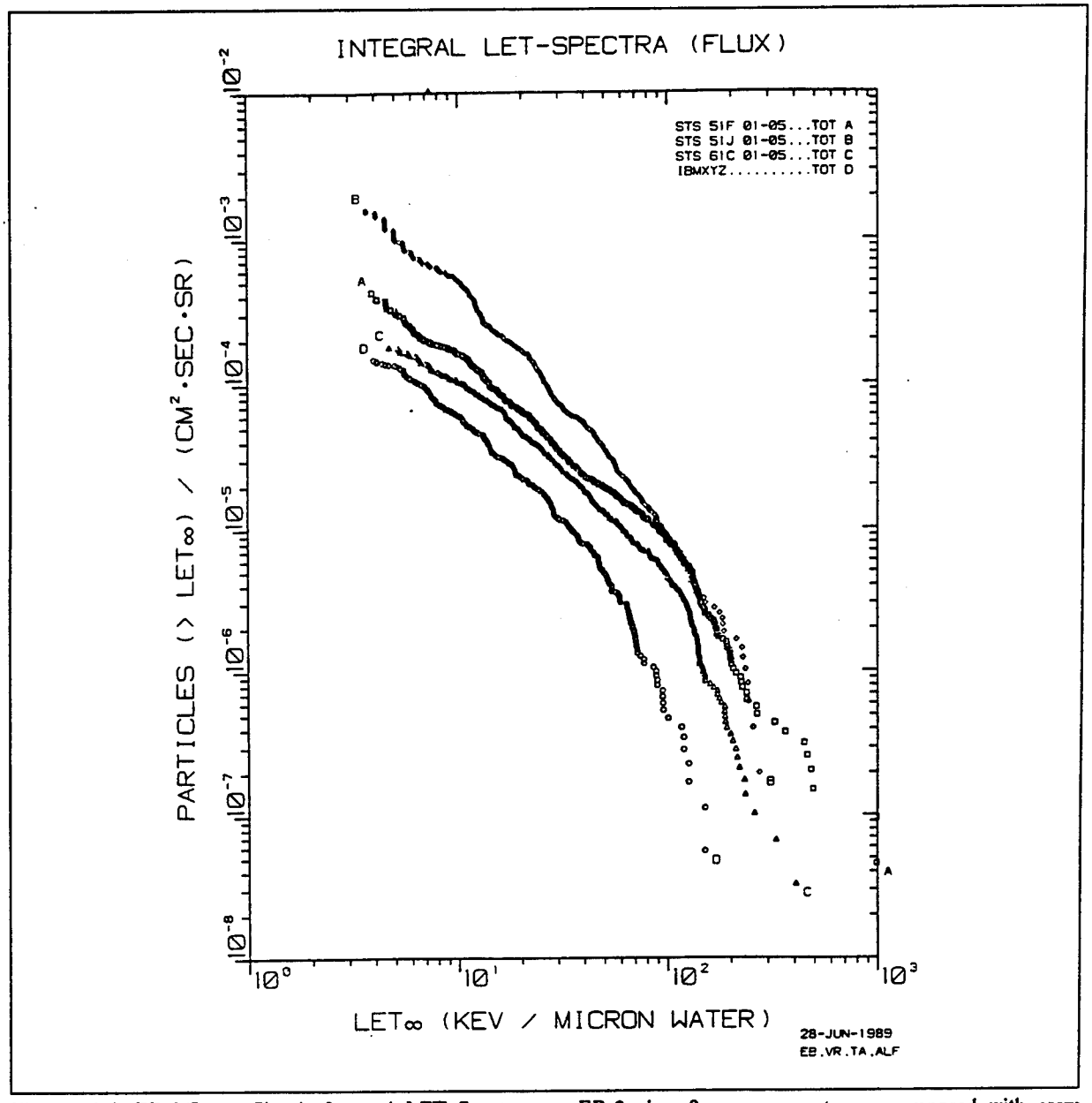

Figure 3-4. ER-2/Space Shuttle Integral LET Spectrums. ER-2 aircraft measurements are compared with crew dosimeters from three Space Shuttle flights: 51F (322x304km, 49.5°), 51J (510km-max., 28.5°), and 61C (324km, 28.5°). For water, stopping power in (keV/micron)x(0.01) = stopping power in MeV/mg-cm².

When the above factors were considered, the main uncertainty in projecting soft fail rates versus altitude was due to the small number of soft fails observed and their random occurrences in time.

Table 3-2. 64K SRAM Soft Error Results.

Altitude	**Sea Level**	**30 kft**	**65 kft**	**65 kft**
North Latitude	39°	39-48°	32-40°	59-82°
Aircraft Type	-	E-3	ER-2	ER-2
Mean Upset Rate *(measured, at battery voltage)*	3.7E-9 f/bd	1.2E-7 f/bd	2.6E-7 f/bd	5.4E-7 f/bd

Section 4. Military Avionics Field Data

Flight tests of military aircraft equipped with a CC-2E Digital computer with semiconductor memory were carried out over two separate areas of Europe during the period of November, 1990 through March, 1992. From the logs of these flights, the status of the five MMU's were determined. Single bit errors detected by the EDAC circuitry were recorded in the AOCP and the AOCP log was read to determine the number of errors for each flight. Most flights were about five to six hours in duration. Most flights were conducted at an altitude of 29,000 feet to optimize the performance of the on-board electronics. Occasionally, portions of a few flights were conducted at lower altitudes.

4.1 European Area 1 Flight Upsets

Test flights of the military aircraft in European Area 1 began in November, 1990. We have obtained data from the first flight and on subsequent flights up to February, 1992. The first flight, the ferry flight, was a polar route from the United States to Europe. One of the two upsets on this flight occurred over Greenland and the other over Iceland. Most of the subsequent flights were in European Area 1 at a minimum latitude of 54°N.

The duration of the test flights varied from less than two hours to more than nine hours. The average flight time was approximately 6.3 hours and more than 78% of the flights were for more than five hours. Three short flights of between three to four hours duration experienced upsets, and one long flight of greater than nine hours experienced no upsets. The largest number of upsets per flight was five and this happened twice. One of these flights was on a north-south path that took the aircraft as far south as 30°N latitude. The 37 flight tests cover 233 hours of flight time. Nine of the 37, about 25%, showed no upsets, clearly indicating the random nature of the upsets. The European Area 1 flight upsets are shown in Figure 4-1 on page 4-2. The data for each of the individual flights, in terms of date, flight duration, and number of upsets, is tabulated in A.1, "European Area 1" on page A-1.

4.2 European Area 2 Flight Upsets

Test flights of military aircraft in European Area 2 began in March, 1991. We have obtained data from that first flight and on subsequent flights up to March, 1992. Most of the flights are in the vicinity of European Area 2 at a minimum latitude of 44°N. One recent flight was conducted considerably further south.

The duration of the test flights ranged from about an hour to more than 10 hours with the average flight length being 6.6 hours. More than 83% of the flights were for more than five hours duration. A short flight of between two to three hours duration had two upsets and several long flights of between eight and nine hours experienced no upsets. The largest number of upsets per flight was four and this occurred twice. The 83 flights cover 552 hours of flight time. About 35% of the flights showed no upsets, clearly showing the random nature of the upsets. The European Area 2 flight upsets are shown in Figure 4-1 on page 4-2. The data for each of the individual flights, in terms of date, flight duration, and number of upsets, is tabulated in A.2, "European Area 2" on page A-2.

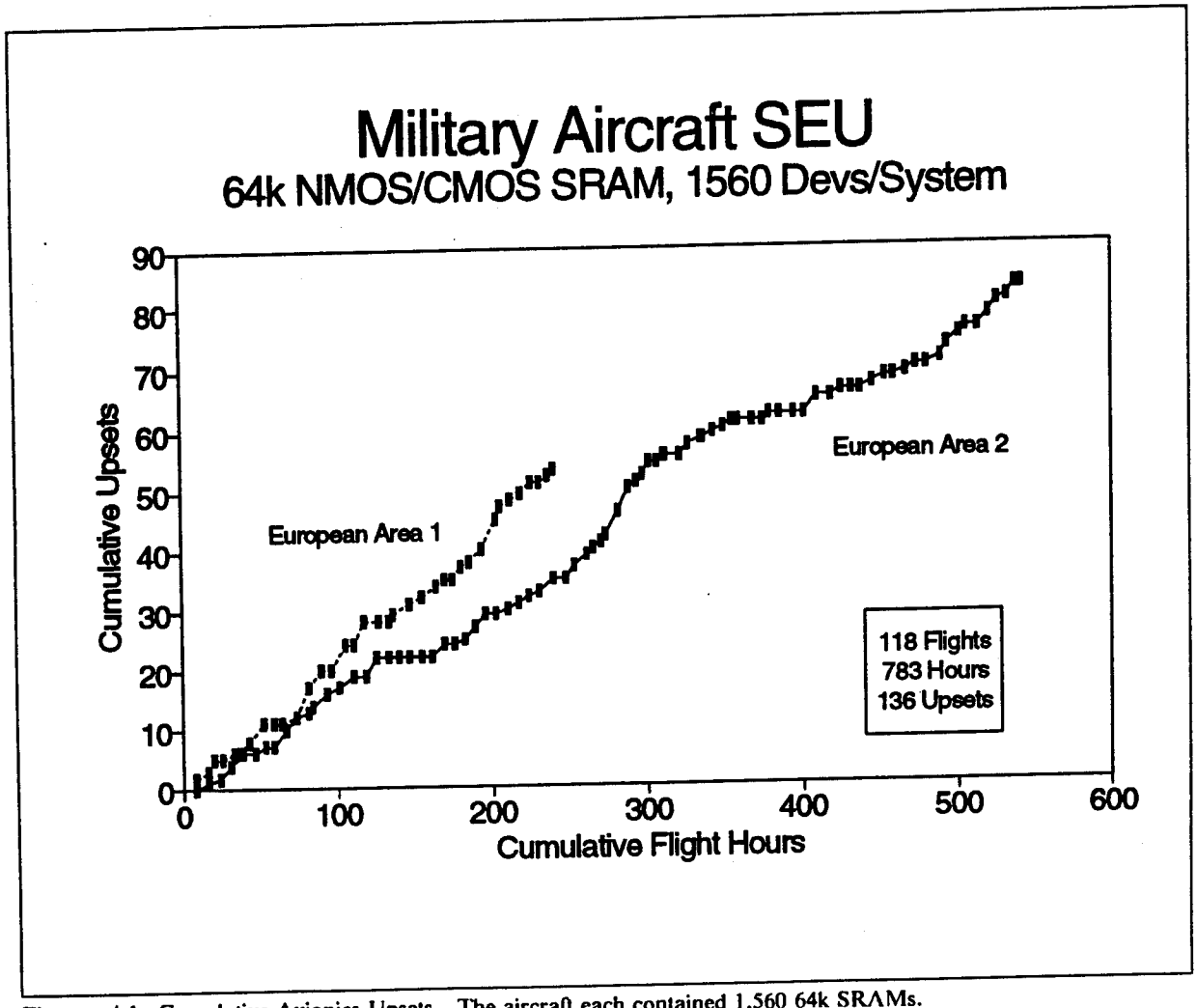

Figure 4-1. Cumulative Avionics Upsets. The aircraft each contained 1,560 64k SRAMs.

4.3 Temporal Variation of Flight Upsets

The flight upset data from the military aircraft can be evaluated in several different ways. One way which appears to give interesting results is to plot the upsets as a function of day as shown in Figure 4-2 on page 4-4. Individual upset points clearly show wide scatter about the long term average value. It would be tempting to ascribe some meaning to the time variation of Figure 4-2. As a first test, we calculated an adjusted, short-term average upset rate, which is indicated by the solid black line. The peaking in the fall of 1991 is seen in the short term average as well as in the individual data points.

The primary issue remains as to whether this time variation is at all meaningful. We believe that this variation is due to poor statistics and is not meaningful because it is based on too little data. When a flight experiences a single upset, one of 1,560 chips have upset, which is 0.064% of all chips. Even when there are four or five upsets in a flight, this represents only 0.2-0.3% of all the chips upsetting. This is just too few to be statistically significant.

If we had upset data averaged from a fleet of at least 10-15 airplanes in flight at the same time, the time variation likely would be statistically significant. The actual data in A.1, "European Area 1" on page A-1 and A.2, "European Area 2" on page A-2 confirm this. Most of the highest daily upset rates shown in Figure 4-2 occurred on days for which we have data from only one of the two flight areas. October 9, 1991 is an exception because there is data from both flight areas on this day. In Area 2, the rate was 0.58

upsets/hr, but in Area 1 it was only 0.15 upsets/hr and if the two were averaged the rate would be 0.37 upsets/hr. We believe that if we had data from another ten airplanes flying on that same day the average upset rate for all the aircraft would closely approach the long term average shown in the figure. This simple example ignores the variation with latitude which is discussed in detail in 8.3, "Effect of Latitude" on page 8-3.

Despite the enormous statistical uncertainty that we have discussed, if we nevertheless wanted to ascribe some significance to the variation, what could be the basis? The reason for the variation in upsets would then have to be due to a variation in the atmospheric neutron flux. As indicated in 4.1, "European Area 1 Flight Upsets" on page 4-1 and 4.2, "European Area 2 Flight Upsets" on page 4-1, the aircraft flew in the same general geographical area and at the same altitude most of the time. Thus we wouldn't expect to see much variation in the neutron flux due to changes in altitude or latitude. The only remaining variable is cosmic ray modulation, i.e. changes in the intensity and/or spectrum of the incoming cosmic rays that produce the atmospheric neutrons.

On earth we measure cosmic ray modulation through the response of specially designed neutron detectors such as the one at Deep River, Canada. However, as discussed in 7.2, "Model of the Atmospheric Neutron Environment" on page 7-1, large changes in the Deep River neutron monitor correlate with only very small changes in the 1-10 MeV atmospheric neutron flux based on the Wilson-Nealy model (see 7.2, "Model of the Atmospheric Neutron Environment" on page 7-1). Thus the wide fluctuations seen in Figure 4-2 on page 4-4 are only statistical in nature, and no physical mechanism can account for a correspondingly large variation in the atmospheric neutron flux.

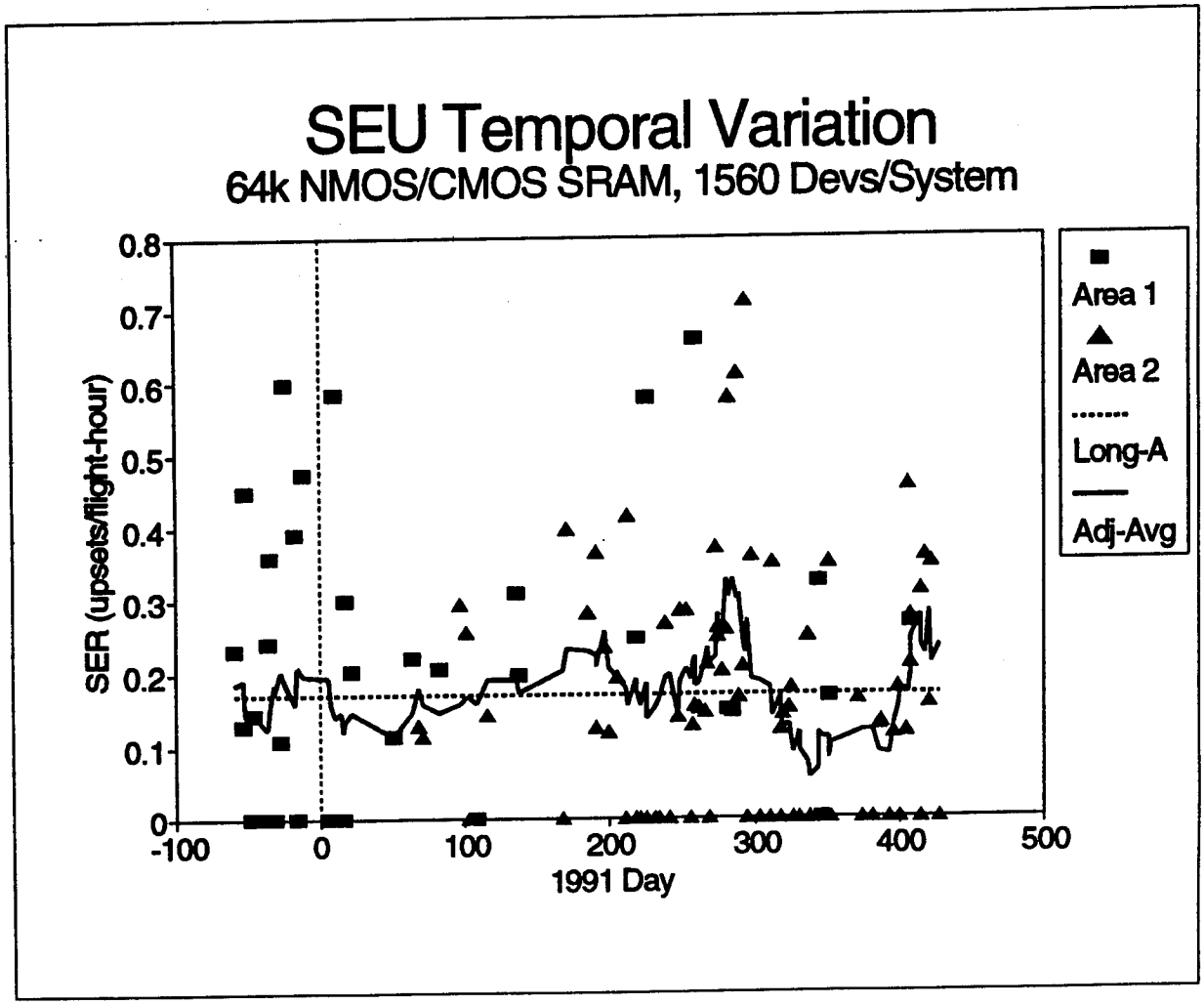

Figure 4-2. Avionics Upset Rate vs Time.

Section 5. Space Shuttle Flight Data

Additional SEU measurements on the same IMS1601 64k×1 SRAM used in this avionics study have been taken in low earth orbit on board recent Space Shuttle flights. This data is included here because it helps corroborate that the soft errors we're seeing in the IMS1601 on aircraft are related to the natural cosmic ray environment and are not due to other effects such as electromagnetic interference, etc.

The IMS1601 is used for the mainstore memory in IBM's upgraded AP101S General Purpose Computers (GPC's) that have been flying on board the Space Shuttle since April, 1991. Each of the five GPC's contains 200 of these 64k×1 SRAMs, along with error detection and correction circuitry. In the active GPC's, the entire mainstore memory is read out every 1.678 seconds so that all single-bit errors can be corrected. The results of each of these "scrub" cycles are sent to Mission Control by telemetry and allow soft errors to be correlated with the time/location of the Shuttle orbiter [Ref. 9].

5.1 Upset Rate Variation with Altitude/Latitude

The soft error rate as a function of altitude and latitude for the first eight flights of the AP101S computer is shown in Figure 5-1 on page 5-2. The IMS1601 soft error rates range from 1.4E-7f/bd at low inclination/altitude to 8.9E-7f/bd at high inclination/altitude. There was about a 2.8× increase in upset rate when going from a 28.5° inclination orbit to a 57.1° orbit at 160nmi. As a function of altitude, the upset rate increased by approximately 3.7E-9f/bd for every nautical mile.

It can be seen that the upset rates measured on the Space Shuttle in low earth orbit are in the same range as those measured on the ER-2 aircraft at 65,000 feet over Norway. Thus, the problem of SEU can be as great a concern for aircraft avionics designers as for designers of spacecraft avionics.

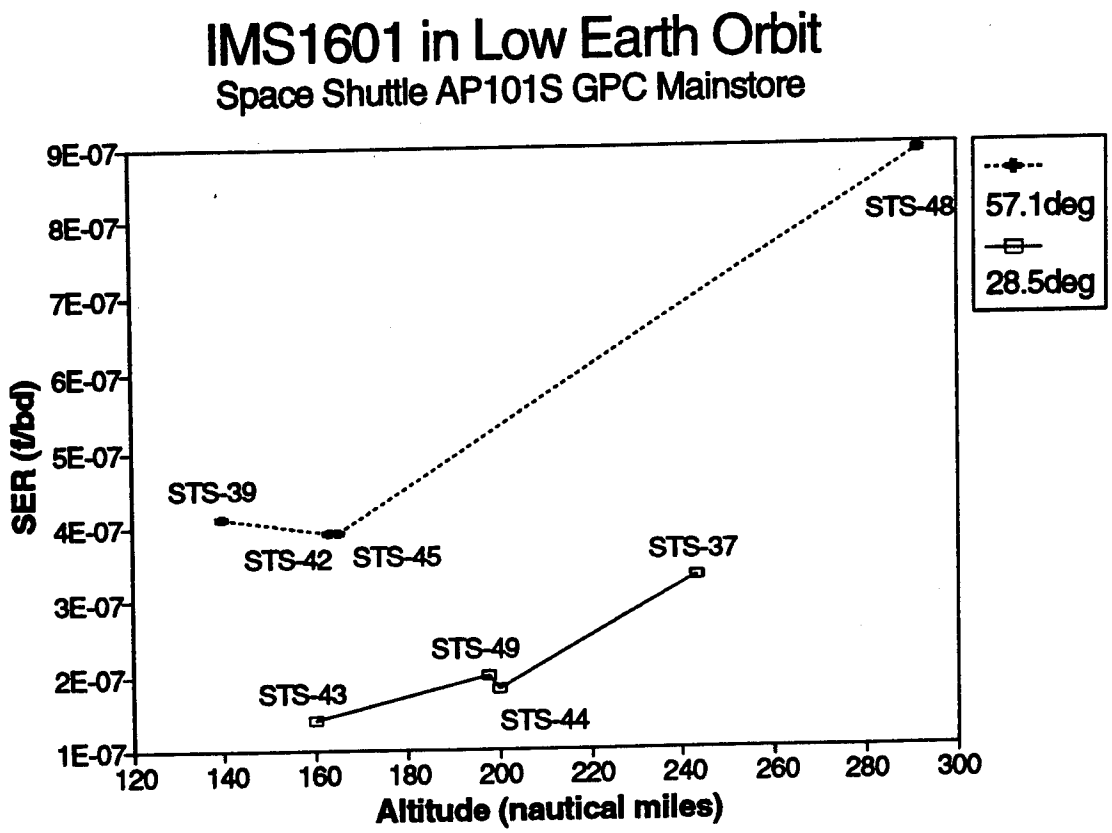

Figure 5-1. Space Shuttle SEU Rate vs Altitude/Latitude. The upset rates were measured on the IMS1601 64k×1 SRAM in the 5V operating mode.

5.2 Multi-Bit Upsets

The Space Shuttle measurements also provide data on multiple-bit upset events. It is consistent with the much larger tabulation of multiple-bit upsets that has been compiled from measurements on the CRRES satellite [Ref. 10]. These Space Shuttle events involve the simultaneous (i.e. within one 1.678 second scrub cycle) upset of more than one memory cell.

Table 5-1 on page 5-3 shows of summary of multi-bit upsets recorded on the first eight flights of the AP101S. In each instance, the multiple upsets were in different ECC words, so that all errors were correctable. The percentage of multiple upset events ranged from 0% of the total events on some of the low inclination flights (STS-44 and STS-37) to as high as 9.0% of the total events on one high inclination flight (STS-42).

Table 5-1. IMS1601 Multi-Bit Upsets on the Space Shuttle. Most multi-bit upset events have occurred at high latitudes.

Flight	Altitude (nmi)	Inclination	Launch Date	SER (f/bd)	Total Events	Multi-bit Events	Ratio (multi/total)
STS-44	200	28.5°	11/24/91	1.8E-7	31	0	0%
STS-37	243	28.5°	4/5/91	3.3E-7	55	0	0%
STS-43	160	28.5°	8/2/91	1.4E-7	39	1	2.6%
STS-49	198	28.5°	5/7/92	2.0E-7	58	2	3.4%
STS-45	165	57.1°	5/24/92	3.9E-7	77	3	3.9%
STS-48	292	57.1°	9/12/91	8.9E-7	151	10	6.6%
STS-39	140	57.1°	4/28/91	4.1E-7	81	7	8.6%
STS-42	163	57.1°	1/22/92	3.9E-7	67	6	9.0%

Notes:

1. The IMS1601 SER is calculated based on all upsets, including multi-bit upsets.
2. The STS-43 multi-bit events consisted of one 2-bit upset.
3. The STS-49 multi-bit events consisted of two 2-bit upsets.
4. The STS-45 multi-bit events consisted of two 2-bit and one 3-bit upsets.
5. The STS-48 multi-bit events consisted of ten 2-bit upsets. Two of these events involved simultaneous upsets in more than one computer (GPC pairs 1&2 and 1&4).
6. The STS-39 multi-bit events consisted of five 2-bit, one 4-bit, and one 11-bit upsets.
7. The STS-42 multi-bit events consisted of five 2-bit and one 4-bit upsets.

About 80% (23/29) of the multiple upset events involved only two memory cells. However, one of the 29 events involved three cells, two involved four cells, and one involved as high as 11 cells. This last event (11 simultaneous upsets on STS-39) occurred when the orbiter was at the southernmost tip of its orbit and the astronauts were viewing an aurora australis display.

The physical location of each memory upset could only be resolved to the card level, so it is not clear whether most upsets occurred within single chips or across multiple chips. In two instances, however, simultaneous upsets occurred in separate computers (on STS-48). The IMS1601 is a 1-bit wide device, so a multiple upset within the same chip would cause only a single-bit error to appear in any individual ECC word.

The Space Shuttle multiple-upset events are also consistent with multiple-bit upsets recorded in SRAMs during heavy ion testing. Koga [Ref. 11] found 10-20% of multi-bit upsets in two different 1Mb SRAMs with the low LET Ne ion. We obtained substantially lower results with a third 1Mb SRAM, the EDI 188128C54 128k×8 device. Our results are shown in Figure 5-2 on page 5-4 in which the single event and multiple-bit upset cross sections are plotted as a function of the LET of the ion. The SEU cross section represents the average for four different parts. For low LET ions (F in our case, 5.5<LET<11), the fraction of multiple bit upsets is only 1-2%, which is about a factor of ten lower than what Koga found.

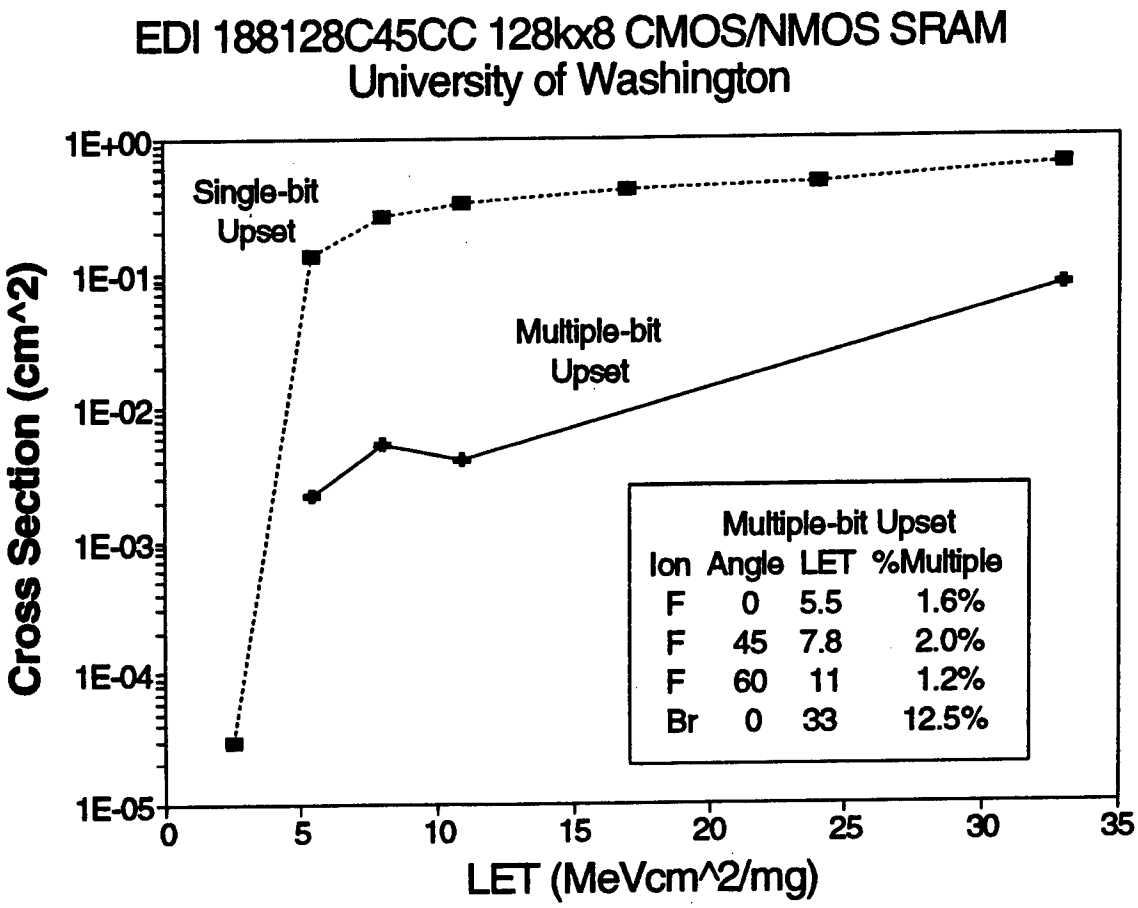

Figure 5-2. Heavy Ion Cross Section for 1Mb SRAM. Testing was performed at the University of Washington Nuclear Physics Laboratory (UWNPL).

We found the multiple-bit upsets because two bits flipped within the same byte (with the F ion we found only two upsets, but with the higher LET Br ion there were instances of three upsets). Koga also found double upsets within the same byte in one of his SRAMs [in this case by a different vendor, Mosaic (Hitachi)] and multiple bit errors, but not within a single byte in another vendor's SRAM (Micron). Thus, contrary to the situation with SEU of similar sensitivity for the same type of commercially available memory technology (see 8.1, "Effect of Memory Size" on page 8-1), there appears to be a wide variation in the sensitivity to multiple-bit upset for the same type of memory technology.

Section 6. Laboratory Testing

The 64K SRAM has previously been tested for SEU using beams of heavy ions and protons. Results of the heavy ion SEU tests, performed at Brookhaven National Laboratory, are given in terms of the SEU cross section as a function of the linear energy transfer (LET) of the ions. The data are presented in Reference 12. Results of the proton SEU tests, in terms of the SEU cross section as a function of proton energy, are also found in Reference 12. These tests were carried out at the Harvard University cyclotron. The heavy ion tests were performed with the SRAMs at the full 5 volt operating voltage. The proton tests were performed with the SRAM at both 5 volt operating voltage and 2.5 volt standby voltage. In addition, the SRAM was tested using the 800 MeV proton beam at the Los Alamos Meson Production Facility (LAMPF). This test was carried out only with the SRAM at 2.5 volt standby voltage, and is documented in Reference 13.

As indicated, at aircraft altitudes, upsets in the SRAMs are induced primarily by the atmospheric neutrons. In order to calculate the upset rate in the SRAM due to neutrons, we required some SEU testing with neutron beams to provide data for the model. The neutron SEU testing was performed at two facilities: the Boeing Physical Sciences Research Center (BPSRC) using the 14 MeV neutron generator and at the University of California at Davis (UCD) using the higher energy neutrons produced by the cyclotron.

6.1 Neutron Facilities and SEU Test Setup

SEU testing of the SRAM was achieved using a standard board of 28 memory chips provided by IBM as the test card. The board was connected through a Boeing-designed interface board to scalars and a diagnostic computer that monitored upsets in the SRAMs. For both neutron sources, only the board with SRAMs and the connecting cable were located within the neutron beam. All other equipment (diagnostic computer, scalars, etc.) were located outside the room containing the neutron source. All 28 SRAMs were loaded with a specific pattern (a psuedo-checkerboard) by a pattern editor and read at regular time intervals. Errors, when detected, were recorded and corrected by the test system.

The two neutron facilities provided significantly different neutron beams. The UCD cyclotron produces a very narrow collimated beam, approximately 1″×2″. We sighted in the test board such that four devices were centered within the beam. Immediately adjacent SRAM devices also received some of the beam so, effectively, five devices recorded upsets due to the neutrons. The BPSRC 14 MeV neutron generator produces neutrons over an approximately 2π field. The test board was located about 12 inches from the head of the generator. Thus, all 28 devices exhibited upsets once the generator was turned on.

6.1.1 Cyclotron Produced Neutron Beam Exposures and Dosimetry

Energetic neutron and proton beams are produced by the Crocker National Laboratory cyclotron at UCD. Energetic neutrons, with energies of 42 and 64 MeV, were used to test some of the devices. Neutrons were produced by directing a beam of protons into a Lithium (^{7}Li) target.

The cyclotron is a magnetic resonance accelerator. It consists of a disc shaped chamber that is split into two halves that are separated by a narrow gap. An electric potential of several thousand volts is placed across this gap and the poles of a strong electromagnet are aligned normal to the radii of the halves. Charged particles (in this case protons) are injected by a source into the gap, near the center of the apparatus and are accelerated to one of the halves by the gap potential. The magnetic field causes the particles to rotate around the semicircle half until they reach the gap, where they are accelerated by the electric potential to the other semicircle half. As this process is repeated, the particle energy is increased with each acceleration across the gap, and the particle's radius of revolution is gradually increased in order to maintain a constant period. After many revolutions, the particle is drawn off for use at the outer walls by an electrostatic field. Specific details of cyclotron operation are presented in Reference 14.

The proton beam drawn off of the cyclotron travels through a beam tube to a steering magnet where it is directed towards one of several experimental stations. The station for proton irradiations is located in the facilities' north cave and the neutron irradiation station is located in the south cave. Because protons have a large range in air, the beam does not require an evacuated path and the DUT exposures do not require an evacuated test chamber. The cyclotron continuously produces beam during a sequence of test trials and DUT exposure is controlled by the operator, who remotely inserts or withdraws a plug into the beam line.

Dosimetry for the proton irradiation beam line is conducted using a Secondary Emission Monitor (SEM) and a Faraday Cup. Both are resident in a Faraday cup box which is evacuated to maintain the stability of the SEM output. The Faraday cup, which prevents beam from reaching the DUT, can be removed from the beamline without being removed from the box. As the beam is steered into the proton irradiation station, it passes through a degrading foil to ensure a reproducible and uniform beam intensity. Before DUT irradiations, the SEM current measurement is calibrated with the Faraday cup current measurement and a Faraday cup to SEM ratio is calculated. This ratio is used in calculations that convert the SEM value, measured with each DUT irradiation, to actual fluence. This dosimetry process for proton irradiations has been automated and is operated from a microcomputer system. This system is described in Reference 15.

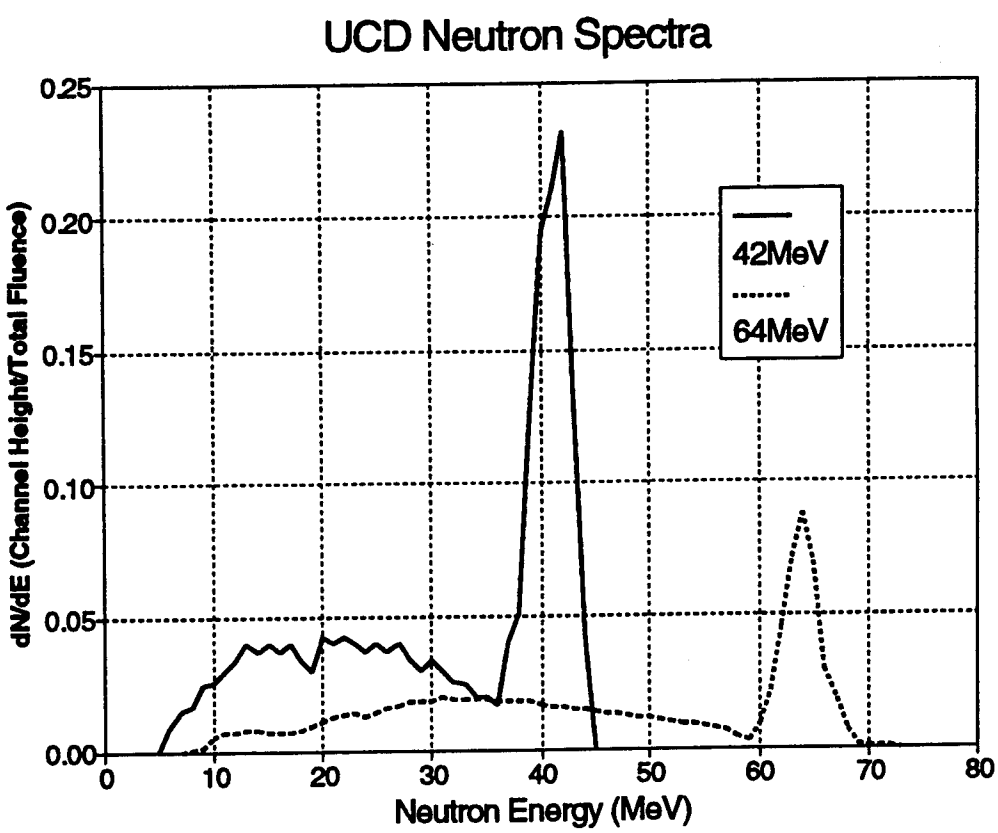

Figure 6-1. Neutron Spectra for Beams Produced at UCD. The neutron beam has a sharp peak near the energy of the incident proton beam, but also has a lower energy "tail" distribution that continues down to approximately 10 MeV.

The neutron beam was produced by bombarding a ^{7}Li target with a beam of protons. The nuclear reaction of interest is $^{7}Li(p,n)^{7}Be$, where the product neutron has very nearly the same energy as the incident proton. The characteristics of the neutron beam were determined with a monitoring system located upstream of the

DUT target. The dosimetry method involved using a multi-wire chamber to measure the energies of recoil protons produced by neutrons interacting with a CH_2 convertor. This dosimetry system is described more completely in Reference 16. The output of this system is the neutron beam energy spectrum, which is shown in Figure 6-1 on page 6-2 for the two peak energies of 42 MeV and 64 MeV. Examination of this spectrum indicates that the neutron beam has a sharp peak near the energy of the incident proton beam, but also has a lower energy "tail" distribution that continues down to approximately 10 MeV. Following each DUT irradiation, UCD personnel provide an approximate measure of the peak fluence, as determined from the dosimetry system, and later provide the accumulated spectrum from all trials at the given peak energy. The objective of this environment simulation was to gather SEU data as a result of mono-energetic neutrons. Although the neutron energy spectrum has a well defined peak, it is not mono-energetic and the low energy tail does have an effect on the test results. The method of compensating for the low energy tail is described in the following section.

6.1.2 Neutron Generator Produced 14 MeV Neutron Exposures and Dosimetry

14.7 MeV neutrons were produced with the 14 MeV neutron generator at BPSRC that uses a Penning Ion Gage type generator. Neutrons are produced by bombarding a titanium tritide target (TiT) with DC accelerated deuteron ions which produces the reaction of interest, $T(d,n)He^4$. The product neutrons have an energy range of approximately 13.4-14.7 MeV. Approximately 1E11 neutrons/second are produced by this generator and a conservative estimate of the flux at a distance of 5 cm from the TiT target is 3E8 n/cm^2-sec. The TiT target is assumed to be a point source and flux varies as $S/4\pi r^2$, where S is the source strength and r is the radial distance from the TiT target. As these neutrons are produced as a result of the (D,T) nuclear reaction, the tail feature exhibited in the cyclotron neutron beams is not observed.

Circuit cards containing the DUTs were placed in the beam a few inches from the TiT target. Irradiations were conducted at ambient atmosphere. The neutron generator was started and stopped with each irradiation, rather than withdrawing and inserting a barrier within a continuous beam as for the other cyclotron simulations.

The neutron fluence for each run (DUT exposure) was determined by measuring the exposure on Thermal Luminescent Detectors (TLDs) that were on the DUT cards. A second verification method was also used by measuring the activation of a Zirconium (Zr) foil that was also irradiated with the DUTs. The TLDs used were TLD-700, which are fully enriched in ^7Li, and have a known response to neutrons of approximately 1E9n/cm^2-sec per rad of exposure. A set of TLDs are collocated on a card with a DUT, or set of DUTs, and accumulate exposure as the DUT undergoes a set of neutron generator irradiations. Following a test sequence, each TLD from each run is taken to a TLD reader where the exposure dose was measured. The total dose a TLD received was converted into the total fluence for each of the corresponding set of irradiations. The fluence measurements determined with the TLDs were verified by Zr foil activation. Zr has a 13 MeV threshold for the (n,2n) reaction and measures the total fluence for neutrons with energy greater than 13 MeV. Following a test sequence using a Zr foil, the activity of each irradiated foil was measured with a Lithium drifted Germanium, Ge(Li), detector. The measured activity was then converted into neutron fluence >13 MeV (see Reference 17).

6.2 Neutron Upset Cross Section Measurements

Neutron upset measurements were made at the neutron energies: 14.7 MeV (using the 14 MeV neutron generator), 42 MeV, and 64 MeV (both using the UCD cyclotron). The upsets recorded using the 14 MeV neutron generator are shown in Figure 6-2 on page 6-4 through Figure 6-4 on page 6-6, which present the data in a three dimensional histogram format.

Figure 6-2 on page 6-4 shows the distribution of 747 of the 836 upsets among the 28 SRAMs when the board was operated in a 5 volt active mode. While in the active mode, errors were detected, recorded and corrected as the memory address lines of the 28 devices were continuously cycled during the exposure. (The

logic analyzer used to record the upset data could capture only 249 upsets at a time; for three cycles this is 747 upsets of the total 836 upsets recorded on the scaler).

Figure 6-3 on page 6-5 presents the distribution of the 369 upsets among the 28 devices when the board was operated at 5 volts, but in the standby mode. For these tests, the memories were loaded with data and then put into a standby mode (with addresses not cycling) during the exposure. Following exposure, the addresses were cycled once to read out the memory contents and count the errors. Figure 6-4 on page 6-6 shows the distribution of 196 of the total 1126 upsets among the 28 devices when the board was operated at 2.5 volts in the standby mode. Again, the 28 devices were written at 5V, put into a standby mode (addresses not cycling), exposed at 2.5V, and then brought back up to the normal 5V operating voltage for readout.

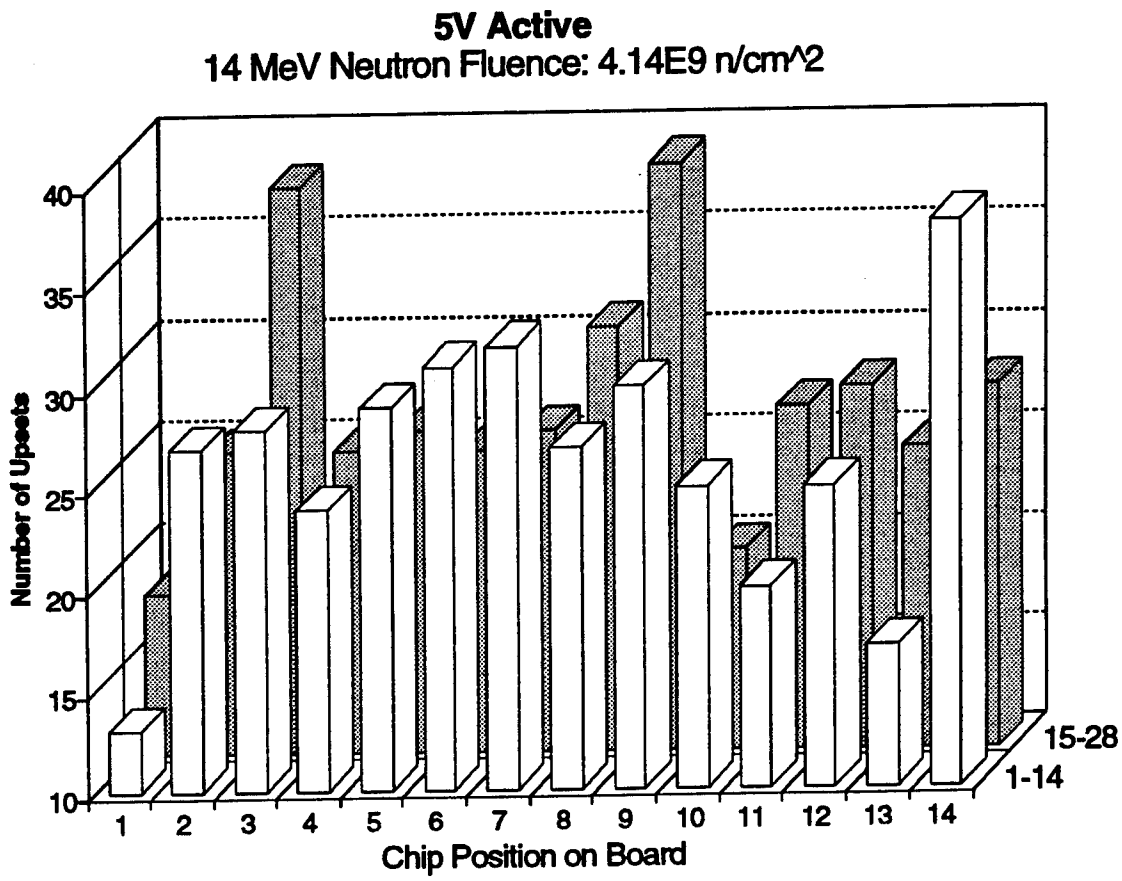

Figure 6-2. 14 MeV Upset Histogram (5V, active).

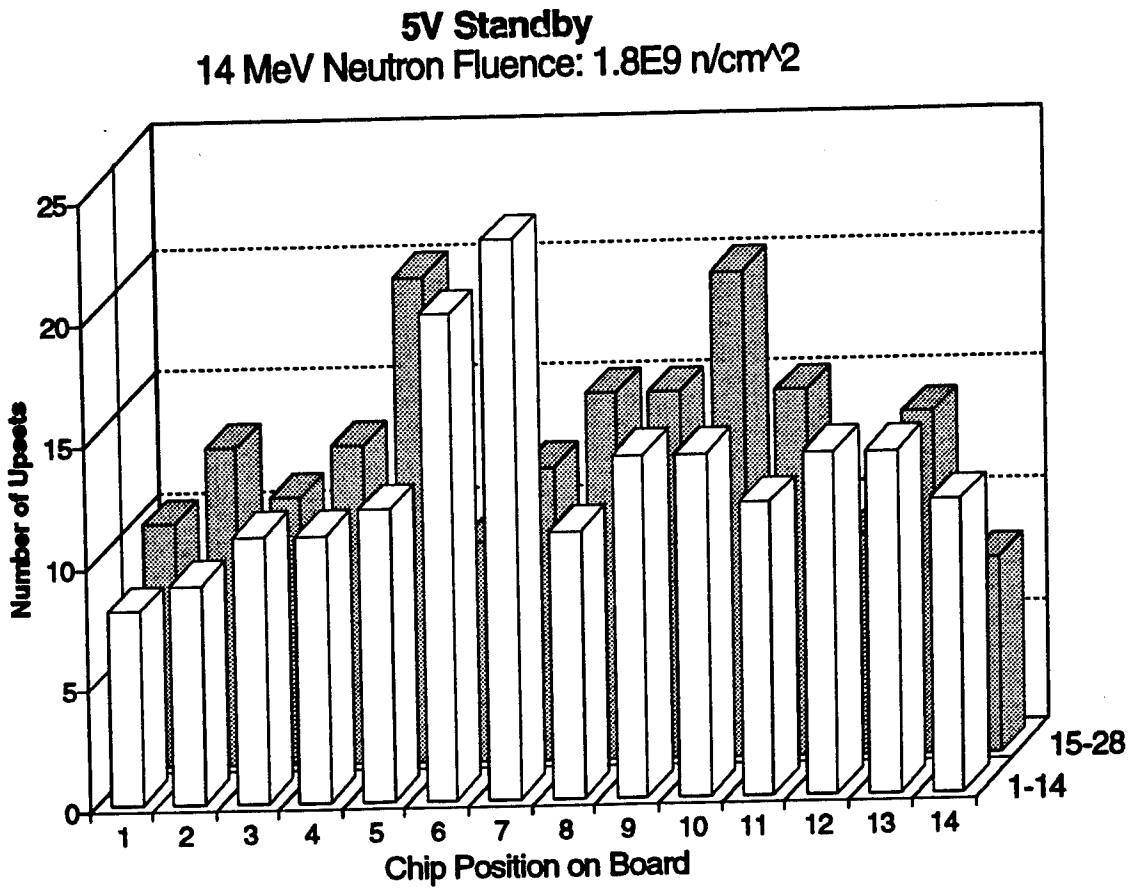

Figure 6-3. 14 MeV Upset Histogram (5V, standby).

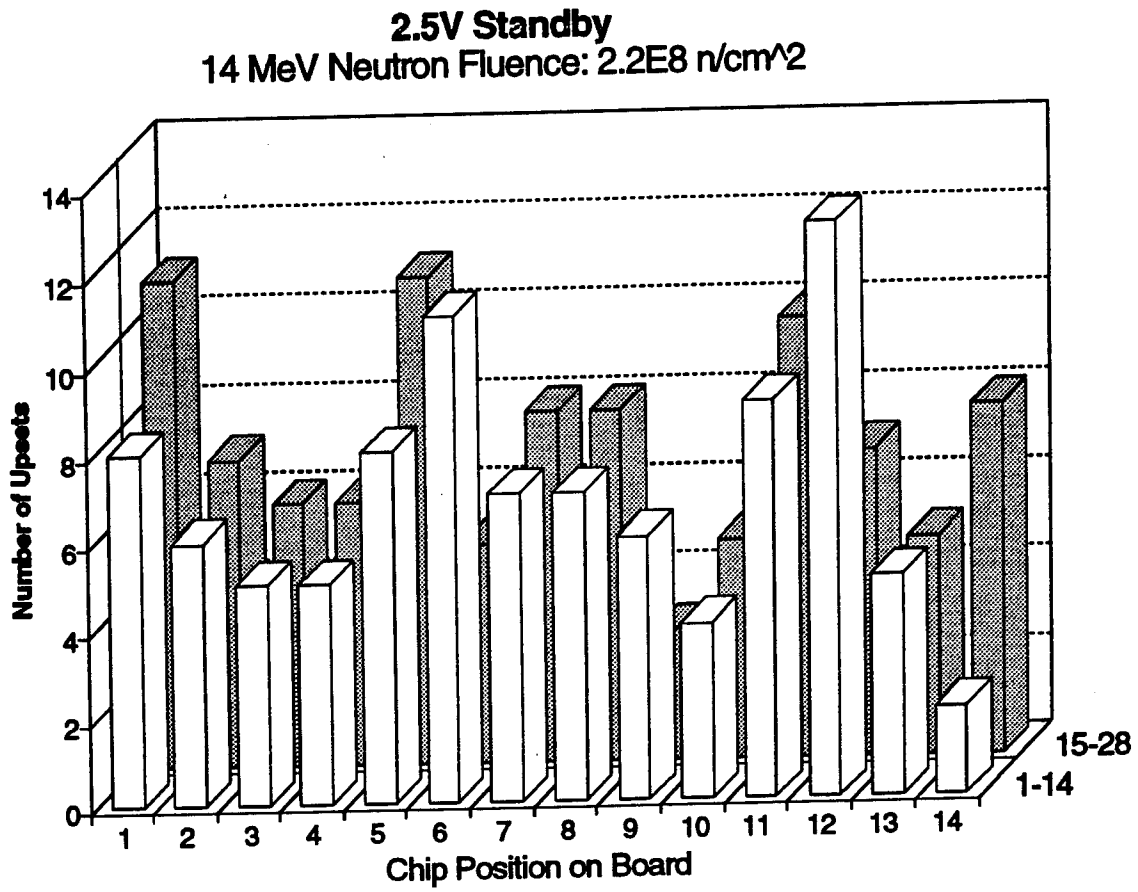

Figure 6-4. 14 MeV Upset Histogram (2.5V, standby).

Only during the second of the three runs did the logic analyzer unequivocally capture all of the 196 upsets. During the first and third runs, when more than the maximum 249 upsets that the logic analyzer could capture at a time were recorded, the distribution was incomplete. The 249 entries were filled up by upsets in only a fraction of the total 28 devices. Thus an accurate distribution of the upsets is only possible for the second run. However, for the purposes of an overall average, the total of the 1126 upsets (297, 196, 633 in the three runs, respectively) will be used, to be divided by the combined fluence for those three runs.

The upsets recorded using the UCD cyclotron neutron source with the peak energy at 64 MeV are shown in Figure 6-5 on page 6-7 through Figure 6-8 on page 6-10. The 76 upsets in the SRAMs when the board was operated at 5 volts in the active mode are shown in Figure 6-5 on page 6-7. Five devices account for nearly all the upsets (13.6 upsets/device because the collimated beam only strikes a small portion of all the 28 devices. Figure 6-6 on page 6-8 and Figure 6-7 on page 6-9 present the distribution of the upsets for two runs when the board was operated at 5 volts in the standby mode. In Figure 6-6 on page 6-8, 55 of the 56 upsets occur in five devices, resulting in an average of 11 upsets/device. Results of the second run with a 13% higher neutron fluence show more scatter. The same five SRAMs average 15.8 upsets/device, but they account for only 84% of the upsets. The remaining 15 upsets are distributed among five separately located devices which we attribute to neutron scatter off of the board.

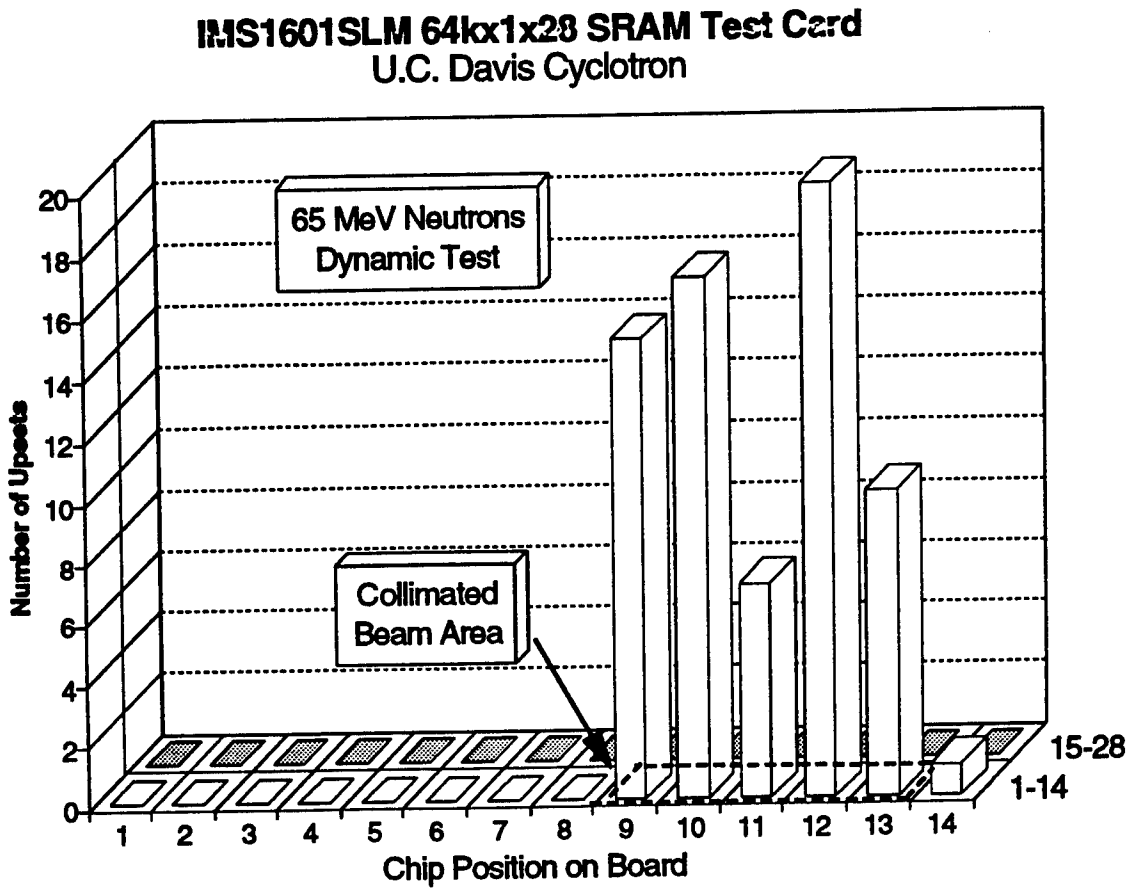

Figure 6-5. Upset Histogram (UCD, 65MeV, Dynamic).

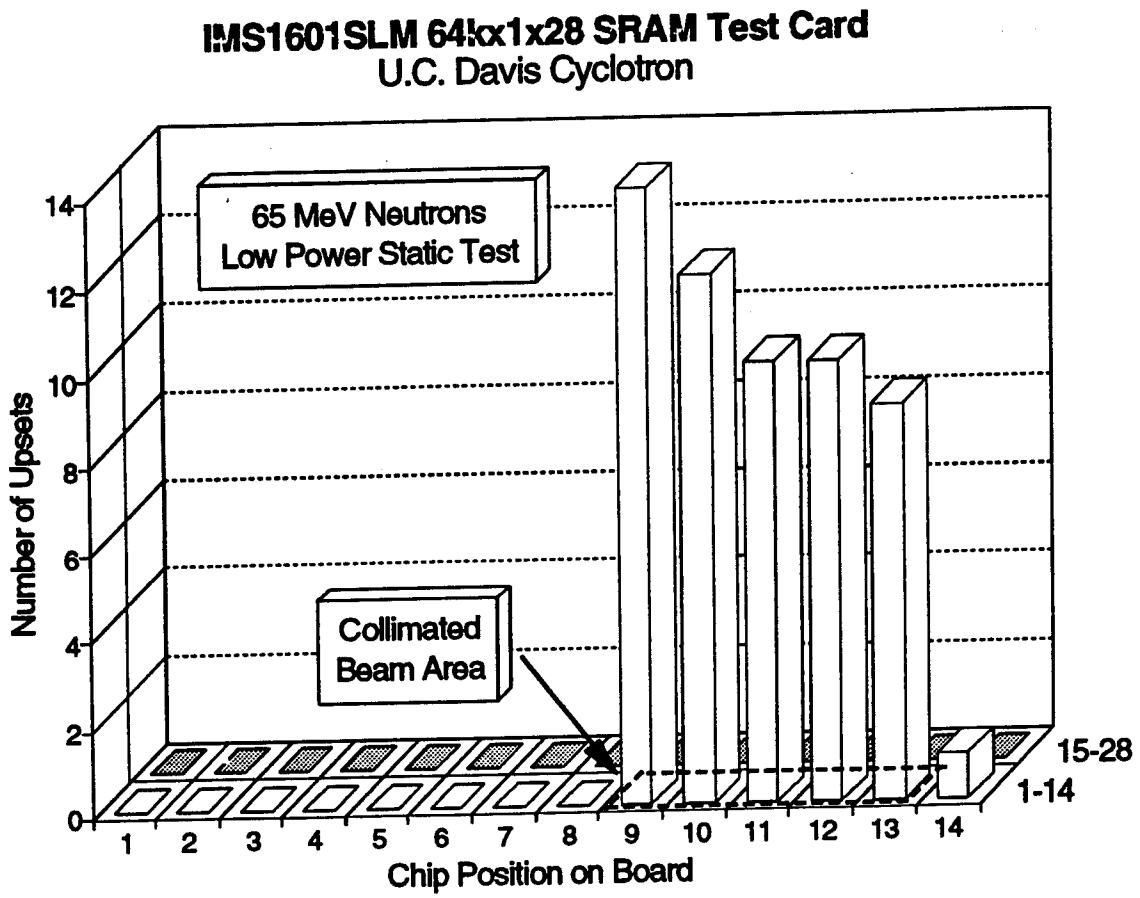

Figure 6-6. Upset Histogram (UCD, 65MeV, Low Power Static, 1st Run).

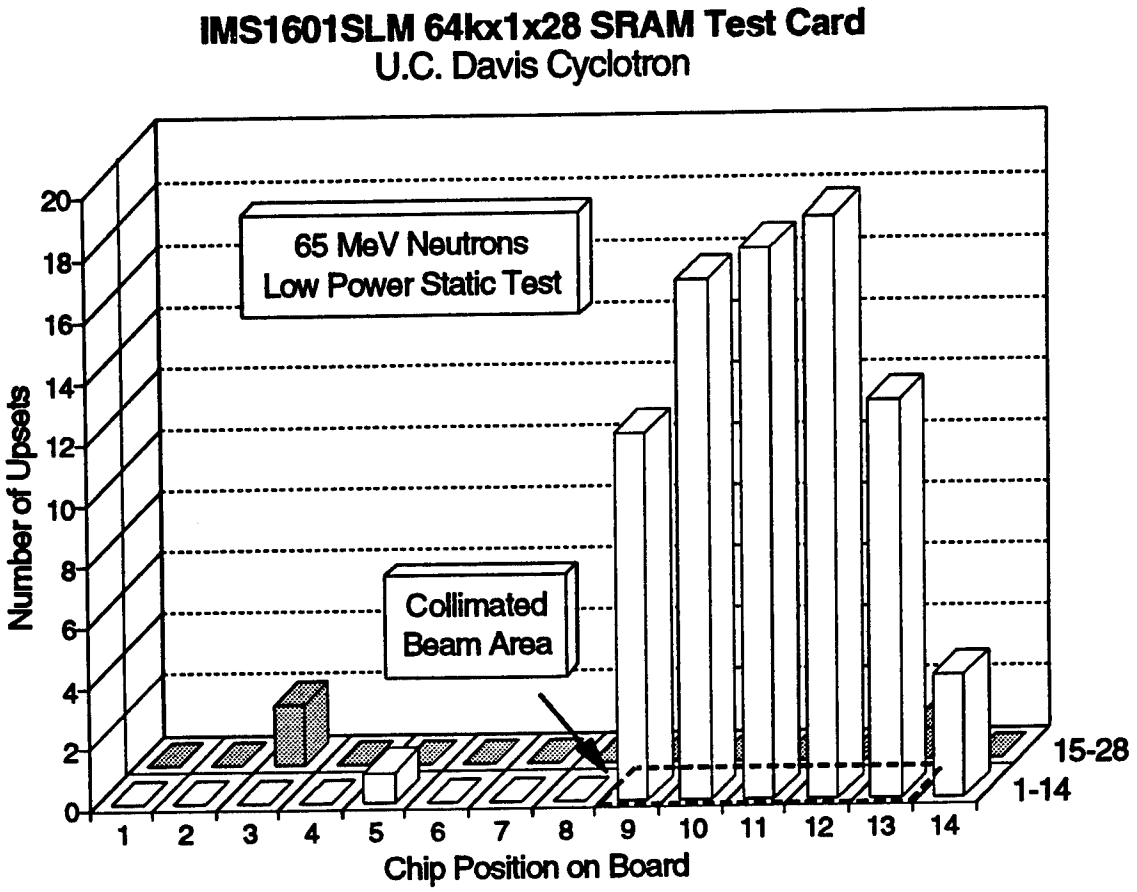

Figure 6-7. Upset Histogram (UCD, 65MeV, Low Power Static, 2nd Run).

Figure 6-8 on page 6-10 and Figure 6-9 on page 6-11 present the upsets recorded at the UCD cyclotron neutron source operated at a peak neutron energy of 42 MeV. In Figure 6-8 on page 6-10 are the results when the SRAMs were operated at 5 volts in the active mode. In Figure 6-8 on page 6-10, 36 of the 37 upsets occur in the same five devices as with the 64 MeV peak neutron source, averaging 7.2 upsets/device. Figure 6-9 on page 6-11 presents the histogram of upsets when the board was operated at 2.5 volts in the standby mode. In Figure 6-9 on page 6-11, 42 of the 45 upsets occur in the same five devices, averaging 8.4 upsets/device, for a fluence 30% of that received by the SRAMs in the 5 volt active mode.

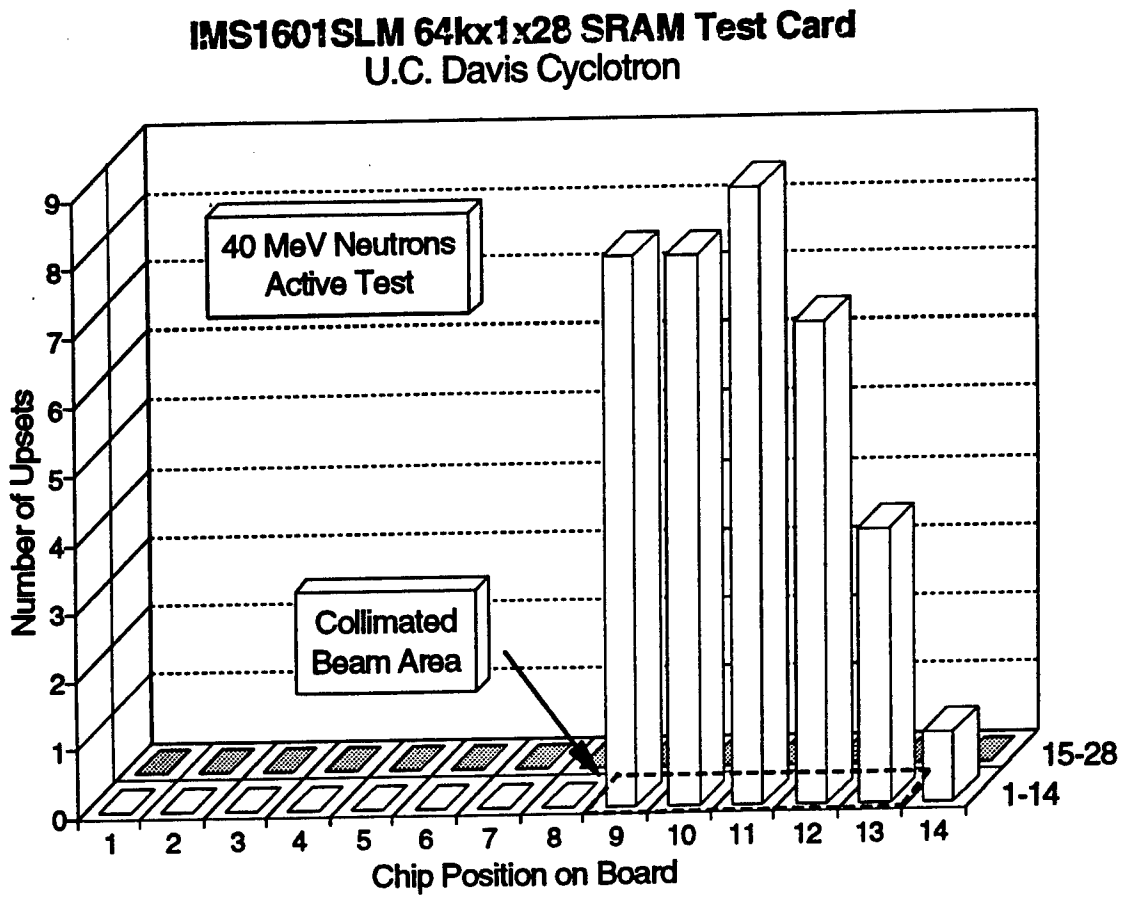

Figure 6-8. Upset Histogram (UCD, 40MeV, Active).

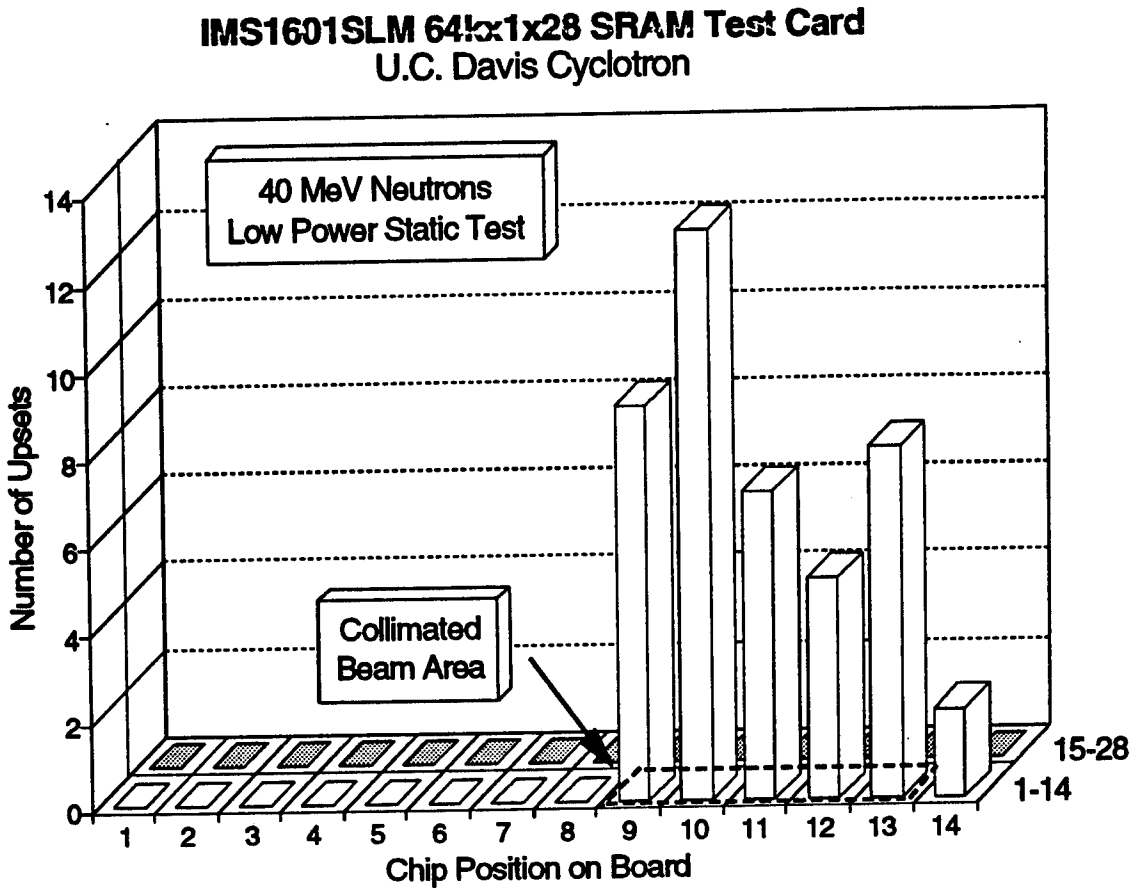

Figure 6-9. Upset Histogram (UCD, 40MeV, Low Power Static).

6.3 Neutron Upset Cross Sections

For a neutron source of specific energy, the neutron upset cross section was obtained following the standard procedure of dividing the number of upsets by the fluence. However, because there is an energy spectrum to the cyclotron source, this source is not mono-energetic and we had to account for the effective contribution of the lower energy neutrons in producing upsets. This was done through the adjustment factor which is fully described in 6.4, "Adjustment Factor" on page 6-16.

The cumulative data from the neutron upset measurements are tabulated in Table 6-1 on page 6-12, including the total number of upsets, upsets per device, neutron fluence, and neutron cross section. For the cyclotron neutron source, the key data is the number of upsets/device in those devices fully within the beam. Some devices that were outside the beam nevertheless received some fluence from neutrons scattered off of the portion of the card directly within the beam.

Table 6-1. Summary of Neutron and Proton Cross Sections.

Particle Type	Particle Source	Particle Energy (MeV)	Supply Voltage (Volts)	Operating Mode	Peak Particle Fluence (/cm²)	Total Neutron Fluence (/cm²)	Total Upsets	Upsets per Device	Upset Cross Section (cm²/device)	Upset Cross Section (cm²/bit)
IMS1601 64k×1 CMOS Static RAM										
Neutron	BPSRC	14.7	5	Active	4.14E9	4.14E9	836	29.9	7.22E-9	1.1E-13
Neutron	BPSRC	14.7	5	Standby	1.80E9	1.80E9	369	13.2	7.33E-9	1.12E-13
Neutron	BPSRC	14.7	2.5	Standby	1.10E9	1.10E9	1124	40	3.64E-8	5.55E-13
Neutron	UCD	42	5	Active	3.90E8	6.60E8	37	7.2	1.09E-8	1.66E-13
Neutron	UCD	42	2.5	Standby	1.20E8	2.00E8	45	8.4	4.2E-8	6.41E-13
Neutron	UCD	64	5	Active	2.00E8	4.60E8	76	13.6	2.96E-8	4.51E-13
Neutron	UCD	64	5	Standby	1.60E8	3.70E8	69	13	3.51E-8	5.36E-13
Neutron	UCD	64	2.5	Standby	6.10E7	1.40E8	56	11 (55)		
Neutron	UCD	64	2.5	Standby	6.90E7	1.60E8	94	15.8 (79)		
Neutron	UCD	64	2.5	Standby	1.30E8	3.00E8		26.8	8.93E-8	1.36E-12
Proton	LAMPF	800	2.5	Standby	6.60E9	6.60E9	10580	2189	3.32E-7	5.06E-12
EDI81256 256k×1 CMOS Static RAM										
Proton	LAMPF	800	2.5	Standby	8.83E9	8.83E9	57504	4107	4.65E-7	1.77E-12

Notes:

1. For 14 MeV neutron generator, total fluence = peak fluence. For cyclotron neutron source, total fluence = A × peak fluence, where A is the adjustment factor described in 6.4, "Adjustment Factor" on page 6-16. For 42 MeV neutrons, A = 1.7 and, for 64 MeV neutrons, A = 2.3.
2. Total upsets include upsets in devices within beam plus in devices outside of direct beam (received some scattered beam).
3. The upsets per device are based on upsets in devices within the beam.
4. The number of upsets per device shown in parentheses are for the 5 devices within the beam.

Table 6-1 also contains one other data point, that based on the same SRAM exposed to a narrow beam of 800 MeV protons at LAMPF (see Ref. 13). In this case, too, four devices were directly within the beam, but virtually all 28 recorded some upsets due to beam scatter. We believe that, at 800 MeV, proton upset cross sections will be the same as neutron upset cross sections. Thus, the 800 MeV proton upset cross section is taken to be the same as an 800 MeV neutron upset cross section.

At lower energies, the proton and neutron interactions in silicon are far from identical. Ziegler (Ref. 18) has shown that the burst generation rates for alpha particles induced in silicon by neutrons and protons become the same as the energy approaches 100 MeV. More recent data from an extensive data generation program (Ref. 19) shows that, based on production cross sections of various light reaction products (neutrons, protons, alpha particles, and deuterons), the neutron and proton cross sections in silicon are still not identical at 100 MeV. These proton and neutron cross sections are much closer at 100 MeV than they are at 50 MeV or even 10 MeV, but they definitely have not converged at 100 MeV. We will therefore assume that, for energies at which the intranuclear cascade/evaporation models apply, i.e., >200 MeV (see Reference 19), the neutron and proton cross sections will be identical. In that case, the number of upsets induced by protons and neutrons will be the same, but this applies only for E>200 MeV.

To utilize the neutron upset cross sections for upset rate calculations, we need the cross sections for all neutron energies, 1-1000 MeV, since the atmospheric neutron spectrum extends over that entire energy range (see 7.2, "Model of the Atmospheric Neutron Environment" on page 7-1). Fortunately, Bendel developed a single parameter model (Ref. 20) for proton induced SEU cross sections that fit the available data on early 1980's microelectronic parts rather well. In this model, the upset cross section in 1E-12 upsets per proton/cm^2 per bit, is

$$\sigma(E) = \left(\frac{24}{A}\right)^{14} [1 - \exp(-0.18 Y^{0.5})]^4, \qquad [6-1]$$

where

$$Y = \left(\frac{18}{A}\right)^{0.5} (E - A). \qquad [6-2]$$

More recently, Stapor [Ref. 21] and Shimano [Ref. 22] have shown that, for more recent microelectronic parts, a two-parameter model is needed to obtain a good fit, where one parameter is related to the asymptotic cross section, and the second to the threshold energy. Following Stapor, this two-parameter cross section fit is expressed as:

$$\sigma(E) = \left(\frac{B}{A}\right)^{14} [1 - \exp(-0.18 Y^{0.5})]^4 \qquad [6-3]$$

and, since Y remains as in Eq[6-2], the two parameters to be specified are A and B.

In examining Table 6-1 on page 6-12 we observe that, based on two sets of measurements; those with the 14 MeV neutron generator and the cyclotron source with the 64 MeV peak neutron energy, there is no real difference in neutron upset cross section when the SRAM is operated at 5 volts. In both the dynamic and standby modes, the upset cross section is essentially the same. With the 64 MeV source, the discrepancy is about 15%, and with the 14.7 MeV source less than 2%.

Thus we will require only two neutron upset cross section curves for the 64K SRAM, one for when it is operated at 5 volts and one for 2.5 volts. The two-parameter mode of Eqs[6-2,3] was fit to the four upset cross section data points for the SRAM operated at 2.5 volts. The results, with A = 10MeV and B/A = 1.125, are shown in Figure 6-10 on page 6-14. The model also shows excellent agreement in fitting the points for the SRAM at 5 volts. Here, a similar fit was made, resulting in A = 10MeV and B/A = 1.01.

Figure 6-11 on page 6-15 shows the resulting curve from the model, which is based on only the three neutron measurements.

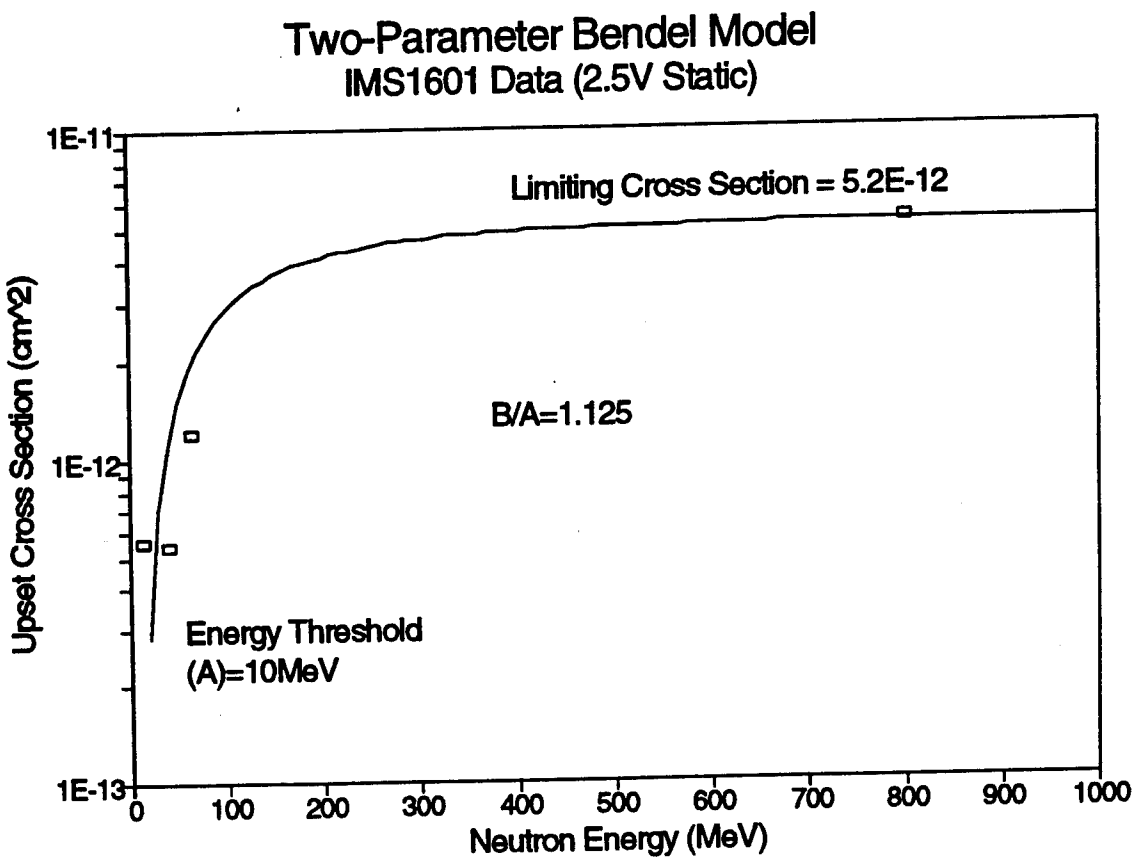

Figure 6-10. Bendel Model of NSEU Cross Section for 64k SRAMs (2.5V Standby Mode).

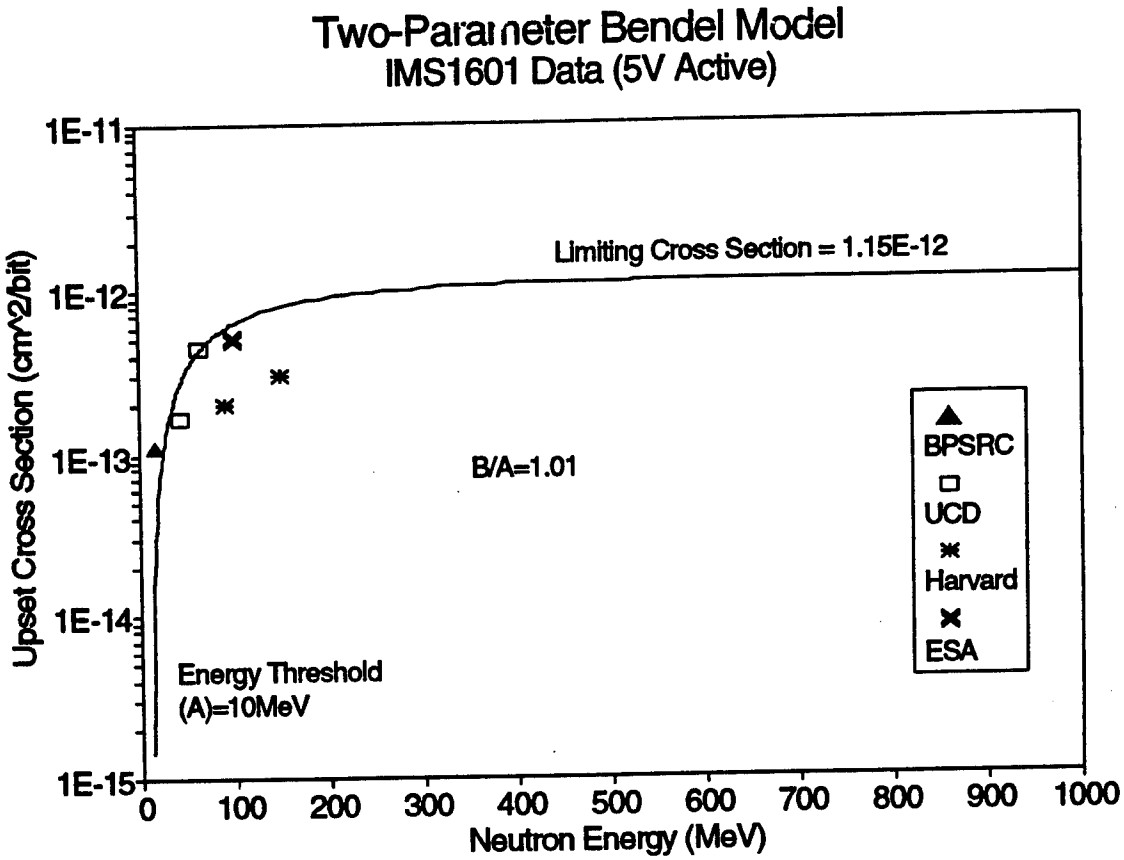

Figure 6-11. Bendel Model of NSEU Cross Section for 64k SRAMs (5V Active Mode).

Figure 6-11 also contains three data points from proton measurements. The two values from Harvard tests are from Reference 12 and the 100 MeV point is from Reference 65. The 100 MeV point was tested by the European Space Agency (ESA) and is for a slightly different 64k×1 SRAM (IMS1600) than the one used in all other tests (IMS1601). Nevertheless, the 100 MeV proton cross section is in good agreement with our fit. The two points from Harvard tests clearly do not fit the model curve very well. However, examination of all the proton data in Reference 12, with the SRAM operated at 5 volts shows a wide variation in cross section responses among different versions of the SRAM (with and without an epitaxial layer) and how the part was operated (dynamic and static modes). For protons with energies of 148 MeV, the upset cross section was 50-70% larger when operated in the static mode compared to the dynamic mode, and this applies to both epitaxial and non-epitaxial memory chips. However, for 50 MeV protons, the epitaxial parts had essentially the same cross section in both the dynamic and static modes, although that cross section is more than two orders of magnitude lower than our results with 64 MeV neutrons.

We can only conclude that the SRAMs responded differently in our neutron tests than they did in the Harvard proton tests and we are not sure exactly why. However, this shouldn't be too surprising. The only other parts that we know of which were tested with both protons and neutrons of several energies are two 16k DRAMs, the Motorola MCM4116AC20 and the Mostek MK4116J-2. The neutron and proton upset cross sections for these parts are given in Reference 44. For the MCM4116AC20, a plot of the cross sections as a function of energy is quite similar to Figure 6-11. However, for the MK4116J-2 part, the plot does not resemble Figure 6-11 nearly as much. For both the MCM4116AC20 DRAM and our 64k SRAM, there is one very high energy point representing the asymptotic cross section for both neutrons and protons

(800 MeV for the 64k SRAM, 4.2 GeV for the 16k DRAM). The cross section/bit for the low energy neutrons are higher than those for protons with at least twice the energy. For example, for both devices, the 14 MeV neutron cross section is approximately the same as that for 50 MeV protons. It thus appears that, for some devices, the geometries of the sensitive volume are such that low energy neutrons (e.g. <40 MeV) are capable of depositing more energy in the sensitive volume through the energetic recoils created than are protons (also see Reference 23).

For purposes of calculating neutron induced upset rates by means of the neutron cross section method (7.3, "Upset Rate by Neutron Cross Section Model" on page 7-8), we will use the two-parameter model fits shown in Figure 6-10 on page 6-14 and Figure 6-11 on page 6-15.

6.4 Adjustment Factor

One of the main disadvantages of the cyclotron neutron source is the low energy tail. Figure 6-1 on page 6-2 shows the energy spectrum of the 64 MeV neutron beam that was used for some of the previously discussed upset measurements. Visual examination indicates that as much as 50% of the cumulative fluence is in the tail. It is reasonable to assume that some of these tail neutrons deposit sufficient energy within the DUT to produce upsets, and that the total number of upsets recorded for a DUT include a contribution from neutrons in the tail. It has been shown that irradiations using this same cyclotron source have produced as much as a factor of three more upsets than predicted in accepted analytic methods [Ref. 23], and the source of this discrepancy appears to be the contribution of the tail neutrons. Since the objective of the cyclotron irradiations is to investigate upset as a function of incident neutron energy, contribution to the upset count by the tail neutrons confuses the issue, particularly if the contribution is significant.

To compensate for the effect of the tail neutrons, an adjustment factor is defined and introduced into the calculation of upset cross section. This adjustment factor may be thought of as a means for adjusting the peak fluence to account for the contribution of the tail neutrons in generating upsets. The sought after result from each DUT irradiation is the upset cross section for the peak neutron energy:

$$\sigma(E_{pk}) = \frac{\text{Upsets produced by peak fluence}}{\text{Peak fluence}} \qquad [6-4]$$

The values actually measured and recorded with each neutron irradiation include upsets caused by the entire neutron energy spectrum. It allows a cross section to be calculated as follows:

$$\sigma(E_{spectrum}) = \frac{\text{Upsets produced by total fluence}}{\text{Peak fluence}} \qquad [6-5]$$

The following adjustment factor is defined and applied to the peak fluence to convert Eq[6-5] into the form of Eq[6-4]:

$$A = \frac{\text{Predicted upsets produced by total fluence}}{\text{Predicted upsets produced by peak fluence}} \qquad [6-6]$$

To a first approximation, Eq[6-6] is simply the ratio of the flux from the total neutron spectrum to that about the peak neutron energy. However, the effectiveness of a neutron in generating upset is not equal across the range of neutron energies. Consequently, an energy dependent weighting function is incorporated into the calculation to account for the relative effectiveness of a neutron with a given energy of producing an upset. The mathematical form of the adjustment factor, A, with the weighting function included is:

$$A = \int_E [dN/dE\ W(E)\ dE]/[N_{pk} W(E_{pk})] \qquad [6-7]$$

where dN/dE is the differential neutron fluence spectrum, W(E) is the weighting function, N_{pk} is the peak neutron fluence, and $W(E_{pk})$ is the weighting function at the peak energy. In practice, this integration is performed numerically.

Two approaches for weighting functions were studied in the calculation of adjustment factors. One approach was to use neutron scattering cross sections (total and inelastic) in the calculations. Another approach was to use the Burst Generation Rate (BGR) as the weighting function. The BGR is defined as the probability that a neutron with energy En will generate a recoil with energy Er or greater in a collision with a silicon atom. The BGR concept was originated by Ziegler and Lanford [Ref. 24] and is more fully described in 7.4, "Upset Rate by the Burst Generation Method" on page 7-9.

Table 6-2 summarizes the results from adjustment factor calculations for the 42 MeV and 64 MeV neutron beams, made with a variety of weighting functions and for several peak widths (width is defined in terms of bins with size ΔE, which was 1 MeV). The energy spectrum for each of these beams is shown in Figure 6-1 on page 6-2. The weighting functions used in the adjustment factor calculations are illustrated in Figure 6-12 on page 6-18. The adjustment factors finally selected for use in the SEU cross section calculations were calculated using the BGRs for a recoil of energy Er = 3.5 MeV or greater, based on considerations discussed in 7.4, "Upset Rate by the Burst Generation Method" on page 7-9 and a peak width definition of seven bins. The results are as follows: for the 64 MeV peak neutron source, A = 2.6, and for the 42 MeV peak neutron source, A = 1.8.

Table 6-2. Peak to Total Spectrum Adjustment Factors. The adjustment factor, A, is equal to the integral of the spectrum weighted by cross section divided by the integral of the peak weighted by cross section.

Bin	s(tot)	s(inelast)	Er = 1	Er = 3	Er = 3.5	BGR = k
42 MeV Neutron Source						
A(1 bin)	4.404563	5.212414	5.538665	5.042053	4.283928	4.321168
A(3 bin)	2.171903	2.554304	2.654919	2.413694	2.090897	2.137184
A(5 bin)	1.956711	2.294084	2.358856	2.143178	1.874155	1.928339
A(7 bin)	1.893604	2.216774	2.267665	2.059708	1.809269	1.867508
A(9 bin)	1.822437	2.128438	2.159885	1.960904	1.734572	1.799392
A(11 bin)	1.739968	2.024989	2.030749	1.842422	1.646601	1.720930
A(13 bin)	1.640132	1.898863	1.871734	1.696511	1.538990	1.626374
A(15 bin)	1.551169	1.782730	1.728077	1.564747	1.441670	1.541667
64 MeV Neutron Source						
A(1 bin)	12.72771	14.08212	19.01474	14.52559	10.19565	11.35942
A(3 bin)	4.898217	5.419543	7.318006	5.590668	3.924177	4.371763
A(5 bin)	3.679500	4.073171	5.503167	4.212678	2.957784	3.287118
A(7 bin)	3.249582	3.597569	4.861077	3.722447	2.613719	2.903518
A(9 bin)	3.104731	3.437644	4.645659	3.559300	2.499347	2.774750
A(11 bin)	3.071929	3.401717	4.597710	3.524186	2.474852	2.746023
A(13 bin)	3.029528	3.355814	4.537293	3.482248	2.445839	2.709700
A(15 bin)	2.971859	3.293841	4.456540	3.428191	2.408670	2.660988

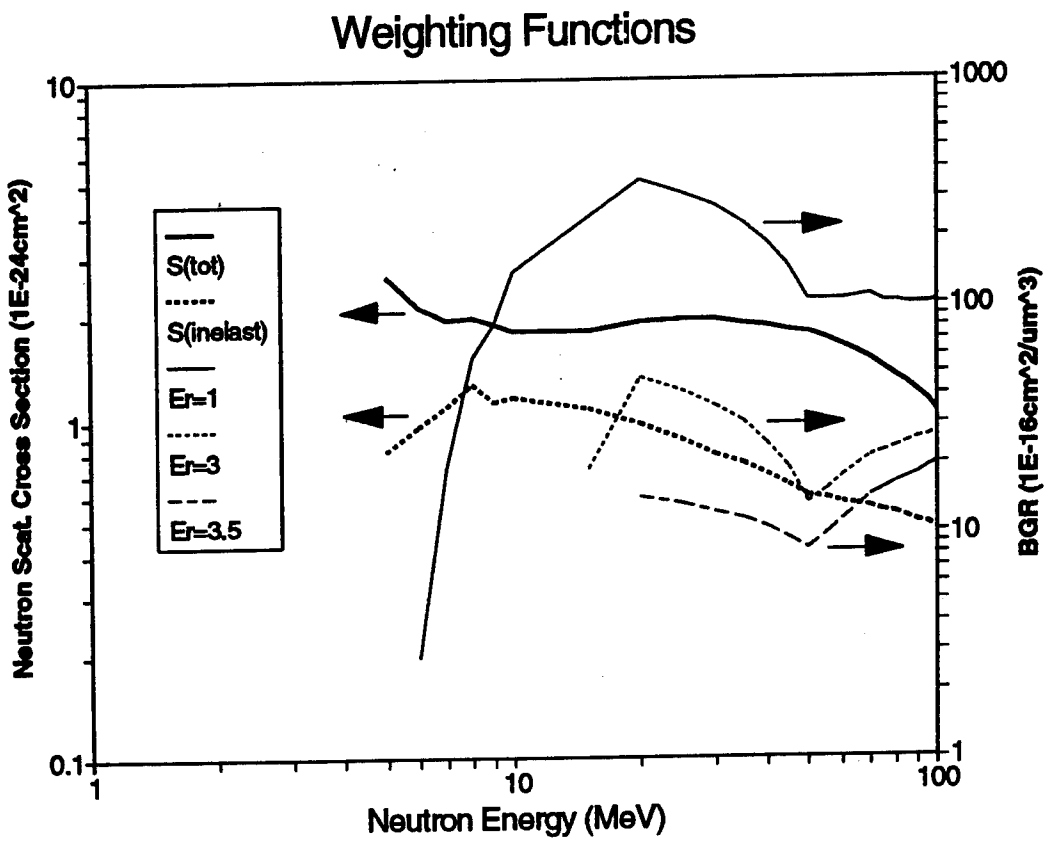

Figure 6-12. Weighting Factors for Adjustment Factor Calculations.

Section 7. Neutron Upset Model

7.1 Radiation Environment of the Atmosphere

The natural radiation environment of the earth is primarily influenced by the galactic cosmic rays. The primary cosmic rays that are continuously bombarding the earth originate outside the solar system, and consist of about 85% protons, 12% alpha particles, and 3% heavy ions, which have extremely high energies (>1000 MeV/amu). As the cosmic rays enter the atmosphere, they interact with the oxygen and nitrogen atoms within the atmosphere, creating neutrons and a host of other secondary particles (see Figure 7-1 on page 7-2).

As a result , the radiation environment at aircraft altitudes consists of a number of different components, including neutrons, protons, electrons, muons, pions, heavy ions, and others. Several studies [Refs. 25, 26, 27] have previously shown that, at aircraft altitudes, it is the neutrons that are most important in terms of inducing single event upsets. Others have shown that this is also true with respect to the radiation dose equivalent delivered to aircraft pilots and crew [Refs. 37, 35].

As a result, we will concentrate on defining only the atmospheric neutron environment. The other environment, e.g. protons, pions, etc. could also be defined. This would not only gain us very little in understanding and predicting how SEU are induced at aircraft altitudes, but it would also add confusion by defining an unnecessarily complex environment. In 7.6, "Correlation with Flight Results" on page 7-15 we will demonstrate that, by focusing on only the neutron environment, we can predict the upset rate very well by comparing calculated values with the measured upset rates tabulated in Section 3, "IBM Flight Experimental Data" on page 3-1 and Section 4, "Military Avionics Field Data" on page 4-1.

At higher altitudes, e.g. >75,000 feet, neutrons may not be the dominant radiation component in terms of inducing upsets (see Refs. 25 and 26). Even at 60,000 feet, the heavy ion component is present at high latitudes, while it cannot be measured at 30,000 feet or at lower latitudes as can be seen in Table 3-1 on page 3-7

Figure 3-4 on page 3-8 contains the LET spectrum measured at the high latitude location. Dyer [Refs. 28, 29] measured the LET spectrum at 50,000-60,000 ft altitude, by flying a pin diode array operated at >100μm depletion in an airplane. He found that, although there were some heavy ions producing counts in the two highest channels, the great majority of counts were by lower LET particles primarily attributable to the neutrons and secondary protons in the atmosphere. Thus, for aircraft altitudes, by defining the atmospheric neutron environment, we provide the practical tool necessary to calculate upset rates in microelectronics devices.

7.2 Model of the Atmospheric Neutron Environment

As indicated, the atmospheric neutron environment is primarily responsible for inducing SEU in avionics systems and so a model for these neutrons was developed. These neutrons cannot be shielded by airplane structures. Furthermore, as the neutrons are created by the cosmic rays, they interact further with the atmosphere, and the equilibrium flux of neutrons in the atmosphere is the result of several competing processes. These processes include:

1. Creation of the neutrons by cosmic ray interactions within the atmosphere;
2. Decrease of the cosmic ray intensity with decreasing altitude;
3. Neutron diffusion;
4. Neutron scattering within the atmosphere; and
5. Neutron absorption in the atmosphere.

The net result is an atmospheric flux that peaks at about 60,000 feet. Between 45,000-75,000 feet the neutron flux is approximately constant; above and below this range of altitudes the flux decreases. At sea level the neutron flux is several hundred times less than the peak flux.

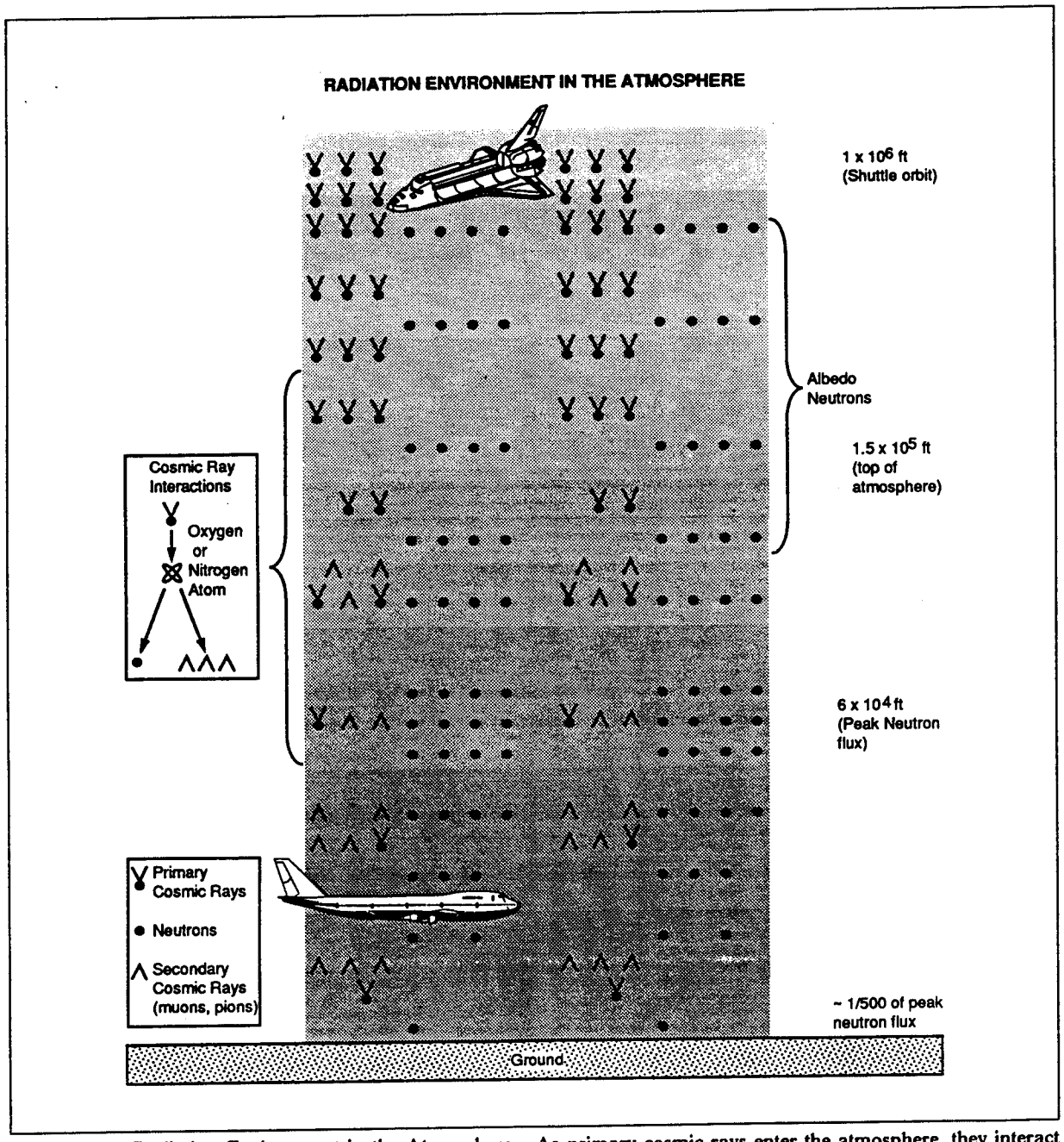

Figure 7-1. Radiation Environment in the Atmosphere. As primary cosmic rays enter the atmosphere, they interact with the oxygen and nitrogen atoms, creating neutrons and a host of other secondary particles.

The neutron flux with energies in the range of 1-10 MeV is shown in Figure 7-2 on page 7-3 as a function of altitude, based on data from References 30 and 31. Due to SEU thresholds in silicon, only neutrons with energies exceeding 1 MeV are important. Additionally, the shape of the neutron energy spectrum does not vary much as a function of altitude. Therefore, the neutron flux in the 1-10 MeV range, for which variations with latitude and altitude have been measured, is representative of the variation in flux over the entire neutron energy spectrum.

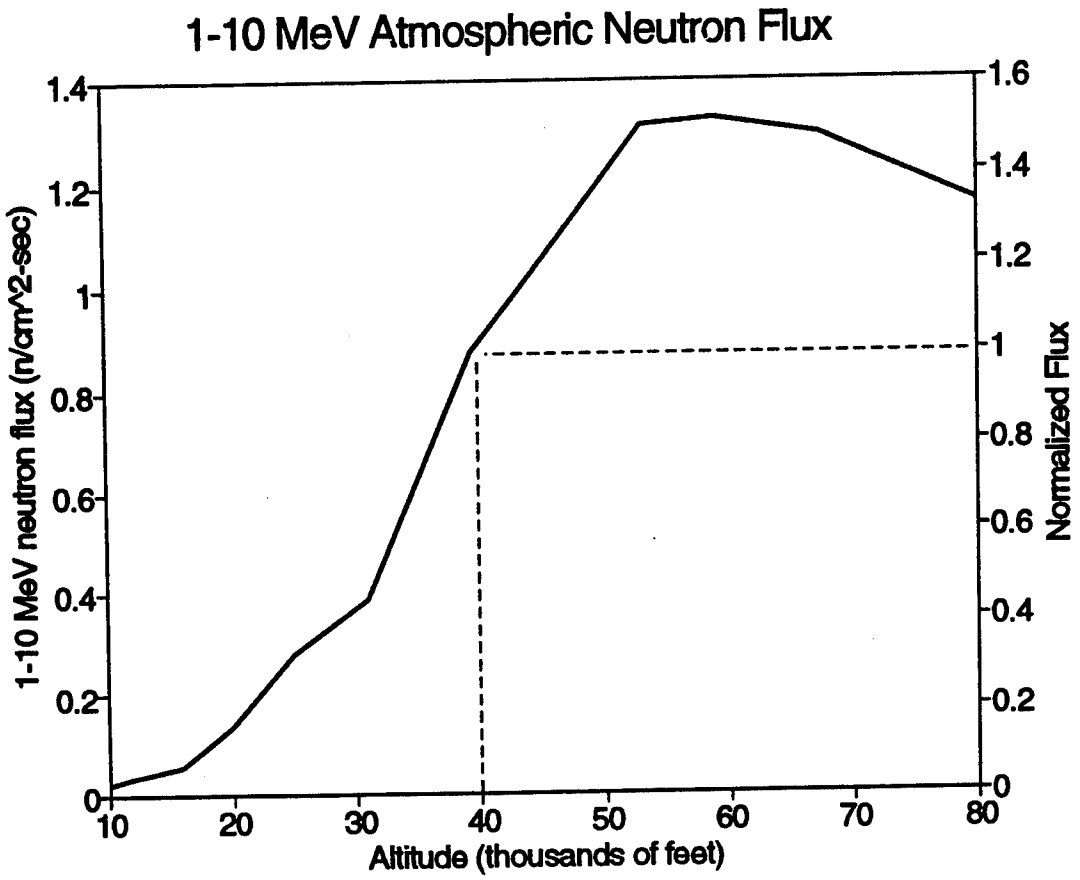

Figure 7-2. Neutron Flux vs Altitude. This graph shows the absolute and normalized 1-10 MeV neutron flux as a function of altitude. It is based on measurements by R.B. Mendell et al, J. Geophys. Res., 68, 1963 and S.S. Holt et al, J. Geophys. Res., 71, 1966. The flux peaks at about 60,000 feet.

The cosmic rays that create the atmospheric neutrons are deflected by the earth's magnetic field. The magnetic field acts as a momentum filter, preventing particles with less than a given momentum from penetrating to certain altitude-latitude combinations. Because the earth's magnetic field is approximately a dipole, the shielding is maximum at the magnetic equator and minimum at the magnetic poles. This results in an atmospheric neutron flux which is approximately six times more intense at the poles than at the equator. At latitudes of greater than 60 degrees the flux is approximately constant. The neutron flux as a function of geographic latitude is shown in Figure 7-3 on page 7-4, and is based on neutron measurements as a function of geomagnetic cutoff from Reference 32, and geomagnetic cutoff values as a function of geographic latitude from Reference 33 which we have averaged over longitude.

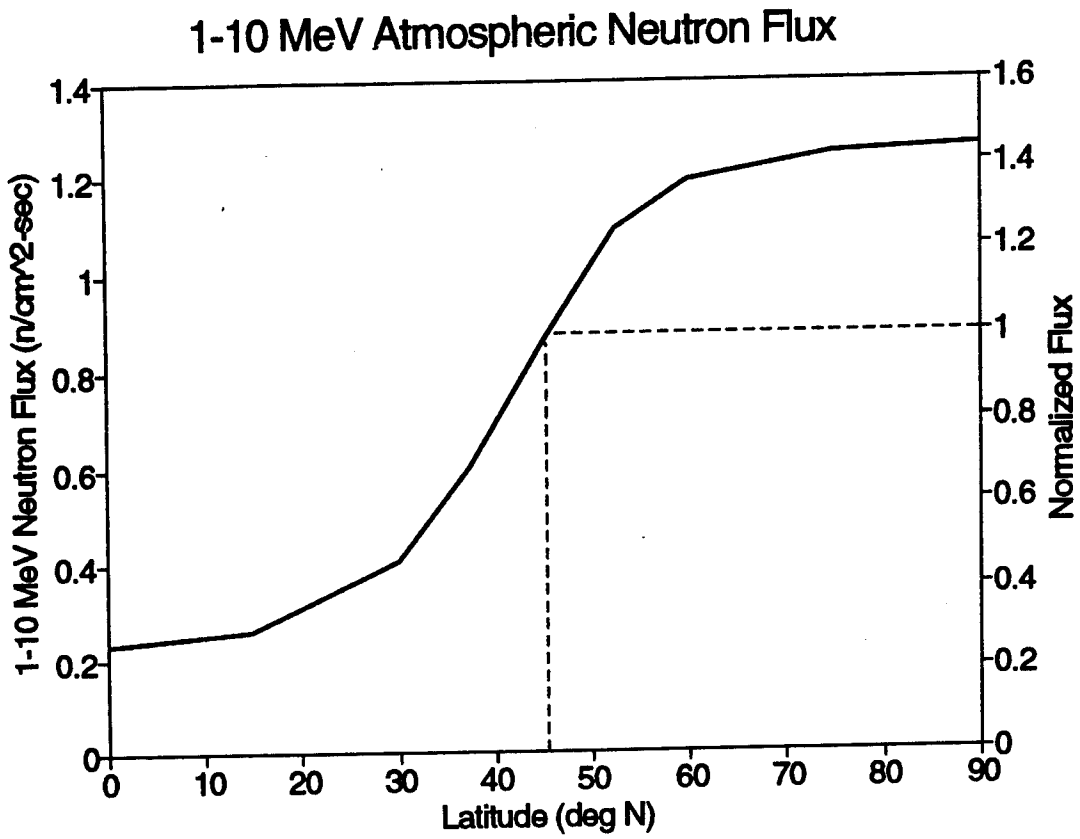

Figure 7-3. Neutron Flux vs Latitude. This graph shows the absolute and normalized 1-10 MeV neutron flux as a function of latitude. It is based on measurements by M. Merker et al, J. Geophys. Res., 78, 1973 and geomagnetic cutoff values from NRL 5901, 1986 (J. Adams). A small scale factor was used to adjust the 1-10 MeV flux to a value of 0.85 n/cm²-sec at 45° and 40,000-ft altitude.

The variation of the neutron flux as a function of the neutron energy is important in characterizing the atmospheric neutrons. This is called the differential neutron flux and several different laboratories have made this measurement obtaining similar, although not identical, results. In Figure 7-4 on page 7-5 the differential neutron flux from Reference 34, which is somewhat more conservative at lower energies compared to other measurements, is plotted as a function of energy. The differential neutron flux in Figure 7-4 on page 7-5 is used in this report for purposes of calculating the induced SEU rate in the various microelectronic devices by the atmospheric neutrons. This curve is designated as the normalized neutron flux at a latitude of 40-50° and an altitude range of 35,000 to 45,000 feet.

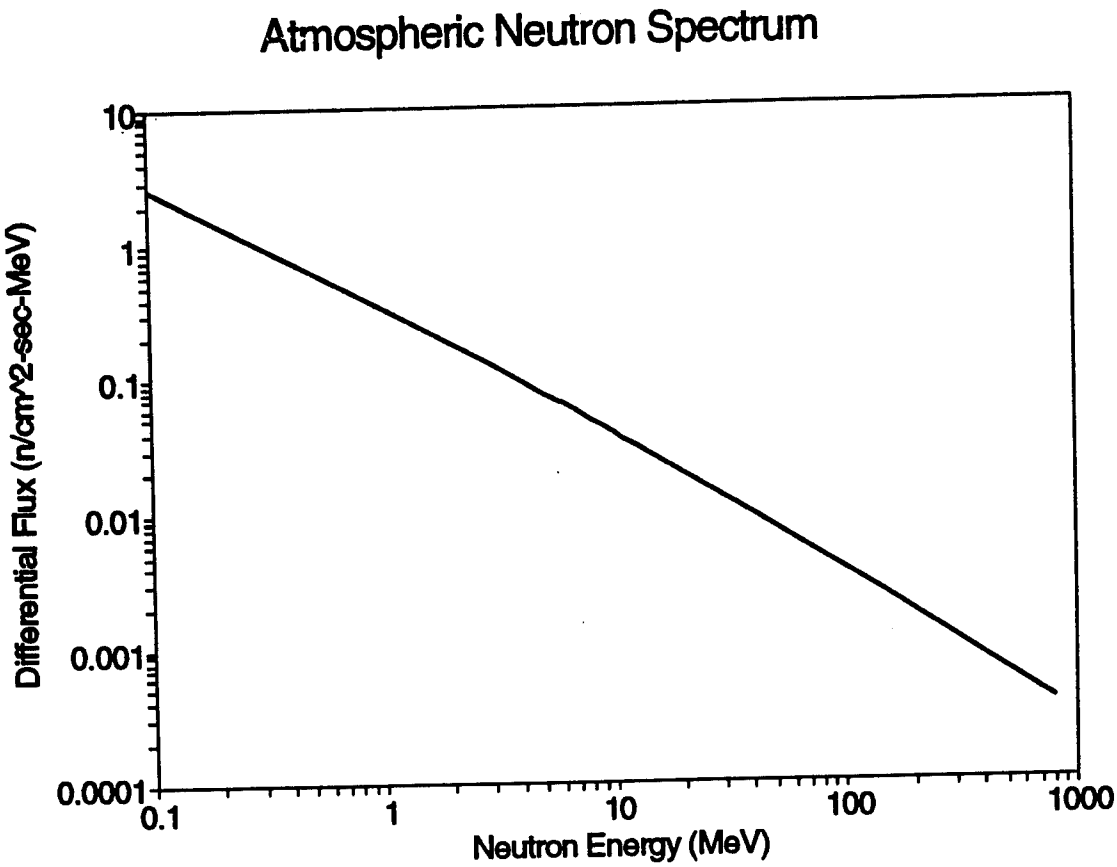

Figure 7-4. Differential Neutron Flux vs Energy. This graph shows the normalized differential neutron flux in the atmosphere as a function of neutron energy. It is based on measurements by NASA-Ames at 40,000 ft and 45° to 50° north (geomagnetic) latitudes and normalized 1-10 MeV neutron flux of 0.85 n/cm^2-sec (J. Hewitt et al, Health Physics, 34, 375, 1978). For the worst-case flare-enhanced differential neutron flux spectrum in the atmosphere, see T.W. Armstrong et al, Nucl. Sci. Eng., 37, 337, 1969.

A new mathematical model of the atmospheric neutron environment was very recently developed by John Wilson and John Nealy of the NASA-Langley Research Center [Ref. 35]. It, too, is based on neutron measurements in the 1-10 MeV range, and uses data taken on both airplanes and balloons. By comparing these two sets of data, they find that the presence of a large commercial airplane decreases the flux by about 10% (i.e. the energetic neutron flux is attenuated 10% due to interactions with airplane structural materials). This new model is more comprehensive than our model which is represented in Figures 7-2, 7-3, and 7-4 and Eq[7-1], although we believe our model to be both easier to use and sufficiently accurate to support any analysis of the flight upsets in microelectronics.

Advantages of the Wilson-Nealy model are a) the explicit incorporation of the geomagnetic rigidity cutoff compared to the averaging of the cutoff over longitude in our model (our model enables the use of the geographic latitude as a parameter, which is more readily available than a map of geomagnetic cutoffs), and b) the incorporation of a factor to account for cosmic ray modulation (i.e. how the atmospheric neutron flux varies with daily changes in the cosmic ray intensity). Cosmic ray modulation is accounted for through the response of one of several well known neutron detectors generally located at high latitude sites, e.g. the Deep River Monitor at Deep River, Ontario, Canada. Wilson's model indicates that the effect of cosmic ray modulation on atmospheric neutrons is very small. From July-December 1991 the Deep River Monitor showed a variation of about 25% (high of 6410, low of 4995, see Ref. 36), yet the Wilson-Nealy model for 1-10

MeV neutrons at 35,000 feet showed a change of less than 2% in the flux. Two other very recent atmospheric neutron models models (see Refs. 37, 38) dealing more with the dose equivalent to passengers and crew than the neutron flux, were also published, along with the Wilson-Nealy model at a session organized by one of the authors (EN).

With respect to inducing SEU in avionics, the altitude variation of the atmospheric neutron flux, shown in Figure 7-2 on page 7-3, is the most important effect. It shows that low flying aircraft, e.g. helicopters and smaller airplanes, are exposed to a neutron environment that is as low as 1-10% of that experienced by the larger and high flying types of military aircraft. However, Figure 7-2, as well as the Wilson-Nealy model, are based only on neutrons in the 1-10 MeV range. To support our contention that this altitude variation is representative of the entire energy spectrum of the atmospheric neutrons, we have examined some recent and some ≃20-year-old neutron measurements to obtain the altitude variation of neutrons in the 10-100 MeV range.

A. Preszler measured the angular distribution and altitude dependence of atmospheric neutrons from 10-100 MeV through balloon-borne instrumentation launched at Palestine, Texas [Ref. 39]. The lowest altitude measurement was made at about 35,000 feet (246 gm/cm^2). F. Ait-Ouamer analyzed atmospheric neutron data recorded on 1981 balloon flights launched at Alice Springs in central Australia (24° S. latitude, in Ref. 40). He used this data to determine the angular distribution of the atmospheric neutrons in the 10-100 MeV range. The lowest altitude measurement was made at approximately 25,000 feet (400 gm/cm^2). R. Saxena, for her Ph.D. thesis [Ref. 41], built a very sensitive neutron spectrometry system similar to that of Preszler that was housed in a trailer. The trailer was set up at three high altitude locations in the United States [Leadville, CO (10,000 ft), Boulder, CO (5,476 ft.) and Mt. Washington, NH (6,070 ft)] where the angular distribution of neutrons up to 170 MeV were measured (see Ref. 41).

For purposes of calculating neutron-induced upset rates, we are interested in only the total neutron flux, i.e. that integrated over all 4π steradians. We therefore integrated the neutron angular fluxes obtained by Preszler and Ait-Ouamer to obtain the total neutron flux at their various balloon altitudes. Saxena made only ground level measurements, so she had a 2π geometry to integrate over (essentially no neutrons directed up off the ground) in order to obtain the total neutron flux. Her total neutron flux values at the three high altitude locations were normalized using Figure 7-3 on page 7-4 to the latitude of Preszler's balloon measurements, and then combined with Preszler's data.

The resulting atmospheric neutron flux curves as a function of altitude are shown in Figure 7-5 on page 7-7. The first curve, that for neutrons with energies of 1-10 MeV, is identical to Figure 7-2 on page 7-3, except that the normalization is based on the peak flux being set to 1.0. In Figure 7-5 on page 7-7 are also shown the two 10-100 MeV atmospheric neutron flux curves, one based on the combined Preszler-Saxena values and the second on the Ait-Ouamer values. The shape of the flux as a function of altitude curves for the two energy groups, 1-10 MeV and 10-100 MeV of the atmospheric neutrons are in very good agreement. This verifies the assertion that the 1-10 MeV neutron group is representative of the entire neutron energy spectrum. We further found that the Preszler and Ait-Ouamer angular neutron fluxes had too much uncertainty in them to allow for a finer energy breakdown.

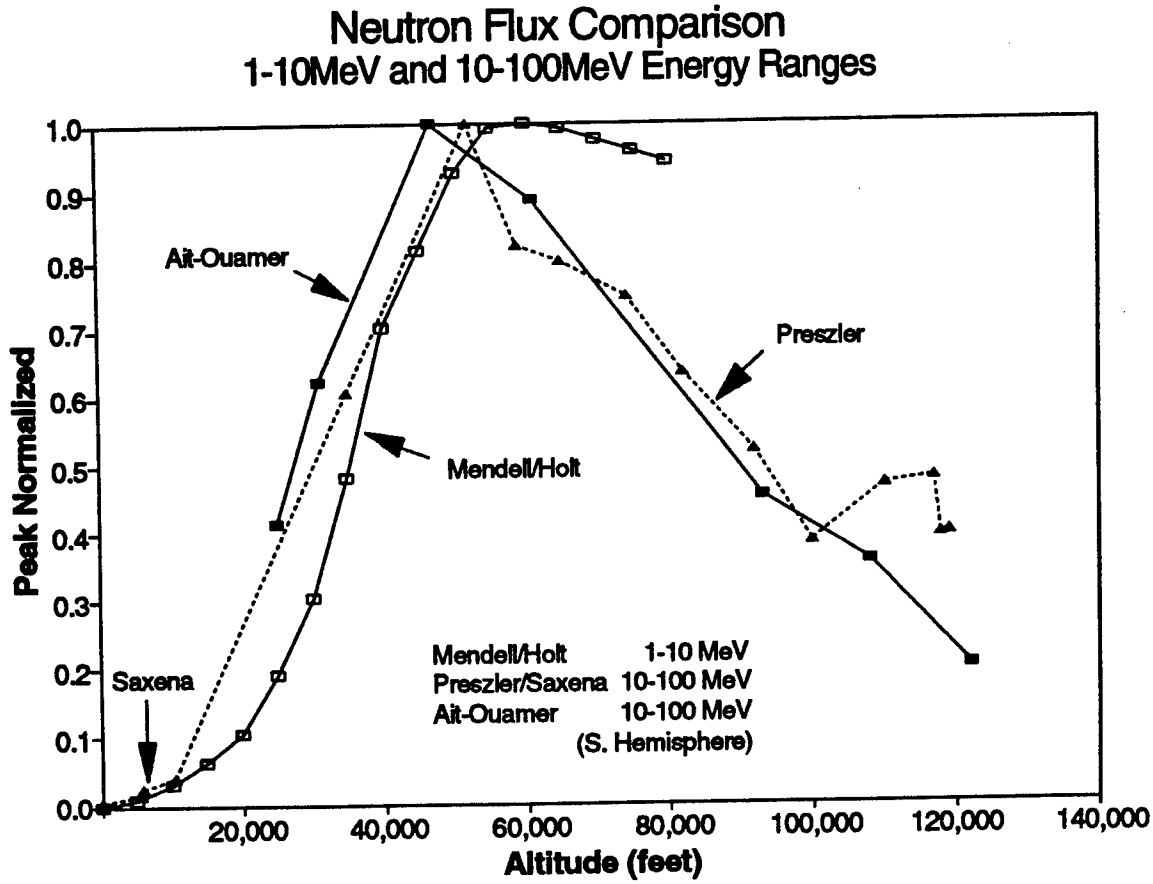

Figure 7-5. Neutron Flux vs Altitude (1-10 and 10-100 MeV Comparison).

Even though some measured atmospheric spectra (e.g. see Reference 39) are flatter in the 10-100 MeV region, the spectrum in Figure 7-4 on page 7-5 is higher at lower energies and so overall serves as a good representation of the differential neutron flux in the atmosphere. The fit we use for this spectrum is:

$$dN/dE = 0.3459E^{-0.9219}\exp[-0.01522(lnE)^2]\ \text{n/cm}^2\text{-sec-MeV} \qquad [7-1]$$

This differential neutron flux is normalized to yield a flux in the 1-10 MeV energy range of 0.85 n/cm^2-sec, which applies at 40,000 feet altitude and 45° latitude. This spectrum also yields similar neutron fluxes at 0.87 n/cm^2-sec over the 10-100 MeV range and 0.75 n/cm^2-sec over the 100 to 1000 MeV range.

1000 MeV appears to be a practical upper limit of the atmospheric neutron energy for purposes of calculating upset rates. The only reliable measurement of the atmospheric neutron spectrum at very high energies (>1000 MeV) is by W. Hess et al [Ref. 42]. For E>1000MeV, this spectrum exhibits a fall-off in energy that can be approximated as $E^{-2.2}$, which is much more rapid than our spectrum (E<1000MeV) which falls off approximately as $E^{-.92}$. Thus, for energies >1000MeV, the neutron flux will decrease much more rapidly than for E<1000MeV, so the contribution to the upset rate from these very high energy neutrons will be minimal and can be ignored.

Solar flares can produce additional radiation and hence cause an increase in neutron flux beyond that of the worst case daily environment. The worst case solar flare was encountered on 23 February 1956. It was conservatively estimated that the peak flux was approximately 1,000 times the normalized neutron flux (see

Reference 43). More recently, during the very intense flare of September 29 - October 7, 1989, measurements from on board Concorde flights at the time of the flare imply a 5-fold increase in the atmospheric neutron flux (see Reference 28). Nevertheless, for the worst case solar flare environment, the multiplier is estimated to be 1,500 times the normalized neutron flux, accounting for the airplane operation at high altitude, high latitude, and the worst case solar flare.

7.3 Upset Rate by Neutron Cross Section Model

The neutron cross section methodology provides a direct correlation between the neutron environment and the device upset rate. In general, a NSEU cross section is defined as the probability that a neutron with energy E_n will interact with a semiconductor device and produce an upset (in units of cm^2/device, or bit). This function is generated for a specific device-type from data collected in neutron and proton testing. The product of the NSEU cross section function and the differential neutron flux spectrum is the differential upset rate which is integrated over the range of neutron energies to obtain the device upset rate (in units of upsets/sec-device, or bit). This is represented mathematically as

$$\text{Upset Rate} = \int_{E_n} dN/dE\sigma_{nseu}(E_n)dE \qquad [7-2]$$

where

dN/dE = atmospheric differential neutron spectrum; and
σ_{nseu} = NSEU cross section.

In 6.3, "Neutron Upset Cross Sections" on page 6-11 we showed how the two-parameter Bendel model provides a good fit to the neutron upset cross sections for the 64k SRAM as shown in Figure 6-10 on page 6-14 and Figure 6-11 on page 6-15. One cross section curve was generated for the condition of the 64k SRAM operated at 5 volts and another for when it was operated at 2.5 volts. The actual cross sections are tabulated in Table 6-1 on page 6-12 and the fit is given by Eqs[6-2,3] in 6.3, "Neutron Upset Cross Sections" on page 6-11. 6.3, "Neutron Upset Cross Sections" on page 6-11 also contains the parameters A and (B/A) for the 2.5 volts and 5 volts operating conditions. Eq[7-1] in 7.2, "Model of the Atmospheric Neutron Environment" on page 7-1 gives the analytical expression for the atmospheric differential neutron flux, dN/dE, shown in Figure 7-4 on page 7-5. This expression applies at an altitude of 40,000 feet and a latitude of 45°. For other altitudes and latitudes, Figure 7-2 on page 7-3 and Figure 7-3 on page 7-4 provide the appropriate correction factors. Thus, having the NSEU cross section makes implementation of the neutron cross section model via Eq[7-2] rather straight forward.

The main difficulty is that only a handful of microelectronic parts have undergone SEU testing with neutrons. References 23, 45, 44, and 46 contain most of the known published data on neutron induced upsets. Many more upset measurements have been made with protons, but even so the number of devices tested for which published data is available is on the order of 80-100 (Ref. 47), but many of these are older, early 1980 devices. Furthermore, as indicated in 6.3, "Neutron Upset Cross Sections" on page 6-11, we assume that proton and neutron upset cross sections are the same only for energies >200 MeV. We have shown (Ref. 48) that for parts tested at UCD with 64 MeV neutrons and 62 MeV protons, the proton cross section may be up to a factor of two larger. Nevertheless, contradicting this is the data shown in 6.3, "Neutron Upset Cross Sections" on page 6-11 from previous SEU testing of the 64k SRAM with protons that gave upset cross sections considerably lower than our neutron results.

We conclude that proton upset cross sections at low energies might be used as neutron cross sections, but there is considerable uncertainty in making this assumptions, possibly as high as a factor of 5-10 based on the results for the 64k SRAM. Proton cross sections at high energies (>200 MeV) are rare, but if such data is found, it can be used as the neutron cross sections with much greater certainty.

7.4 Upset Rate by the Burst Generation Method

The Burst Generation Rate (BGR) methodology utilizes:

1. device SEU characteristics determined in heavy ion testing; and
2. tabulated calculated values of energy deposition in silicon by neutron interactions (the BGRs)

to predict the upset rate for a given device-type due to interactions with the atmospheric neutron environment. As stated in 2.1.1, "Soft Error Mechanisms" on page 2-1, the mechanism for NSEU is the burst of charge produced by the reaction products of a neutron-silicon interaction. When this burst of charge is generated within the sensitive volume of a device and is greater than the critical charge, Q_c, then an upset can occur. This alternative method is more indirect than the neutron cross section method discussed in 7.3, "Upset Rate by Neutron Cross Section Model" on page 7-8. However, it has one great merit in that it utilizes heavy ion SEU test data, and many hundreds of microelectronic devices have undergone such SEU testing.

The BGR methodology is formulated in terms of two key parameters: a) the sensitive volume, V, which is a device-specific value representing the size of the sensitive region within which the burst of charge generated by the neutron-induced recoil will produce an upset, and b) the recoil energy, E_r, that is equivalent to Q_c for the device [E_r(MeV) = Q_c(pC)×22.5MeV/pC in silicon], and in terms of two functions: a) the BGR(E_n,E_r), and b) the differential flux of atmospheric neutrons, Eq[7-1]. In mathematical terms the BGR methodology gives the upset rate as (see Reference 49):

$$\text{Upset Rate} = VC\int_{E_n} BGR(E_n,E_r)dN/dE\ dE, \qquad [7-3]$$

where

V = sensitive volume;
dN/dE = differential neutron flux spectrum;
E_n = neutron energy; and
E_r = recoil energy.

An additional constant factor, C, is used to account for collection efficiency, the contribution from light ions, and other effects. In practice, this integration is performed numerically.

Neutron BGR is defined as the probability that a neutron with a given energy, E_n, will interact with a silicon atom and produce a recoil with energy E_r or greater (see Reference 49). These BGRs are generated from neutron cross section data by performing the reaction kinematics to determine the energy distributions of the recoils for each type of neutron-silicon reaction. For neutrons with energies less than approximately 20 MeV, these are straight forward calculations that involve only two reaction products - a recoil and a secondary - and there are nine reactions to consider (see Reference 50). For neutrons with energies greater than 20 MeV, the calculations are complicated by the addition of more reaction products and many more reactions, so a probabilistic approach is used. A complete description of the BGR methodology and the BGR data set is given in References 49 and 50.

The BGR methodology is performed in five steps. First, the two key device SEU characteristics, the asymptotic cross section and LET threshold, are obtained from the heavy ion upset cross section curve. Second, the device sensitive thickness is determined (in units of μm) and is multiplied by the asymptotic cross section (in units of cm^2/bit or device) to obtain the device sensitive volume (in units of cm^2-μm). Third, the assumed sensitive thickness is multiplied with the LET threshold and the density of silicon to obtain the recoil energy, E_r, necessary to produce an upset (MeV-cm^2/mg×μm×0.233mg/cm^2-μm in silicon). This recoil energy can be further converted to the critical charge necessary to produce upset (E_r/22.5MeV/pC). Fourth, the BGR function, BGR(E_n,E_r), is obtained for the calculated recoil energy by

extracting values from tabulated BGR data. Fifth, the integration of Equation 7-3 is performed using the differential neutron spectrum, sensitive volume, and BGR values.

As the flux is given in units of neutrons/cm^2-sec, the upset rate has units of upset/sec-device (or bit), but this is typically converted to upsets per hour or day. The sensitive thickness can be considered to consist of three components: the depletion region, the funnel region, and the diffusion region. The sensitive thickness and collection efficiency were determined on a trial and error basis by comparing calculated results against the measured upsets tabulated in Table 6-1 on page 6-12 for the various neutron tests. Thus, for a given test result, several thickness's were assumed, the BGR methodology steps listed above were carried out for the appropriate neutron environment, and the calculated upset rate prediction was compared with the measured upset rate to select the appropriate thickness and collection efficiency. This process is described in 7.5, "BGR Upset Rate Model for 64K SRAM" on page 7-12.

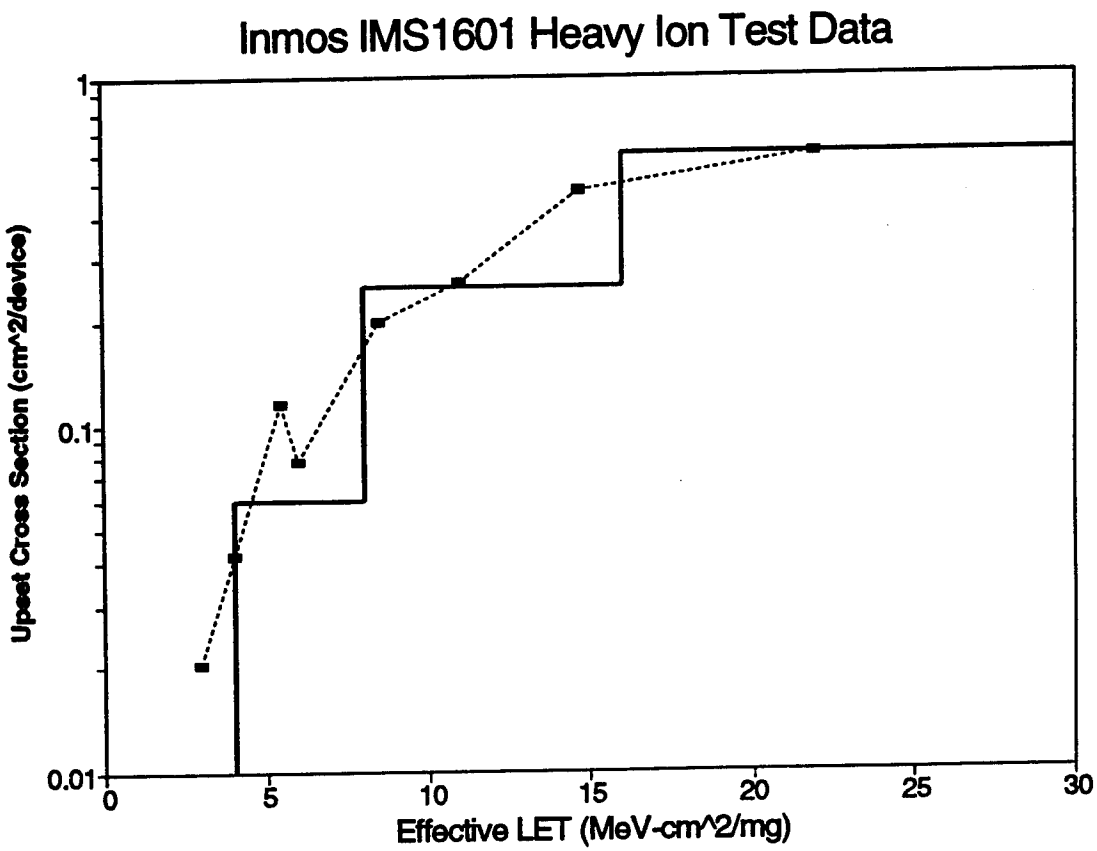

Figure 7-6. Heavy Ion Cross Section for 64k SRAM.

In actual practice we found that, in examining heavy ion cross section curves as a function of LET, we could not easily identify a single LET threshold for the entire curve that would not be overly conservative. Instead, we found it preferable to make simplified fits to the cross section curve that are equivalent to two or three effective thresholds, each of which has a corresponding cross section. This is illustrated in Figure 7-6, that shows the actual cross section curve with a three-part simplified fit for the 64k SRAM: the lowest LET threshold is 4 MeV-cm^2/mg with a 0.06 cm^2 cross section, the middle LET threshold is 8 MeV-cm^2/mg with a 0.25 cm^2 cross section, and the highest effective LET threshold is 16 MeV-cm^2/mg with a 0.6 cm^2 cross

section. The use of the stair-step fit to the actual heavy ion cross section curve is an important refinement over the description of a single effective LET threshold described in Reference 49.

To assist in evaluating Eq[7-4] in general terms, we have carried out the integration of the BGR function with the differential neutron flux in the atmosphere over the neutron energy range of $1<E_n<1000$MeV for various values of recoil energy, E_r. The BGR values used are similar to those in References 49, 50, and 51. The resulting curve of the integral of BGR with dN/dE is shown in Figure 7-7 as a function of E_r and is similar to one presented in Reference 49 except that the latter is expressed as a function of critical charge, Q_c, in units of pC rather than E_r (E_r(MeV) = 22.5×Q_c in silicon).

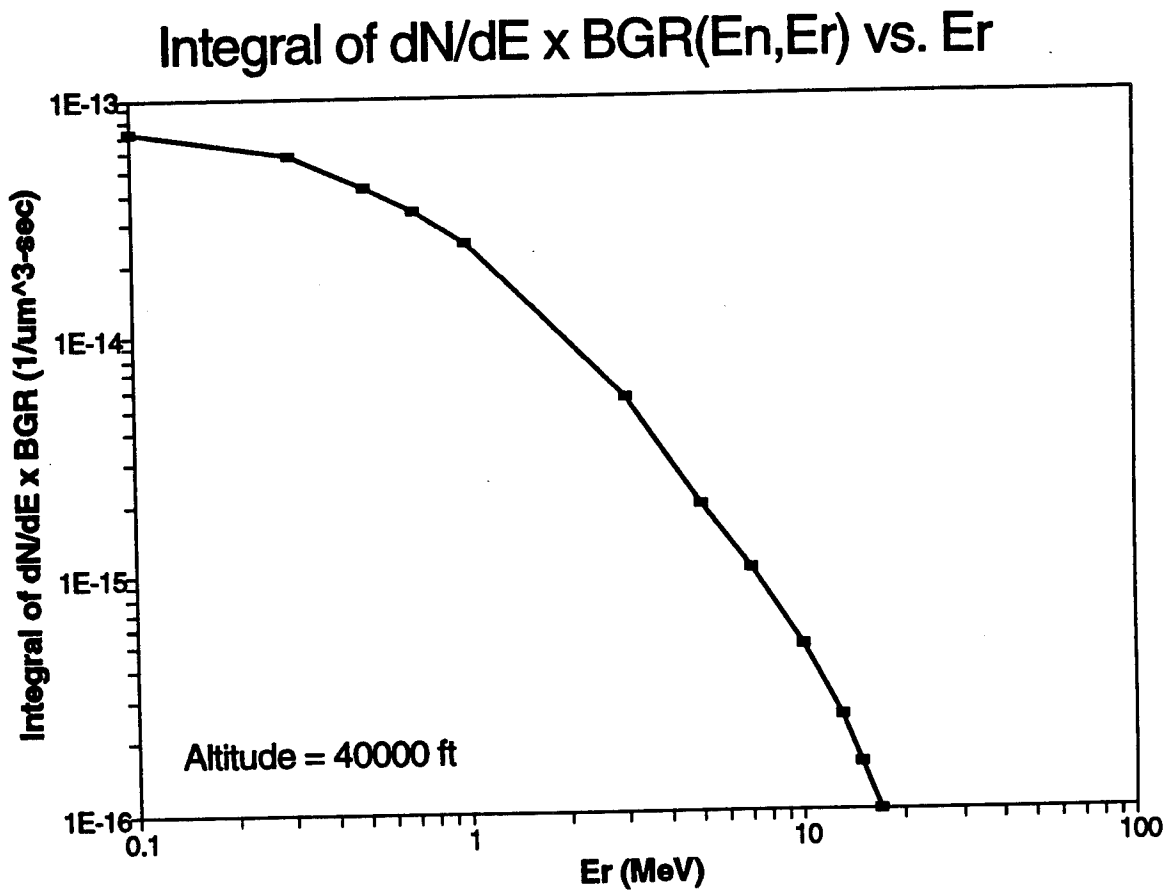

Figure 7-7. Integral of dN/dE × BGR(En,Er) vs. Er.

As indicated above, one of the merits of the BGR method is that heavy ion SEU data is available for hundreds of microelectronic devices from previous testing. To utilize the BGR method in order to calculate upset rates through Eg[7-3], we need to know two key parameters, *t*, the sensitive thickness which is needed to calculate E_r and V, and *C*, the collection efficiency. Neither *t* nor *C* are generally known for the hundreds of devices that have undergone SEU testing.

In this study our purpose is to calculate the upset rate at aircraft altitudes accurately in order to compare to measured values. For many applications that is not necessary; a conservative estimate of the upset rate will suffice. We know from experience that the smaller the sensitive thickness, the larger the upset rate, because it forces E_r to be low and therefore the BGR to be high (see 7.5, "BGR Upset Rate Model for 64K SRAM"

on page 7-12). Therefore, for parts with no neutron upset data to verify against, we recommend using $t = 1\mu m$ and $C = 1$ to obtain a conservative upset rate.

Following Reference 52, t can be considered as comprised of three parts: the depletion region, a funnel region, and a diffusion region. Based on values typical for current microchips, t is expected to be $2\mu m$ or larger. Thus, using a value of $1\mu m$ for t yields a conservatively large BGR and hence a conservative upset rate.

7.5 BGR Upset Rate Model for 64K SRAM

As indicated in 7.4, "Upset Rate by the Burst Generation Method" on page 7-9, we intend to develop the BGR upset rate model for the 64K SRAM based on Eq[7-3] and the three-part fit to the SEU cross section as a function of LET shown in Figure 7-6 on page 7-10.

There are now three effective sensitive areas. When multiplied by the sensitive thickness these become three effective sensitive subvolumes, each with a separate LET threshold. Eq[7-3] has to be modified to reflect the contributions from each of the i subvolumes:

$$\text{Upset Rate} = C \sum_i \left[\Delta V_i \int BGR(E_n, E_{ri}) dN/dE \, dE \right] \qquad [7-4]$$

Each sensitive subvolume ΔV_i has a corresponding LET threshold. Once the sensitive thickness t is assumed, not only are the sensitive subvolumes defined, but so too are the corresponding burst energies, E_{ri}. With the ΔV_i and E_{ri} specified, the upset rate can be calculated. Calculated upset rates will be compared with those actually measured in the neutron tests. The collection efficiency C will then be defined as the ratio of the measured to calculated upset rates.

This is a different approach than is used in Ref. 49, where C would ordinarily be taken to be 1 in order to obtain a conservative estimate of the upset rate. In our case, we know the upset rate, or in this case, the number of upsets, so our objective is to obtain an accurate estimate rather than a conservative one.

The starting point for the procedure is the sensitive thickness, t. Following Reference 52, t can be considered as comprised of three parts: the depletion region, a funnel region, and a diffusion region. Based on values typical for current silicon microchips, t is expected to be $2\mu m$ or larger. Using a value of $1\mu m$ for t would yield a conservatively large BGR and hence a very conservative upset rate. In the case of the 64K SRAM, $1\mu m$ and $2\mu m$ are still considerably too small, so we chose three larger values to obtain closer agreement, 3.5, 3.8, and $4.0\mu m$.

For illustrative purposes we apply the method in detail to the test corresponding to the first entry in Table 6-1 on page 6-12. This was with the SRAM at 5 volts being exposed to the 14 MeV neutron generator. The neutron fluence was 4.14E9 n/cm^2 and 836 upsets were recorded in all 28 chips. Choosing $t = 3.5\mu m$, we obtain $E_{r1} = 3.2$MeV, $E_{r2} = 6.4$MeV, and $E_{r3} = 12.8$MeV. The maximum recoil energy that a 14-15 MeV neutron can produce in silicon is about 3.8 MeV, so only recoils of $E_{r1} = 3.2$MeV are possible. The corresponding volume ΔV_i is $2.17E7\mu m^2$ and the BGR for $E_n = 14.7$MeV is $BGR(14.7,3.2) = 13.5E\text{-}16 cm^2/\mu m^3$ for the essentially mono-energetic neutrons ($E_{avg} = 14.7$MeV) produced by the neutron generator. Thus the integral in Eq[7-4] is replaced by point values for the neutron fluence and BGR, yielding 113.4 upsets per device or 3175 upsets for all 28 devices. To calculate the actual number of upsets measured, a collection efficiency of 0.263 would be needed, that is, 836/3175.

Similar calculations were carried out for $t = 3.8$ and $4.0\mu m$ and for the 42 and 64 MeV peak energy neutron tests. For the 42 and 64 MeV neutron sources, an adjustment factor has to be used to account for upsets

induced by neutrons in the low energy tail of the spectrum. Theoretically, the adjustment factor, A, will vary with each value of t, because the recoil energy is different for each t. In practice, though, this variation is small, so we have applied the adjustment factor for $t = 3.8\mu m$ to the calculations for all three values of t.

The results are tabulated in Table 7-1. Figure 7-8 on page 7-14 shows the ratio of calculated/measured upsets for each of the three tests, as well as the average for the three tests. It is clear from Figure 7-8 on page 7-14 that $t = 3.8\mu m$ gives the most consistent results when measurements from all three neutron sources are considered. This becomes especially clear when the curve for the average of all three measurements is examined, and account is taken of the standard deviation between the three sets of measurements. From Figure 7-8 on page 7-14, the ratio for $t = 3.8\mu m$ for the average of the three tests is 1.81 and therefore the collection efficiency, C, is $1/1.81 = 0.55$.

Table 7-1. Variation of Calculated/Measured Upsets with Sensitive Thickness.

t (μm)	Calculated Upsets	Ratio, Calc/Meas Upsets	1/Ratio
14.7 MeV BPSRC Source (836 upsets/device measured)			
3.5	3175	3.80	0.263
3.8	1456	1.74	0.574
4.0	190	0.227	4.4
64 MeV UCD Source (13.6 upsets/device measured)			
3.5	20.3	1.49	0.670
3.8	17	1.25	0.8
4.0	14.7	1.08	0.925
42 MeV UCD Source (7.2 upsets/device measured)			
3.5	23	3.19	0.313
3.8	17.5	2.43	0.411
4.0	14	1.94	0.514
t (μm)	**Average Ratio**	**Avg.+Std. Dev. Ratio**	**Avg.−Std. Dev. Ratio**
3.5	2.83	3.80	1.85
3.8	1.81	2.29	1.32
4.0	1.08	1.79	0.383

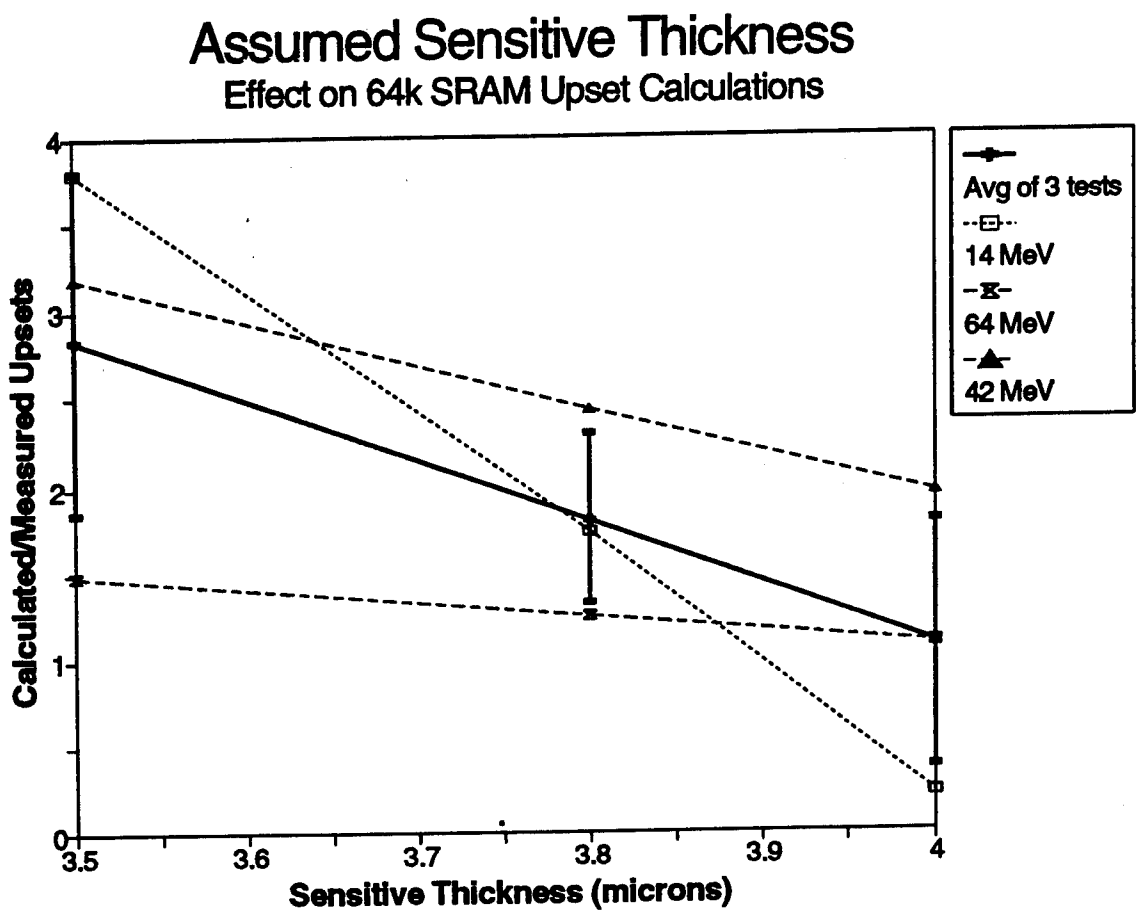

Figure 7-8. Variation of Calculated/Measured Upsets with Sensitive Thickness.

Selection of 3.8μm as the sensitive thickness can be corroborated in another way. Figure 7-6 on page 7-10 presents the heavy ion testing performed by IBM. The lowest LET at which upsets occurred is 3 MeVcm^2/mg. However, from this data the LET threshold cannot be determined; all we can observe is that the LET threshold is $\leq$3. Fortunately, separate heavy ion testing was performed on this same 64K SRAM and, as reported in Reference 8, the LET threshold is given as 2 MeVcm^2/mg. Using the absolute LET threshold of 2 MeVcm^2/mg and the 3.8μm sensitive thickness, we obtain a threshold energy deposition of 1.75 MeV, which is equivalent to a critical charge of 78 fC. Taber has reported several estimates of the critical charge in Reference 6. Based on estimates of the cell capacitance and signal margin, for operation at 5 volts, the critical charge was determined to be between 73-130 fC, in good agreement with our estimate of 78 fC based on neutron induced SEU and the BGR method.

Having determined the collection efficiency, the BGR upset rate model for the 64K SRAM is:

$$\text{Upset Rate} = 0.55\left[\begin{array}{l} 2.28E7\int BGR(3.5,E_n)(dN/dE)dE \\ +\,7.22E7\int BGR(7,E_n)(dN/dE)dE \\ +\,1.33E8\int BGR(14,E_n)(dN/dE)dE \end{array}\right] \qquad [7-5]$$

7.6 Correlation with Flight Results

The two different models to calculate the upset rate induced by atmospheric neutrons in the 64K SRAM were described in 7.3, "Upset Rate by Neutron Cross Section Model" on page 7-8 and 7.4, "Upset Rate by the Burst Generation Method" on page 7-9. In Section 3, "IBM Flight Experimental Data" on page 3-1 and Section 4, "Military Avionics Field Data" on page 4-1, we presented the actual flight data recorded. We now would like to compare the calculated upset rates against the rates actually measured in flight. This comparison is made in Table 7-2 on page 7-16.

Eq[7-2] provides the model for the neutron cross section. All calculations were carried out for the differential neutron flux at 40,000 feet and 45°N latitude, i.e. given by Eq[7-1]. When the integration required by Eq[7-2] is carried out, we obtain an upset rate of 3.28E-9 upsets/bit-hour, which applies at 45°N latitude and 40,000 feet. From Figure 7-2 on page 7-3, we obtain a normalization factor of 0.4 for the atmospheric neutron flux at 29,000 feet compared to that at 40,000 feet. Thus, for European Area 2, the calculated upset rate is 1.3E-9 upsets/bit-hour.

For European Area 1, which we have taken to be at an average latitude of 55°N, the additional normalization factor for latitude is obtained from Figure 7-3 on page 7-4 (value of 1.37). Thus, for European Area 1, the upset rate is 1.8E-9 upsets/bit-hour.

For the BGR method, a similar procedures was used. Eq[7-5] presents the model and Figure 7-7 on page 7-11 contains the values of the integral of BGR with dN/dE. After the integrations are performed, the upset rate obtained is 5.8E-9, which applies at 45°N latitude and 40,000 feet. We again use the same normalization factors as above, 0.4 for an altitude of 29,000 feet and 1.37 for a latitude of 55°N, to obtain the corrected values listed in Table 7-2 on page 7-16.

All the aforementioned applies to the 5 volt operating mode. When the 64K SRAM is operated at 2.5 volt standby, it is more susceptible to upset. From Table 6-1 on page 6-12, the increased susceptibility is a factor of 3.8 based on the 42 MeV peak neutron test and 3.0 for the 64 MeV peak neutron test. Thus we will use an average factor of 3.4 for the increased susceptibility for 2.4 volt standby operation compared to achieve 5 volt operation. This value of 3.4 is very close to the 3.5 scaling factor that was previously obtained [Ref. 3] as described in 3.5, "Dosimetry" on page 3-6. This enables us to calculate the upset rate for the low altitude (29,000 feet elevation) measurements described in 3.3, "Low-Altitude Measurements" on page 3-3.

Table 7-2. Comparison of Calculated to Actual Upset Rates. Calculated versus actual recorded upset rates are compared for static RAMs at aircraft altitudes.

SRAM Type	Operating Voltage (V)	Flight Latitude (degrees)	Average Latitude Assumed (degrees)	Flight Altitude (ft)	Measured Upset Rate (upsets/bit-hr)	Rate Calc. w/NCS Method (upset/bit-hr)	Rate Calc. w/BGR Method (upsets/bit-hr)
64k	5	54-60	55	29k	2.26E-9	1.80E-9	3.20E-9
64k	5	44-50	45	29k	1.57E-9	1.30E-9	2.30E-9
64k	2.5	39-48	45	29k	5.00E-9	4.40E-9	7.90E-9
64k	2.5	32-40	35	65k	1.10E-8	9.70E-9	1.75E-8
64k	2.5	59-82	70	65k	2.25E-8	2.30E-8	4.16E-8
256k	2.5	59-82	70	65k	4.60E-9	8.20E-9	1.36E-8

Notes:

1. Calculated upset rates are scaled to altitude and average latitude.
2. The 256k×1 NCS calculation is based on the 64k results, normalized by upset cross sections measured with 800 MeV protons.
3. The 256k×1 BGR calculation is based on a heavy ion cross section curve for the same vendor's 32k×8 SRAM, and assumed a sensitive thickness of 3μm and a collection efficiency identical to that for the 64k SRAM.

For the 64K SRAM measurements recorded on the ER-2 flights (at 65,000 feet), we need different normalization factors. For 65,000 feet altitude, it is 1.4, rather than 0.4 for 29,000 feet. For the latitude normalization factor from Figure 7-3 on page 7-4, it is 0.63 for 35° latitude and 1.5 for 70° latitude.

For the 256k SRAM, the only actual SEU test data we have is for a single proton test at LAMPF with 800 MeV protons [Ref. 13], the data for which is contained in Table 6-1 on page 6-12. It was obtained with the SRAM operating at 2.5 volts, just as the 64k SRAM was tested. If we use the 800 MeV proton upset cross section as a means of normalizing, we may utilize the neutron cross section model to calculate the upset rate. For the 64k SRAM, we showed above that the neutron cross section model gives 3.28E-9×1.4×1.5×3.4 = 2.3E-8 upsets/bit-hr. Applying this to the 256k SRAM, and normalizing by the 800 MeV upset cross section, we obtain 2.34E-8×1.77E-12/5.06E-12 = 8.2E-9 upsets/bit-hr, which is less than a factor of two higher than the measured value.

The BGR method may also be used to calculate the upset rate in the 256k SRAM, but in a more indirect manner. There is data available for a similar 256k SRAM from the same vendor (32k×8 organization and 1.3μm feature size compared to the 256k×1 organization and 1.1μm feature size of the SRAM that was flown). Figure 7-9 on page 7-17 shows the SEU cross section as a function of LET curve for the 32k×8 SRAM as measured by Koga et al [Ref. 53], along with our simplified fit to the curve, namely: lowest LET threshold of 2 MeVcm^2/mg with a cross section of 1E-3 cm^2, middle LET threshold of 4 MeVcm^2/mg with a cross section of 0.1 cm^2, and highest LET threshold of 12 MeVcm^2/mg with a cross section of 0.3 cm^2.

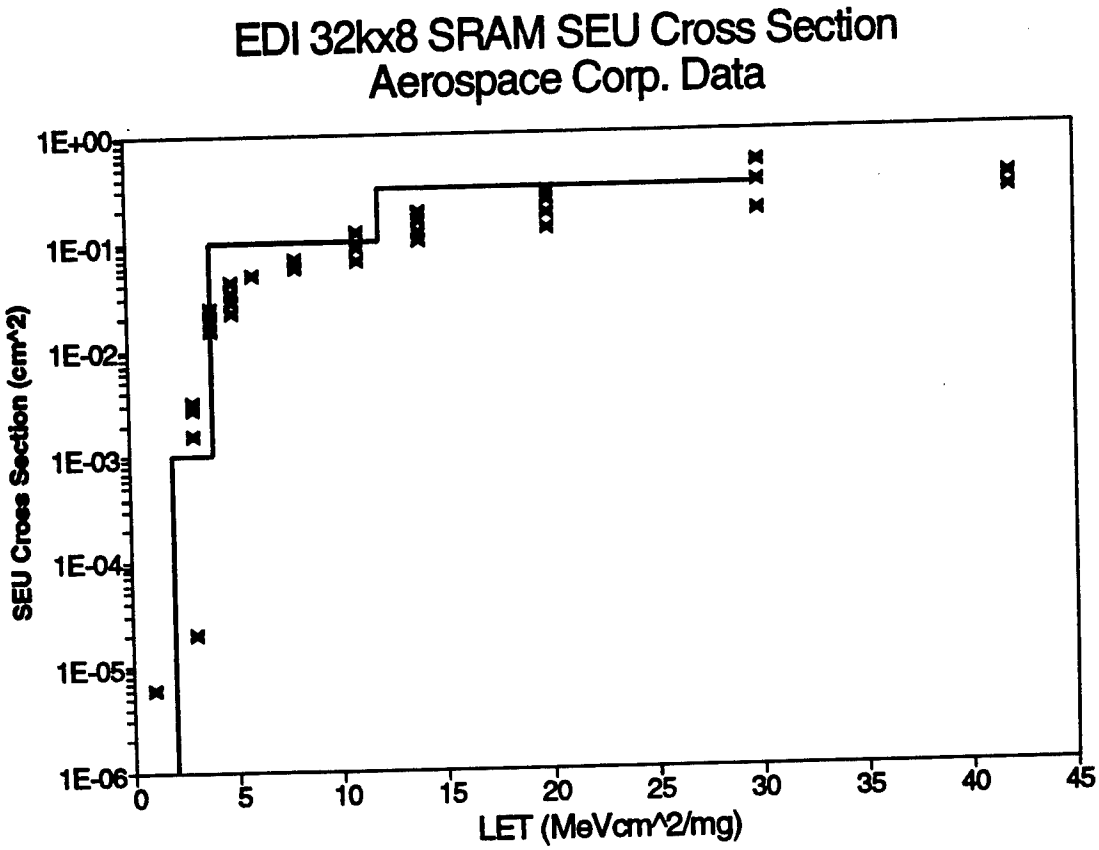

Figure 7-9. EDI 32kx8 SRAM Heavy Ion Upset Cross Section. The EDI 32k×8 SRAM is similar to the EDI 256k×1 SRAM flown over Norway in this study.

We have no actual data to allow us to calculate the sensitive thickness, so we estimate as follows. As shown in 7.5, "BGR Upset Rate Model for 64K SRAM" on page 7-12, the sensitive thickness for the 64k SRAM is 3.8μm. This is a mid-1980's part and its sensitive thickness is about 4μm. We have performed a similar analysis on a 1M SRAM [Ref. 54], a 1990's era part, and found its sensitive thickness to be about 2μm. For the 256k SRAM, a late 1980's part, we will assume the sensitive thickness to be approximately midway between, i.e. $t = 3\mu$m. We will further assume that the collection efficiency is similar to that for the 64k SRAM, $C = 0.55$.

Thus, for $t = 3\mu$m, we obtain the following BGR method upset model for the 256k SRAM:

$$\text{Upset Rate} = 0.55\left[\begin{array}{l} 3E5\int BGR(1.4\text{MeV},E_n)(dN/dE)dE \\ +\,3E7\int BGR(2.8\text{MeV},E_n)(dN/dE)dE \\ +\,6E7\int BGR(8.3\text{MeV},E_n)(dN/dE)dE \end{array}\right] \qquad [7-6]$$

After the integrations are carried out, the upset rate obtained is 1.9E-9 upsets/bit-hr, which applies at 45° latitude, 40,000 feet and the full 5 volt operating voltage. Using normalization factors of 1.4 for the altitude,

1.5 for the latitude, and 3.4 for the 2.5 volt operation, we obtain a calculated upset rate of 13.6E-9 upsets/bit-hr, which is almost a factor of three higher than the measured value.

Considering the large uncertainties in this particular calculation, this is still good agreement. The uncertainties include use of an SEU cross section curve for a different, although similar, SRAM by the same vendor, an assumed sensitive thickness based on general trends in SRAM structure, and an assumed collection efficiency identical to that for the 64k SRAM.

Examining the calculated upset rates listed in Table 7-2 on page 7-16, we note the excellent agreement with the rates from actual flight data. This applies to the rates calculated by both the neutron cross section method and the BGR method. The neutron cross section method gives upset rates that are 20-25% lower than the measured rates and the BGR method gives upset rates that are generally 40-60% higher. The fact that the two different methods give such good agreement reinforces our confidence in the two methods. The only case of less than good agreement is for the 256k SRAM, but, as indicated above, we had much poorer actual data to base our calculations upon. In addition, the measured data for the 256k SRAM is also poorer, since only 6 upsets were measured on the 14 flights out of Norway.

Section 8. Impact on Current/Future Avionics

The real payoff in this research is in knowing how to better specify and design future avionics equipment to be less susceptible to NSEU. Consequently, the model and knowledge gained in this work were applied to predict the sensitivity of future devices and systems.

8.1 Effect of Memory Size

The total amount of semiconductor memory on board an aircraft is a key factor in determining what kind of a problem neutron-induced SEU will cause for an avionics system. This is clearly seen in Figure 8-1 on page 8-2, in which the number of memory bits per aircraft are plotted against the mean time to fail (MTTF). Figure 8-1 on page 8-2 is based on an SEU upset rate of 2.3E-9 upsets/bit-hour for 5 volt operation. It is taken from Table 7-2 on page 7-16 and applies to flight at an altitude of 29,000 feet and a latitude of 55° (atmospheric neutron normalization factors of 0.4 and 1.37). It serves as a representative flight path only.

Similarly, we have somewhat arbitrarily assumed that an upset rate of more than one per flight would be noticeable but that less than one per flight would not. This is based on our experience in collecting avionics field reliability data, in which memory alterations potentially attributable to NSEU are difficult to separate from memory/system errors due to other causes such as power supply fluctuations, electromagnetic interference, or software/procedure errors.

The point of the curve is that, as the total memory density increases, the mean time between upsets decreases and we can easily reach a situation of 1-2 hours per upset for a memory of approximately 0.2-0.4 Gbit. Of course this applies only to unprotected memory. For memory protected by EDAC, the mean time between upsets increases enormously, as discussed in 9.2, "Fault Tolerance" on page 9-2. It also very significant that, on a per-bit basis, there is not very much difference in susceptibility to SEU for the same type of commercially available memory technology, in this case NMOS four-transistor cells. Koga in Reference 11 performed heavy ion testing on 12 different commercially available NMOS SRAMs and all but one exhibited very similar SEU sensitivity.

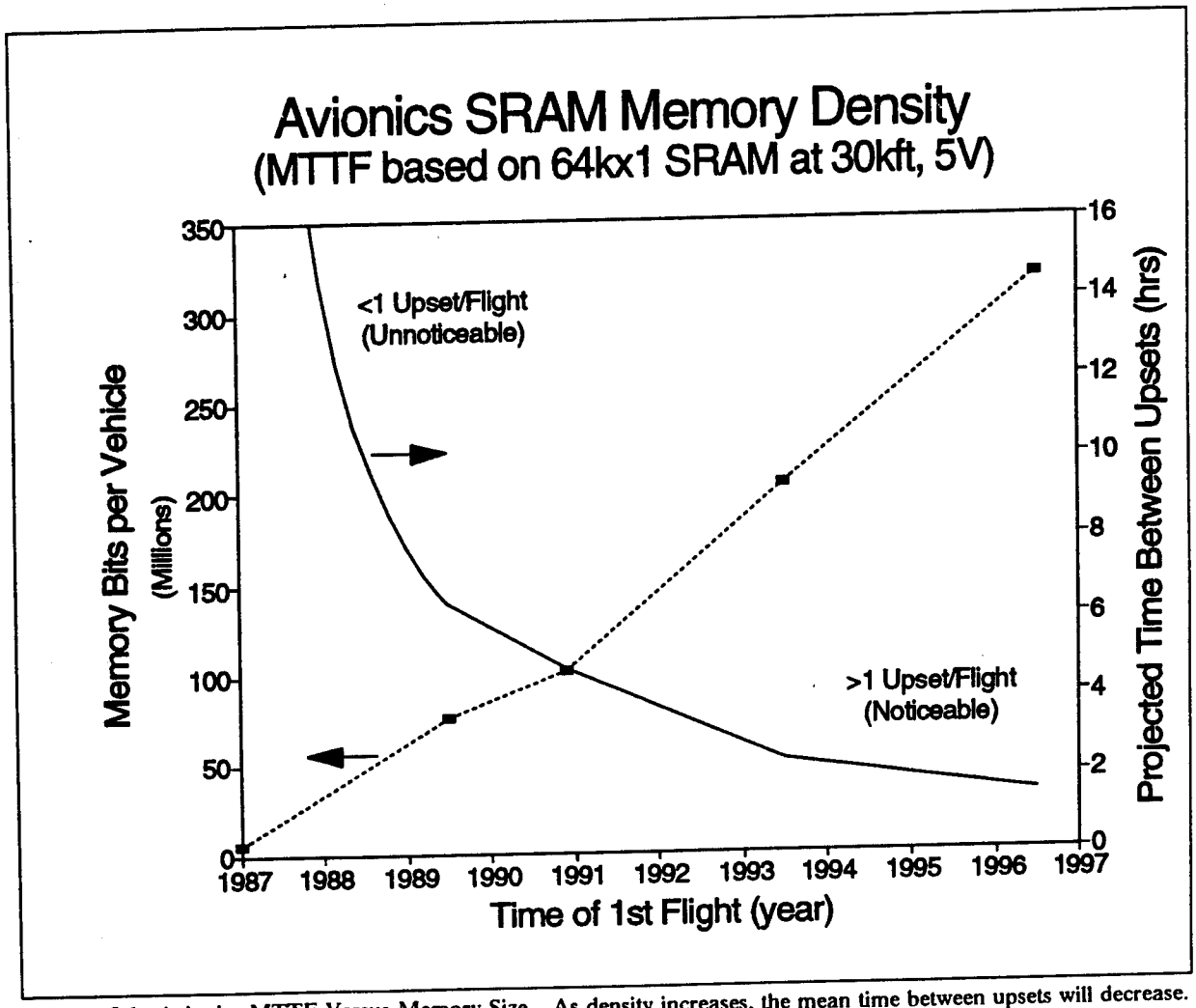

Figure 8-1. Avionics MTTF Versus Memory Size. As density increases, the mean time between upsets will decrease.

8.2 Effect of Altitude

Military avionics designers should note that atmospheric neutron single event upset rates will increase with increasing altitude. This is seen convincingly in Figure 8-2 on page 8-3, which shows the SEU rate as a function of altitude, and Figure 8-3 on page 8-4, which shows the SEU rate as a function of latitude. For the altitude variation, the IBM flight experimental data from Table 3-2 on page 3-8 is more useful than the military avionics field data, since the latter were all conducted at one altitude. The shape of the curve for the upset rate in the 64k SRAM operated at 2.5 volts as a function of altitude is in excellent agreement with the 1-10 MeV atmospheric neutron flux curve. This is further verification of the energetic atmospheric neutrons as the cause of the upsets.

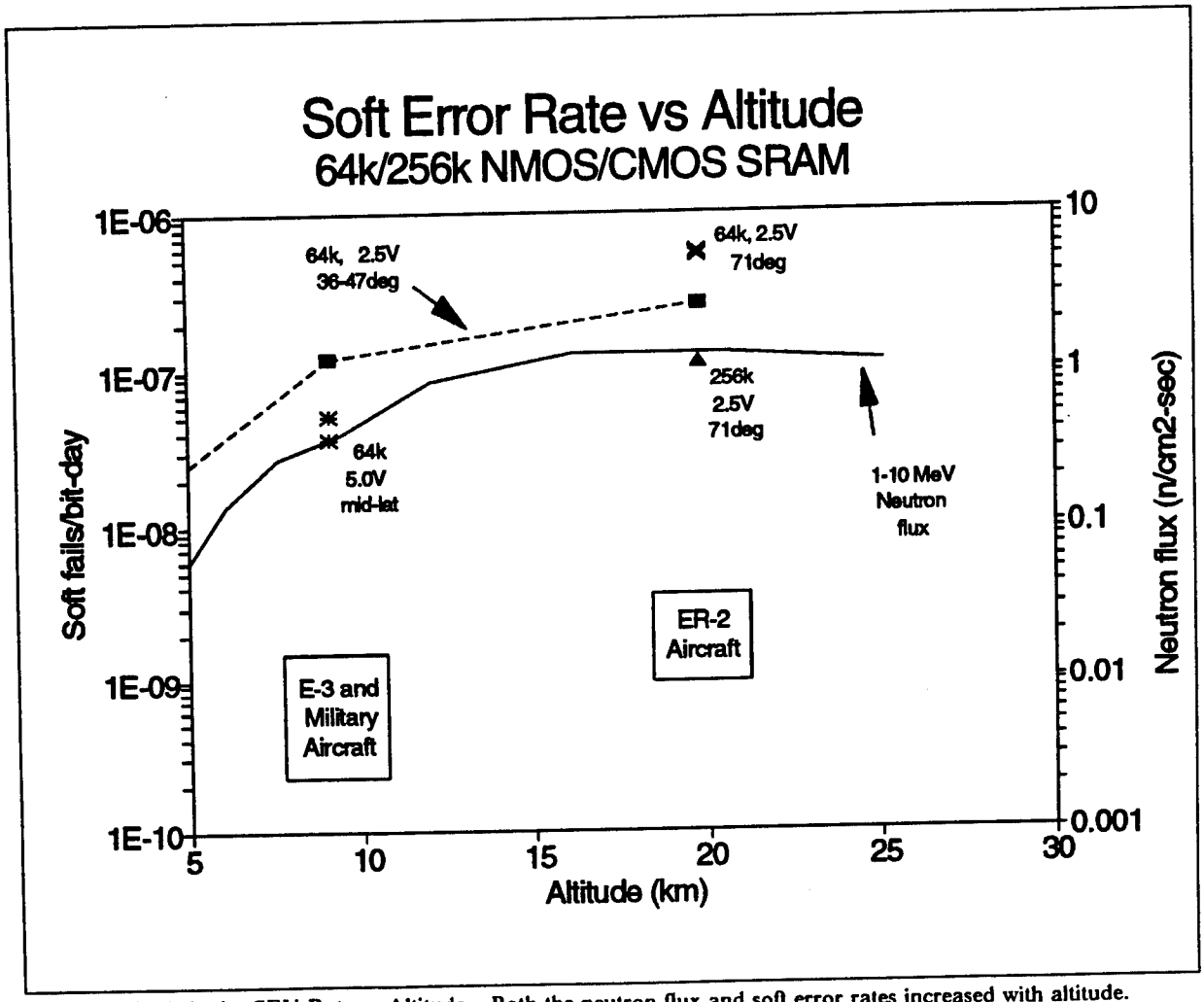

Figure 8-2. Avionics SEU Rate vs Altitude. Both the neutron flux and soft error rates increased with altitude.

8.3 Effect of Latitude

Soft error rates will also tend to increase with increasing latitude. For the latitude variation, both the IBM flight experimental data at 2.5 volts and the military avionics field data at 5 volts are useful, but both provide upset rates at only two latitudes. Nevertheless, the slope of the the two partial upset curve lines. at 2.5 volts and 5 volts, are in good agreement with the shape of the atmospheric neutron flux curve as a function as a function of latitude. This again corroborates our identification of the atmospheric neutrons as the cause of the upsets.

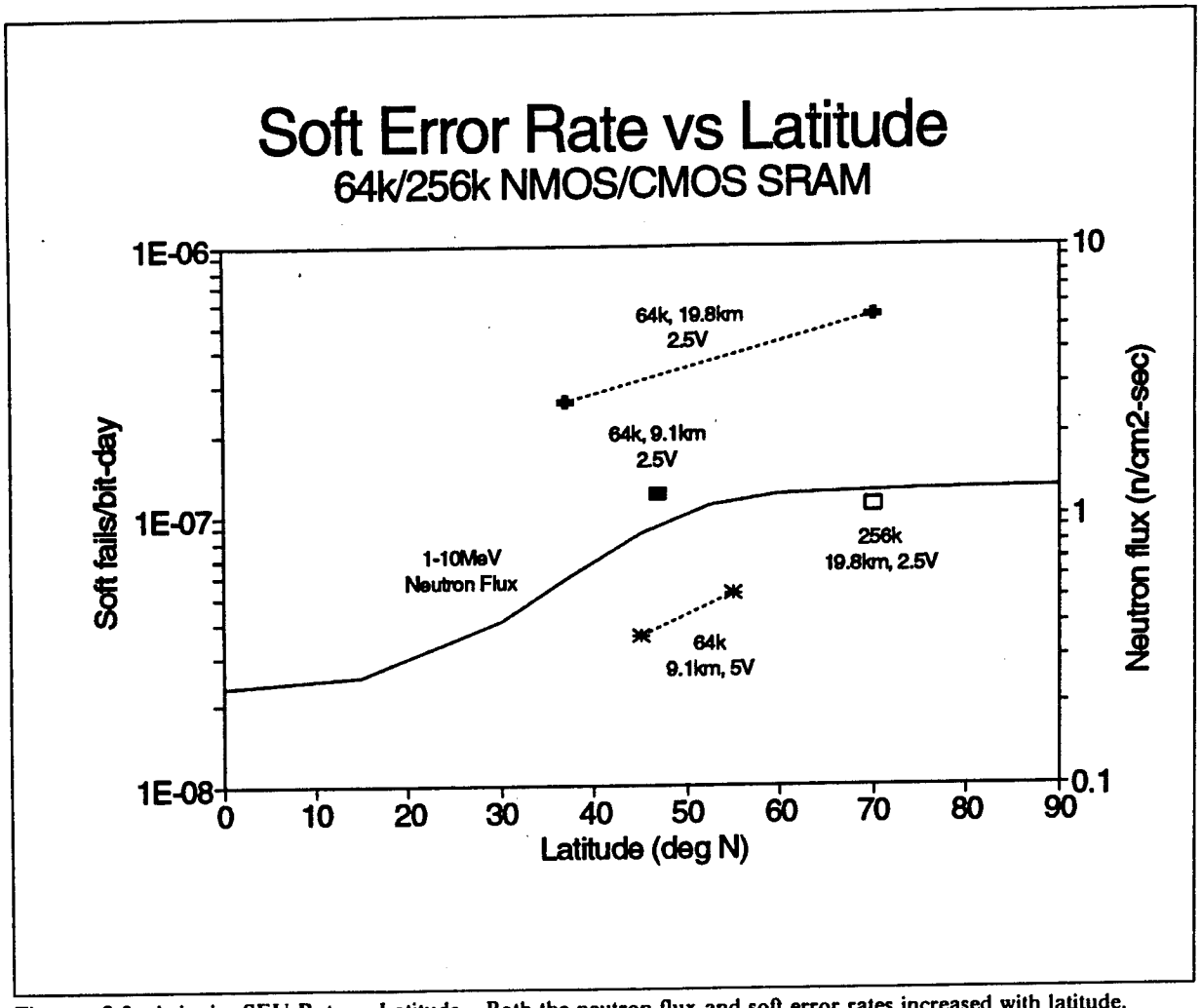

Figure 8-3. Avionics SEU Rate vs Latitude. Both the neutron flux and soft error rates increased with latitude.

8.4 Effect of Multi-Bit Upsets

When implementing soft error protection, designers should also consider the potential impact of multi-bit upsets. As described in 3.4.2 and 5.2, there have been several instances where two or more upsets appear to have occurred simultaneously (i.e. in known physically adjacent cells or within the same time measurement interval. Such bursts of upsets may overwhelm a soft error protection scheme if considerations aren't made in the initial design (see Section 9, "Hardening Strategies" on page 9-1).

Our limited data indicates that multi-bit upsets may account for up to 2% of the total events at both 29,000 feet and 65,000 feet. These are neutron induced double bit upsets. They can be compared to the multiple bit upsets induced by heavy ions of relatively low LET (15≤LET) because of the similar energy deposition between these ions and the neutron-induced recoils. We described in 5.2 multiple bit upset measurements in three different 1Mb SRAMs that indicated the multi-bit upsets comprise about 2%, 10%, and 20% of all events in the three devices. We noted the apparent wide variation in sensitivity to multi-bit upset for the same type of memory technology.

The Space Shuttle multiple upsets are interesting. However, because most upsets are caused by the heavy ion portion of the galactic cosmic rays (GCR) and some by the trapped protons in the South Atlantic Anomaly, the frequency of these multiple events can only serve as a general guide for similar effects at aircraft altitudes. For example, Table 5-1 on page 5-3 shows that the higher inclination orbits, for which the

GCR is more important, have the higher multiple bit frequencies (average of 7% compared to 1.5% at lower inclination.

Little is known about the physical distribution of such upsets. We expect that, in most cases, simultaneous upsets would involve physically adjacent memory cells. An instance of two adjacent cells being flipped was noted on the return of one of the 64k SRAM boards from flights over Norway (see Section 3). However, we did not have a time history to show that the two upsets occurred simultaneously. The two instances on the military avionics flights (see Section 4) were known to be coincident in time, but we have not yet traced the logical computer memory addresses back to the corresponding physical devices/cells.

There are at least two cases for the 64k SRAM, however, where we are certain that simultaneous upsets did *not* occur in adjacent cells. These were on Space Shuttle flight STS-48 (see Section 5) and involved simultaneous upsets in *separate computers*. Such an instance is thought to be very rare and likely caused by heavy ions, so it is not expected to apply at aircraft altitudes. However, it is presented here to indicate that such a possibility exists.

For now, avionics designers may assume that most, but not all, multi-bit upset bursts involve clusters of two or more cells in a very localized area (usually the same chip). This would not cause serious problems for designs using one-bit-wide memory devices, since multiple upsets on the same chip would, by definition, appear at different addresses and not cause multiple bits to fail in a single output word.

However, those designs using greater than one-bit-wide memory devices (such as ×4, ×8, ×9, or ×16) should consider the chance that a cluster of two or more upsets in the array could propagate to the same output word and overwhelm a single-bit soft error protection scheme. Furthermore, based on the data presented in 5.2, this effect has been seen in commercially available 1Mb SRAMs, and the percentage of the total number of upsets ranges from at least 2-20% for relatively low LET ions. We believe that these percentages also apply to neutron-induced multiple bit upsets in the same devices. More explicitly, having a multiple bit cross section curve as a function of LET such as Figure 5-2 allows us to calculate the multiple bit upset rate at aircraft altitudes by means of the BGR method.

The chance of multiple upsets occurring will be dependent on the array topology of the memory devices. Koga [Ref. 11] has shown that some static RAM memory devices have such tight column interleaving that upsets in physically adjacent cells of the same row will always propagate to the same output word. Other memory devices are designed with eight or more cells separating those in the same word, so that the chance of multiple faults in the same output word is greatly reduced.

Section 9. Hardening Strategies

Soft error hardening strategies can generally divided into two types; fault avoidance and fault tolerance. These are discussed below.

9.1 Fault Avoidance

Fault avoidance involves preventing faults from happening in the first place, as opposed to recovering from them once they've occurred.

9.1.1 Circuit Hardening

Efforts to protect semiconductor circuitry from the effects of packaging, space, and nuclear weapon radiation environments have resulted in the development of many circuit hardening techniques. These include increasing signal margin, reducing charge collection, and time filtering of SEU transients. Many of these techniques are expected to help reduce or even eliminate NSEU, but the cost and availability of such hardened parts may preclude their use on a typical avionics system.

9.1.2 Component Selection

When more than one manufacturer produces the same semiconductor device, it is possible to measure the candidate devices' sensitivity to NSEU and then select the device(s) with the lowest error rates. This technique has been used to reduce heavy ion soft error rates on the Space Shuttle General Purpose Computers.

9.1.3 Shielding

Localized and spot shielding have been used in the past for reducing the intensity of other types of radiation and thereby controlling the induced failures (e.g. die coatings for alpha particle protection, titanium package lids for gamma ray protection, etc.). However, shielding is not expected to be a practical method for controlling NSEU in aircraft. This is because the very energetic atmospheric neutrons (energies >150MeV) are highly penetrating and would require a large amount of shielding material to obtain a significant reduction in soft error rate.

With these very high energy neutrons, the fall off of the flux as neutrons are transported through a material is often characterized in terms of the attenuation length λ, in units of gm/cm^2. For a variety of materials (e.g. concrete, soil, iron) λ is similar (see Ref. 55). The attenuation length is large, e.g. we will use 80 gm/cm^2 which is applicable to the 100 MeV neutrons (from Ref. 56), although it is $\simeq$100 gm/cm^2 for E>400MeV. Attenuation of these high energy neutrons is primarily due to inelastic neutron interactions which decrease with increasing energy to an essentially constant value above about 150 MeV. To achieve a factor of ten reduction (i.e. $0.1 = e^{-2.3}$), we would need 2.3×80/2.7 or 68 cm of aluminum. This is totally impractical in terms of serving as a shield on an airplane. (To shield a 6"×6"×10" avionics box would require six aluminum slabs, each about 26" deep, with a combined weight of more than 800 pounds).

9.2 Fault Tolerance

A more likely candidate for NSEU hardening is the use of fault tolerance. Fault tolerance involves the use of redundancy to allow a system to continue functioning during or after a NSEU. It relies on the assumption that NSEU is not likely to occur simultaneously in widely separated locations (physical redundancy) or that, if an operation is repeated (time redundancy), a second NSEU will not occur in exactly the same manner.

In practice, fault tolerance can be implemented at many different levels, including chip, card, box, and system. A fault tolerant design may also involve the use of firmware, software, and procedures to recover from errors. In the following sections, we discuss some of the most common types of fault tolerance that are implemented for memory arrays.

9.2.1 Single-Error Detection With No Correction

One of the most common types of memory fault tolerance is the use of parity checking in hardware, coupled with recovery mechanisms in firmware, software, or procedures. The reason for parity checking's widespread use is its simplicity and speed. It requires as little as one extra bit per word.

Parity checking can be either "odd" or "even." In "odd" parity checking, the parity check bit is adjusted so that there is an odd number of 1's in word. In "even" parity checking, the parity bit is adjusted for an even number of 1's. An example of a nine-bit odd parity checker is shown in Figure 9-1.

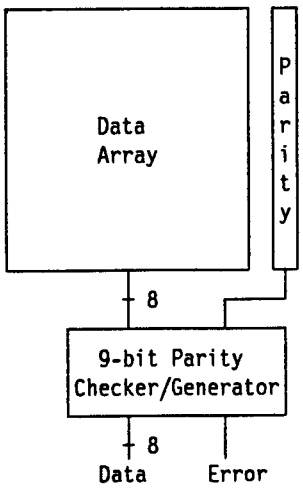

Data Bits	Check Bit
1 0 1 0 1 1 0 0	1
0 1 0 0 0 1 0 1	0
0 0 0 0 0 1 0 1	1

Figure 9-1. Example of Nine-Bit Odd-Parity Checker.

Some of the disadvantages of single-bit/word parity checking are that it can not detect an even number of errors (such as 2, 4, 6, etc.) and that it doesn't provide any means of correcting the error. Therefore, some of the concerns in implementing it are:

1. How often will higher-level recovery procedures have to be invoked (performance impact)?
2. How often will undetectable errors occur (safety impact)?

The frequency with which soft errors are observed and subsequently have an impact on performance will depend on the radiation environment, the size and sensitivity of the memory, and the way in which the memory is used. If all (100%) of the memory is used and it is read much more frequently than the time between errors, then the mean time t_e between observed errors will be:

$$t_e = \frac{1}{\lambda_s \times r \times c} \qquad [9-1]$$

where

t_e = mean time between observed errors (in days);
λ_s = single-bit upset rate in fails/bit-day;
r = number of rows (memory depth); and
c = number of columns (word width, including parity).

For example, a 1M×32 array with one parity-check column would have 1,048,576 rows and 33 columns. If the single-bit upset rate were 1E-7 f/bd, the mean time between events would be 0.29 days, or once every 6.9 hours.

The chance R_m of no events during a mission of time t_m would be:

$$R_m = e^{-\lambda_s r c t_m} \qquad [9-2]$$

where

R_m = probability of no events; and
t_m = mission time in days.

For example, if the above memory array was flown on a five-hour mission, the chance of no events would be less than half, or 0.49. Factors such as these must be considered where the recovery procedures are "painful," such as requiring a pilot to manually re-boot a system each time an error is detected.

9.2.2 Double-Error Detection With Single-Error Correction

Another popular soft error protection technique is the use of single-error-correction/double-error-detection (SEC-DED) coding. This technique employs a Hamming [Ref. 57] distance-4 code, usually optimized for minimum gate delay as in Hsiao's odd-column-weight code [Ref. 58]. See Reference 59 for a survey of various SEC-DED coding techniques.

An example of a 4M×32 memory array with SEC-DED coding is shown in Figure 9-2 on page 9-4 Each 32-bit wide data word requires seven extra check bits to perform the SEC-DED operation. These extra check bits are supplied by expanding the memory array to 4M×39 (22% increase in size).

On write operations, a 7-bit check word is generated (based on the incoming 32-bit data word) and stored in memory. On read operations, another 7-bit check word is generated (based on the outgoing 32-bit data word) and compared with the 7-bit check word previously stored in memory. If there is a mismatch, then one or more errors have occurred. If it is a single-bit error, the circuitry will invert the flipped bit and output correct data. If it is a detectable multi-bit error, the circuitry will provide an error flag indicating that the data is uncorrectable.

Our basic quantitative assumption about single-bit soft errors is that they are *exponentially distributed.* That is, the probability that a single-bit soft error has not occurred after time t is equal to $e^{-\lambda t}$, where λ is the average single-bit soft error rate. We can then calculate the soft error reliability of a SEC-DED protected system.

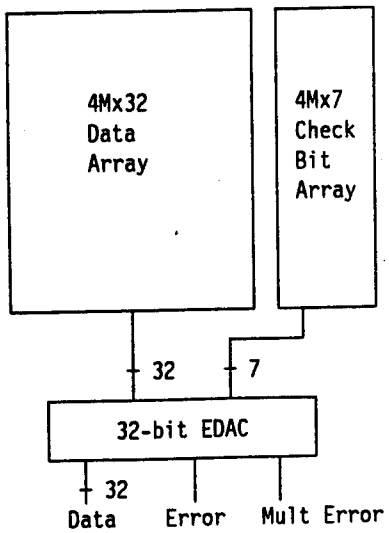

Data Bits	Check Bits
00000000000000000000000000000000	0011000
00000000000000000000000000000001	1100001
00000000000000000000000000000010	0010001
00000000000000000000000000000011	1001101
00000000000000000000000000000100	0010101
00000000000000000000000000000101	1001101

Figure 9-2. Example of 32-Bit SEC-DED Configuration. Single error correction/double error detection capability can be added to a 32-bit wide memory array using 7 extra check bits per word (22% additional memory).

First, we examine one word of memory. Each individual bit has a chance p of experiencing a soft fail equal to

$$p = 1 - e^{-\lambda t}, \qquad [9-3]$$

where

λ = bit soft error rate in fails/bit-day; and
t = time in days.

Therefore, the chance $Pf(1)_w$ of exactly one soft fail in a memory word would be equal to

$$Pf(1)_w = n(1-p)^{n-1}p, \qquad [9-4]$$

where

n = number of bits in the word.

Similarly, the chance $Pf(1)_w$ of zero soft fails in a memory word would be equal to

$$Pf(0)_w = (1-p)^n. \qquad [9-5]$$

Then, the combined chance $Pf(0,1)_w$ of zero or one soft fails in a word (correctable error situation) would be

$$Pf(0,1)_w = Pf(0)_w + Pf(1)_w. \qquad [9-6]$$

Since we assume that single-bit soft fails occur independently in each word of memory, then the array reliability R would be equal to the combined chance $Pf(0,1)_a$ of zero or one soft fails in *all* words of memory, or

$$R = Pf(0,1)_a = [Pf(0,1)_w]^w = \left[(1-n)e^{-\lambda tn} + ne^{-\lambda t(n-1)}\right]^w, \qquad [9-7]$$

where

w = the number of words in the memory array.

The mean time to fail ($MTTF$) for soft fails would be

$$MTTF = \frac{t}{-\ln[Pf(0,1)_a]} = \frac{-t}{w\ \ln\left[(1-n)e^{-\lambda tn} + ne^{-\lambda t(n-1)}\right]}. \qquad [9-8]$$

The above equations apply for a SEC-DED coding scheme without scrubbing capability. For example, if we assume that the memory array shown in Figure 9-2 on page 9-4 is flown on a six-hour mission using a memory device technology with a soft fail rate of 1E-7 f/bd at altitude (w=4,194,304, n=39, λ=1E-7, t=0.25), then the reliability R would be equal to 0.999998 and the MTTF would be approximately 352 years.

The advantage of SEC-DED coding can be seen when we examine what happens without it. In the case above, if only parity error detection were used (n=33 instead of 39), any single soft error would be uncorrectable. Unless some means of recovering/reloading memory existed, there would only be about a three percent chance of completing the mission without a fail (R=0.031420) and the $MTTF$ would be an average of 1.7 hours.

Figure 9-3 on page 9-6 shows graphically the probability of success (R) for the above examples as a function of soft error rate. Three important points are to be made. First, the use of SEC-DED coding alone provides a significant (3-4 orders of magnitude) improvement in soft error rate tolerance. Secondly, the soft error rates we've measured on the 64k SRAM at 29kft clearly dictate the necessity for SEC-DED coding or some similar means of protection on a memory array of this size. Finally, if other types of memory devices have soft upset rates within 1-2 orders of magnitude of our measurements, the same conclusions will still apply.

9.2.2.1 Soft Error Scrubbing

The reliability of memory arrays having SEC-DED code can usually be improved by periodically "scrubbing" the contents to remove any single-bit errors. This helps reduce the chance that single-bit errors will accumulate to the point where they overwhelm the EDAC (>1 error in one or more words).

An example of a system with soft error scrubbing is the IBM AP101S General Purpose Computer used on the U.S. Space Shuttle. The Space Shuttle system uses five computers, each containing four 128k×25 static RAM memory arrays that are scrubbed every 1.678 seconds. Without scrubbing, it is likely that there would have been a multiple fault alignment on at least one of the missions, since there have been 31 to 161 upsets per mission at the time of this writing. To date, the SEC-DED code and scrubbing have successfully corrected all upsets.

The reliability R (chance of no uncorrectable errors) for a SEC-DED system with scrubbing is equal to

$$R = \left[(1-n)e^{-\lambda t_s n} + ne^{-\lambda t_s(n-1)}\right]^{\frac{wt_m}{t_s}}, \qquad [9-9]$$

where

n = number of bits in parity word;
λ_s = soft error rate in fails/bit-day;
t_s = scrub time interval in days;
w = number of words in array; and
t_m = mission length in days.

It follows that the mean time to fail (MTTF) for multiple fault alignment is equal to:

$$MTTF = \frac{t_m}{-\ln(R)} \qquad [9-10]$$

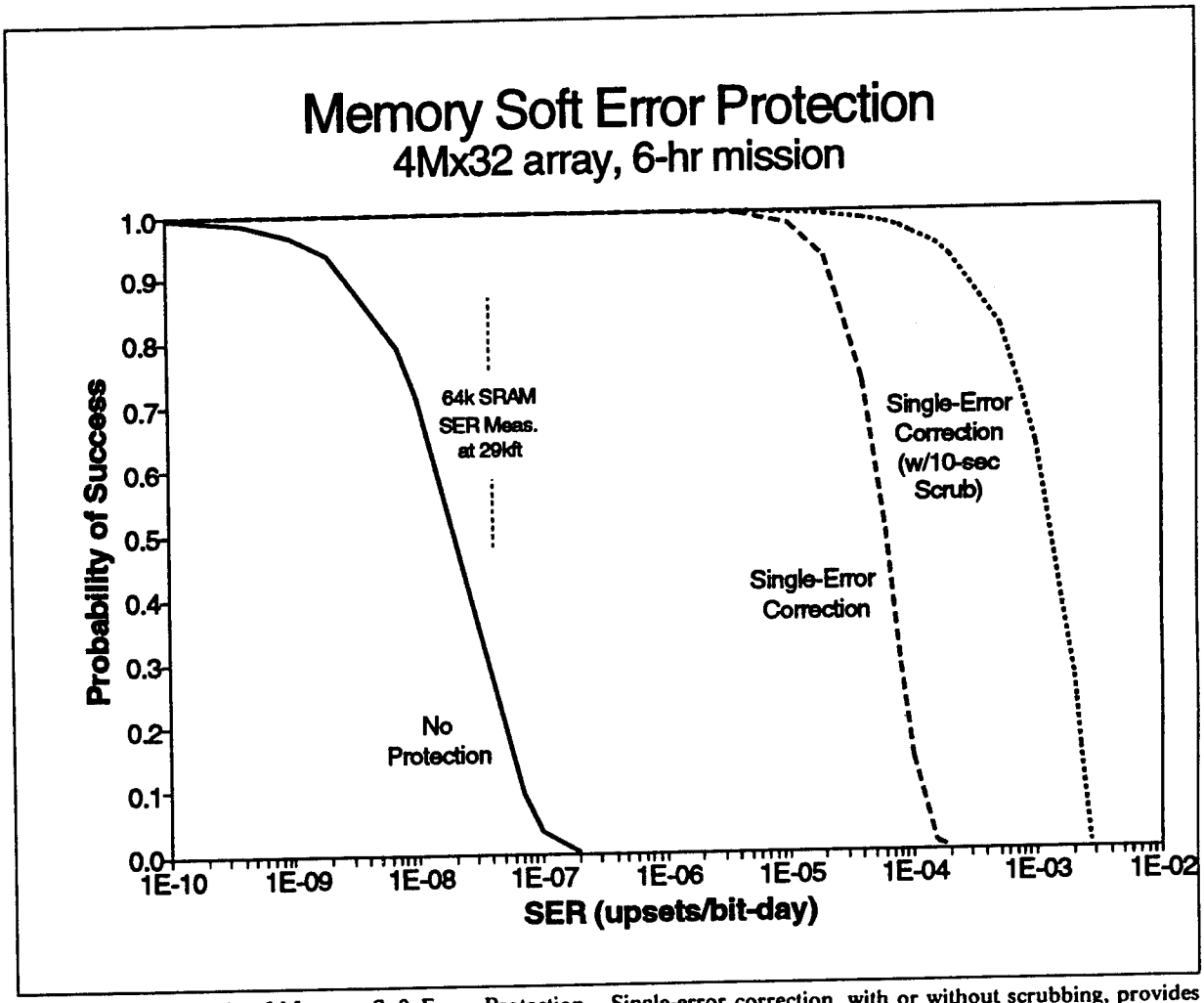

Figure 9-3. Example of Memory Soft Error Protection. Single-error correction, with or without scrubbing, provides significant protection against single-bit soft errors.

9.2.2.2 Multi-Bit Upsets

In order to circumvent the problem of multi-bit/chip upsets described in Section 8, "Impact on Current/Future Avionics" on page 8-1, it is suggested that each memory device output be wired to a separate EDAC circuit so that no more than one upset can occur per word. See Reference 60 for more information on this approach.

9.2.2.3 On-Chip Error Correction

There has been a trend towards inserting more testability and error detection features directly onto logic and memory chips. In one case, SEC-DED coding has been incorporated directly into a 16 megabit dynamic RAM to improve its manufacturability [Ref. 61].

Such on-chip error correction features should dramatically improve the soft error reliability of these devices when used in systems without external ECC. However, it is cautioned that, if there are any single-bit manufacturing defects on the chip, then those particular memory words would not be protected against an additional soft error. For instance, if 1000 bits out of a total 16,777,216 bits had hard fails, then 1000 words would be unprotected against further hard or soft fails. This means that a soft upset in any of 137-bits/word×1000-words = 137,000-bits would cause an uncorrectable error.

It is recommended that, if on-chip error correction is used to replace external error correction circuitry in avionics designs, that devices be screened to select only those with no single-bit manufacturing defects or other defects that would limit their soft error protection.

If on-chip error correction is used in combination with external error correction circuitry, then one might achieve a significant improvement in reliability and perhaps reduce or eliminate the need for soft error scrubbing.

9.2.3 Voting Technique

Another means of providing memory fault tolerance is the use of voting. This is not often used for memory arrays, since it requires a significant amount of redundancy, but it can be effective if the resources are available.

In a voting configuration, the outputs of three or more memory arrays are compared against each other. If a majority of the outputs are in agreement, the voter assumes their values are correct. The minimum voting configuration is a set of three redundant modules, or Triple Modular Redundancy (TMR), as shown in Figure 9-4 on page 9-8. The reliability of a system using triple modular redundancy (TMR), assuming an ideal voter, is equal to the chance that all three modules work, plus the chance of two modules working and one failing, or

$$R_{sys}(t) = R_m^3(t) + 3R_m^2(t)[1 - R_m(t)] = 3R_m^2(t) - 2R_m^3(t), \qquad [9-11]$$

where

$R_{sys}(t)$ = reliability of system as a function of time; and
$R_m(t)$ = reliability of module as a function of time.

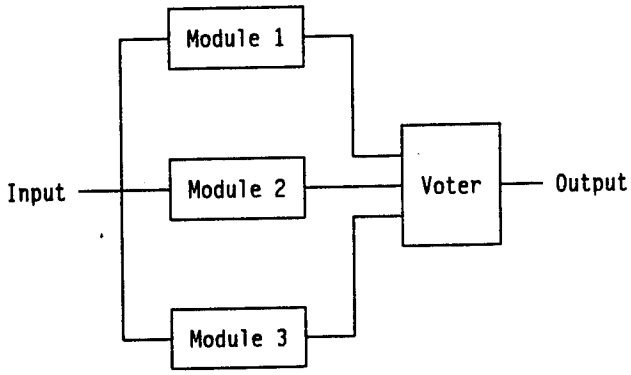

Figure 9-4. Example of Triple Modular Redundant Memory.

For example, if we take the case of the memory array described in 9.2.1, "Single-Error Detection With No Correction" on page 9-2, a single module (simplex system) would have a reliability of 0.87 for a one-hour mission. The same modules, if used in a TMR system, would provide a system reliability of 0.95.

Since a TMR system relies on a majority of the modules being good, it is only effective for short duration missions. This can be seen when we compare $MTTF_{tmr}$ to $MTTF_{mod}$. If we assume that the modules obey the exponential failure law, then the single module reliability as a function of time is equal to

$$R_m(t) = e^{-\lambda t}, \qquad [9-12]$$

where

λ = module failure rate; and
t = time.

Since

$$MTTF = \int_0^\infty R(t)dt, \qquad [9-13]$$

then

$$MTTF_{mod} = \int_0^\infty e^{-\lambda t}dt = \frac{1}{\lambda}. \qquad [9-14]$$

Using Equations 9-11 and 9-12 for a TMR system, the reliability would be

$$R_{sys}(t) = 3[e^{-\lambda t}]^2 - 2[e^{-\lambda t}]^3 = 3e^{-2\lambda t} - 2e^{-3\lambda t}. \qquad [9-15]$$

Then, $MTTF_{tmr}$ for the TMR system would be

$$MTTF_{tmr} = \int_0^\infty 3e^{-2\lambda t} - 2e^{-3\lambda t}dt = \frac{5}{6\lambda}. \qquad [9-16]$$

This compares with an MTTF of $1/\lambda$ for a simplex system. Therefore,

$$MTTF_{tmr} < MTTF_{\text{mod}}.$$

So, the TMR system is not suitable for long life applications because of its short MTTF compared to the MTTF of a single module. It is, however, useful for short duration missions where very high reliability is required.

Section 10. Conclusions

We conclude that a significant single event upset phenomenon exists at airplane altitudes, that it is most likely due to energetic neutrons created by cosmic ray interactions within the atmosphere, and that memory error correction coding (ECC) is likely to be necessary for most high density avionics memory systems.

We have demonstrated this by compiling flight upset data from more than 1000 hours of flight that included well over 100 upsets. All flights carried at least 280 64k SRAMs and a few also carried 84 256k SRAMs. The 64k SRAM was exposed to beams of neutrons and protons in the laboratory in order to obtain its neutron-induced upset cross section. Models were developed to correlate the laboratory results with the atmospheric neutron environment. The calculated upset rates are in very good agreement with the measured values. With the models verified we were able to predict the impact of SEU on current and future avionics systems and to evaluate various hardening strategies.

This is a comprehensive study. Earlier work [Refs. 62, 63] had addressed the subject in largely qualitative terms. A more recent approach [Ref. 64] reached similar conclusions to ours with regard to the impact of neutron-induced SEU on avionics designs, but based theirs on very limited flight upset data and supporting calculations. Nevertheless, using data based on totally different avionics systems, but which also contained SRAMs, they obtained a flight upset rate within a factor of about six of what we had measured. Factors such as altitude, latitude, and the SEU sensitivity of specific devices, all of which we have examined in detail, may alter the agreement factor some, but it still corroborates the basic phenomenon. Having developed a comprehensive approach, we believe that it can be used to both evaluate present/future avionics design concepts and analyze flight upset data from other systems.

Section 11. Recommendations

It is recommended that avionics developers consider NSEU phenomena in current and future designs. Also, government specifications should be developed to guide contractors in the analysis, prevention, and verification of NSEU effects. In addition, more work is needed to better quantify the problem. As this is a relatively new field, data on different memory devices, and eventually logic devices, will be invaluable in understanding and controlling the problem.

Finally, neutrons are likely to induce single event effects other than upset, in particular, latchup. Heavy ion-induced latchup has been a known and measured effect in CMOS devices for many years. Very recently, however, two papers were presented indicating that proton-induced latchup was measured in a memory [Ref. 66] and in a microprocessor [Ref. 67]. The energies of the protons that induced the latchup ranged from 30 to 150 MeV. Thus, based on our discussion in 6.3, "Neutron Upset Cross Sections" on page 6-11 on the similarity between energetic protons and neutrons in causing single event effects, we expect that the atmospheric neutrons will also induce latchup in parts that are sensitive to latchup with ions of very low LET. Because latchup is a potentially more serious problem than upset (recovery may require power cycling or switching to redundant hardware), we recommend that a flight experiment program be undertaken with parts very sensitive to latchup, to demonstrate that latchup can occur in flight. Furthermore, CMOS parts with known extreme sensitivity to latchup (very low LET thresholds) ought to be identified to avionics designers as parts to avoid.

Section 12. References

1. D. Binder, E.C. Smith, and A.B. Holman, "Satellite Anomalies from Galactic Cosmic Rays," IEEE Trans. Nucl. Sci., Vol. NS-22, 2675, 1975.
2. C.M. Hsieh, P.C. Murley, and R.R. O'Brien "Collection of Charge from Alpha-Particle Tracks in Silicon Devices," IEEE Trans. Elec. Dev., Vol. ED-30, No. 6, June 1983.
3. E.R. Berger, M.K. House, G.J. Manzo, and A.H. Taber, "Single Event Upsets in Microelectronics: Third Cosmic Ray Upset Experiment," IBM Technical Directions, Vol. 11, No. 1, 1985.
4. T.C. May and M.H. Woods, "Alpha-Particle-Induced Soft Errors in Dynamic RAMs," IEEE Trans. Electron Devices, ED-26, 1979.
5. A. Constantine, "SEU Project Update," RPI memo to R. Block, October 31, 1988.
6. A.H. Taber, "Soft Fail Rate Projections for the Inmos 64K×1 CMOS SRAM," IBM Technical Report no. 84-PN6-001, April 2, 1984.
7. E.V. Benton, "Radiation Measurements for the IBM Aircraft Nos. 1, 2, and 3 High Altitude Aircraft Experiment," ERIL Research Report, August 15, 1989.
8. D.K. Nichols et al, "Latest Trends in Parts SEP Susceptibility from Heavy Ions," IEEE Trans. Nucl. Sci., NS-36, 2388, 1989.
9. P.M. O'Neill, "Post-Flight Analysis Report of Radiation Effects on New General Purpose Computer (GPC) and Local Store Memory Devices," NASA/JSC technical memorandums for STS-37 through STS-49, 1991-92.
10. P.T. McDonald, W.J. Stapor, and D. Gonyea, "CRRES MEP Multiple Bit Upsets," presented at the Eighth Single Event Effects Symposium, Los Angeles, CA, April, 1992.
11. R. Koga et al "On the Suitability of Non-Hardened High Density SRAMs for Space Applications," IEEE Trans. Nucl. Sci., NS-38, No. 6, Dec. 1991.
12. T.M. Scott, "Cosmic Ray Upset Experiment Results," IBM Report 89-PN6-023, Manassas, VA, November 1989.
13. A.H. Taber, "Cosmic Ray Flight Upset Experiment/Analysis," IBM letter 92-FLUX-01 to E. Normand, January 2, 1992.
14. D. Halliday, Introductory Nuclear Physics, J. Wiley & Sons, 1950.
15. H.M. Murray, W.J. Stapor, and C.M. Castaneda, "Calibrated Charged Particle Radiation System with Precision Dosimetric Measurement and Control," Nucl. Instr. and Meth., A281, p 616, 1989.
16. F.P. Brady et al, "Multi-Wire Chamber System for Measurements of Neutron Spectra," Nucl. Instr. and Meth., 228, p 89, 1984.
17. J.R. Lamarsh, Introduction to Nuclear Engineering, 2nd Edition, Addison-Wesley 1983.
18. J.F. Ziegler and W.F. Lanford, "The Effect of Sea Level Cosmic Rays on Electronic Devices," J. Appl. Phys., 52 (6), 4305, 1981.
19. P.G. Young et al, "Transport Data Libraries for Incident Proton and Neutron Energies to 100 MeV," LA-11753-MS, Los Alamos National Laboratory, July 1990.
20. W.L. Bendel and E.L. Petersen, "Proton Upsets in Orbit," IEEE Trans. Nucl. Sci., NS-30, 4481, 1983.
21. W.J. Stapor et al, "Two Parameter Bendel Model Calculations for Predicting Proton Induced Latchup," IEEE Trans. Nucl. Sci., NS-37, 1966, 1990.
22. Y. Shimano et al "The Measurement and Prediction of Proton Upset," IEEE Trans. Nucl. Sci., NS-36, 2344, 1989.
23. E. Normand et al "Quantitative Comparison of Single Event Event Upset Induced by Protons and Neutrons," IEEE Trans. Nucl. Sci., NS-38, 1457, 1991.
24. J.F. Ziegler and W.A. Lanford, "Effect of Cosmic Rays on Computer Memories," Science, 206, 776, November 1979.
25. R. Silberberg, C.H. Tsao, and J.R. Letaw, "Neutron Generated Single Event Upsets in the Atmosphere," IEEE Trans. Nucl. Sci., NS-31, 1183, Dec. 1984.
26. C.H. Tsao, R. Silberberg, and J.R. Letaw, "Cosmic-Ray Heavy Ions at and Above 40,000

Feet," IEEE Trans. Nucl. Sci., NS-31, 1066, Dec. 1984.

27. J. Dicello, M. Paciotti, and M. Schillaci, "An Estimate of Error Rates in Integrated Circuits at Aircraft Altitudes and at Sea Level," Nucl. Instr. and Meth., B40/41, 1989.

28. C.S. Dyer, A.J. Sims, J. Farren, and J. Stephen, "Measurements of Solar Flare Enhancements to the Single Event Upset Environment in the Upper Atmosphere," IEEE Trans. Nucl. Sci., NS-37, 1929, Dec. 1990.

29. C.S. Dyer, A.J. Sims, J. Farren, and J. Stephen, "Measurements of the SEU Environment in the Upper Atmosphere," IEEE Trans. Nucl. Sci., NS-36, 2275, Dec. 1989.

30. R.B. Mendall and S.A. Korff, "Fast Neutron Flux in the Atmosphere," J. Geophys. Res., 68, 5487, 1963.

31. T.W. Armstrong et al "calculation of Neutron Flux Spectra Induced in the Earth's Atmosphere by Galactic Cosmic Rays," J. Geophys. Res., 78, 2715, 1973.

32. M. Merker et al "Time Dependent Worldwide Distribution of Atmospheric Neutrons and Their Products," J. Geophys. Res., 78, 2727, 1973.

33. J.H. Adams, "Cosmic Ray Effects on Microelectronics," NRL-5901, Naval Research Laboratory, 1986.

34. J. Hewitt et al "Ames Collaborative Study of Cosmic Ray Neutrons & Mid-Latitude Flights," Health Physics, 34, 375, 1978.

35. J.W. Wilson and J.E. Nealy, "Model and Data Base for Background Radiation Exposure of High Altitude Aircraft," Proceedings of the Topical Meeting in New Horizons in Radiation Protection and Shielding, American Nuclear Society, April, 1992.

36. "Cosmic Ray Measurements by Neutron Monitor," National Geophysical Data Center, Solar Geophysical Data Prompt Reports, Part I, No. 571, March, 1992.

37. K. O'Brien et al, "Extraterrestrial Radiation Exposure of Aircraft Crews," Proceedings of the Topical Meeting in New Horizons in Radiation Protection and Shielding, American Nuclear Society, April, 1992.

38. D.F. Smart and M.A. Shea, "The Distribution of Galactic Cosmic Rays and Solar Particles to Aircraft Altitudes," Proceedings of the Topical Meeting in New Horizons in Radiation Protection and Shielding, American Nuclear Society, April, 1992.

39. A.M. Preszler, G.M. Simnett, and R.S. White, "Angular Distribution and Altitude Dependence of Atmospheric Neutrons from 10-100 MeV," J. Geophys. Res., 79, 17, 1974.

40. F. Ait-Ouamer, "Atmospheric Neutrons at 8.5 GV Cutoff," UCR/IGPP-87/20, M.S. Thesis (Physics), University of California at Riverside, June, 1987.

41. R. Saxena, "Ground Level Atmospheric Neutron Flux Measurements in the 10-170 MeV Range," Ph.D. Dissertation (Physics) University of New Hampshire, May 1990.

42. W. Hess, H.W. Patterson, R. Wallace, and E.L. Chupp, "Cosmic-Ray Neutron Energy Spectrum," Phys. Rev., 116, 445, 1959.

43. T.W. Armstrong, R.G. Alsmiller, and J. Barish, "Calculation of the Radiation Hazard at Supersonic Aircraft Altitude Produced by an Energetic Solar Flare," Nucl. Sci. Eng., 37, 337, 1969.

44. C.S. Guenzer, E.A. Wolicki, and R.G. Allas, "Single Event Upset of Dynamic RAMs by Neutrons and Protons," IEEE Trans. Nucl. Sci., NS-26, 5048, 1979.

45. C.S. Guenzer et al "Single Event Upset in RAMs Induced by Protons at 4.2 GeV and Protons and Neutrons Below 100 MeV," IEEE Trans. Nucl. Sci., NS-27, 1485, 1980.

46. E. Normand, "Use of PuBe Source to Simulate Neutron-Induced Single Event Upsets in Static RAMs," IEEE Trans. Nucl. Sci., NS-35, No. 6, Dec. 1988.

47. Single Event Effects Data Base, Exciton Science Corporation, Aliso Viejo, CA, July, 1991.

48. E. Normand, D.L. Oberg, J.L. Wert, T.J. Baker, and C.M. Castaneda, "Considerations in Single Event Upset Testing with Energetic Neutrons," presented at the Eigth Single Event Effects Symposium, Los Angeles, CA, April 1992.

49. J.R. Letaw, and E. Normand, "Guidelines for Predicting Single-Event Upsets in Neutron Environments," IEEE Trans. Nucl. Sci., NS-38, 1500, 1991.

50. E. Normand, "Incorporation of ENDF-V Neutron Cross Section Data for Calculating Neutron-Induced Single Event Upsets," IEEE Trans. Nucl. Sci., NS-36, Dec. 1989.

51. C.H. Tsao, R. Silberberg, and J.R. Letaw, "A Comparison of Neutron-Induced SE Rates in Si and GaAs Devices," IEEE Trans. Nucl. Sci., NS-35, 1634, Dec. 1988.

52. P.J. McNulty, W.G. Abdelkader, and J. Lynch, "Modeling Charge Collection and Single Event Upsets in Microelectronics," Nucl. Instr. Meth., B61, 52, 1991.

53. R. Koga et al, "SEU Test Techniques for 256k Static RAM and Comparisons of Upsets by Heavy Ions and Protons," IEEE Trans. Nucl. Sci., NS-35, 1638, 1988.

54. "Guidelines for Predicting Single Event Upset (SEU) Rate in Microelectronic Parts for ------- Program," Boeing Proprietary Document D201W601, March, 1992.

55. W.P. Swanson, "Radiological Safety Aspects of the Operation of Electron Linear Accelerators," IAEA Technical Report 188, 1979.

56. "Shielding for High Energy Electron Accelerator Installations," National Bureau of Standards Handbook 97, July, 1964.

57. R.W. Hamming, "Error Detecting and Error Correcting Codes," Bell System Technical Journal, Vol. XXVI, No. 2, April 1950, 147-160.

58. M.Y. Hsiao, "A Class of Optimal Minimum Odd-Weight-Column SEC-DED Codes," IBM J. Res. Develop. 14 (July 1970), 395-401.

59. C.L. Chen and M.Y. Hsiao, "Error-Correcting Codes for Semiconductor Memory Applications: A State-of-the-Art Review," IBM J. Res. Develop. 28 (March 1984), 124-134.

60. G. Buskirk, "32-Bit-Wide Memory Tolerates Failures," NASA Tech Briefs June 1990, pp. 38-42.

61. C.H. Stapper, J.A. Fifield, and H.L. Kalter, "High-Reliability Fault-Tolerant 16-Mbit Memory Chip," Proceedings of the Annual Reliability and Maintainability Symposium, 48, 1991.

62. H. May, "A New Enemy - Homotrons," International Federation of Airline Pilots Association (IFALPA) newsletter, September 1980.

63. B. Nordwall, "Avionics Vulnerable to Particles From Solar Flares, Cosmic Rays," Aviation Week and Space Technology, July 25, 1988.

64. J.P. Raymond and C.P. Capps, "Aircraft SEU Phenomena," presented at the Eighth Single Event Effects Symposium, Los Angeles, CA, April, 1992.

65. R. Harboe-Sorensen, "Proton and Heavy Ion Testing of Electronic Devices for Analysis of SEU at Low Altitudes," paper ESA WPP-23 presented at the European Space Agency Workshop on Space Environment Analysis, ESTEC, Noordwisk, Netherland, Oct, 1990.

66. L. Adams et al, "A Verified Proton Induced Latchup in Space," paper presented at the 1992 IEEE Nuclear and Space Radiation Conference, July 1992, New Orleans, LA.

67. D.K. Nichols et al, "Discovery of Proton-Induced Latchup," paper presented at the 1992 IEEE Nuclear and Space Radiation Conference, July 1992, New Orleans, LA.

Appendix A. Flight Data Logs

A.1 European Area 1

Table A-1. Flight Log - European Area 1.

Date	AOCP (H)	Flt Hrs (Cum)	SEU	SEU (Cum)
02-Nov-90	8.600	8.600	2	2
07-Nov-90	7.870	16.470	1	3
09-Nov-90	4.430	20.900	2	5
13-Nov-90	5.400	26.300	0	5
14-Nov-90	6.990	33.290	1	6
23-Nov-90	2.630	35.920	0	6
25-Nov-90	8.380	44.300	2	8
26-Nov-90	8.380	52.680	3	11
29-Nov-90	6.510	59.190	0	11
30-Nov-90	5.660	64.850	0	11
04-Dec-90	9.200	74.050	1	12
06-Dec-90	8.360	82.410	5	17
14-Dec-90	7.670	90.080	3	20
15-Dec-90	7.380	97.460	0	20
19-Dec-90	8.430	105.890	4	24
08-Jan-91	5.320	111.210	0	24
10-Jan-91	6.870	118.080	4	28
14-Jan-91	9.210	127.290	0	28
15-Jan-91	6.380	133.670	0	28
17-Jan-91	3.340	137.010	1	29
22-Jan-91	9.920	146.930	2	31
19-Feb-91	8.940	155.870	1	32
05-Mar-91	9.160	165.030	2	34
23-Mar-91	4.900	169.930	1	35
19-Apr-91	4.700	174.630	0	35
16-May-91	6.500	181.130	2	37
17-May-91	5.110	186.240	1	38
07-Aug-91	8.120	194.360	2	40
14-Aug-91	8.690	203.050	5	45
16-Sep-91	3.050	206.100	2	47
09-Oct-91	6.710	212.810	1	48
11-Oct-91	6.770	219.580	1	49
10-Dec-91	6.210	225.790	2	51
13-Dec-91	5.520	231.310	0	51
17-Dec-91	6.010	237.320	1	52
11-Feb-92	3.740	241.060	1	53

A.2 European Area 2

The Airborne Operational Control Program (AOCP) duration, or length of time that upsets were recorded on each flight, was assumed to be 15 minutes shorter than the actual flight duration.

Table A-2 (Page 1 of 2). Flight Log - European Area 2.

Date	Flt Dur (H/M)	AOCP Dur	AOCP (H)	Flt Hrs (Cum)	SEU	SEU (Cum)
06-Jan-91	08:38:11	08:23:11	8.386	8.386	0	0
08-Mar-91	07:57:12	07:42:12	7.703	16.090	1	1
12-Mar-91	08:59:00	08:44:00	8.733	24.823	1	2
07-Apr-91	07:05:00	06:50:00	6.833	31.656	2	4
11-Apr-91	08:05:00	07:50:00	7.833	39.490	2	6
12-Apr-91	07:30:00	07:15:00	7.250	46.740	0	6
25-Apr-91	07:11:02	06:56:02	6.934	53.674	1	7
17-Jun-91	06:00:00	05:45:00	5.750	59.424	0	7
20-Jun-91	07:50:00	07:35:00	7.583	67.007	3	10
04-Jul-91	07:23:00	07:08:00	7.133	74.140	2	12
09-Jul-91	08:09:00	07:54:00	7.900	82.040	1	13
10-Jul-91	03:00:00	02:45:00	2.750	84.790	1	14
16-Jul-91	08:48:00	08:33:00	8.550	93.340	2	16
18-Jul-91	08:34:00	08:19:00	8.317	101.657	1	17
25-Jul-91	10:34:00	10:19:00	10.317	111.974	2	19
30-Jul-91		07:12:00	7.200	119.174	0	19
01-Aug-91	07:30:00	07:15:00	7.250	126.424	3	22
06-Aug-91	07:02:00	06:47:00	6.783	133.207	0	22
08-Aug-91	07:01:00	06:46:00	6.767	139.974	0	22
13-Aug-91	07:10:00	06:55:00	6.917	146.890	0	22
20-Aug-91	08:38:00	08:23:00	8.383	155.274	0	22
22-Aug-91	06:46:00	06:31:00	6.517	161.790	0	22
26-Aug-91	07:46:00	07:31:00	7.517	169.307	2	24
29-Aug-91	07:13:00	06:58:00	6.967	176.274	0	24
03-Sep-91	07:25:00	07:10:00	7.167	183.440	1	25
05-Sep-91	07:15:00	07:00:00	7.000	190.440	2	27
09-Sep-91	07:18:00	07:03:00	7.050	197.490	2	29
12-Sep-91	06:32:00	06:17:00	6.283	203.774	0	29
14-Sep-91	08:02:00	07:47:00	7.783	211.557	1	30
16-Sep-91	06:44:28	06:29:28	6.491	218.048	1	31
19-Sep-91	06:52:00	06:37:00	6.617	224.665	1	32
23-Sep-91	07:05:00	06:50:00	6.833	231.498	1	33
24-Sep-91	09:45:00	09:30:00	9.500	240.998	2	35
26-Sep-91	07:50:00	07:35:00	7.583	248.581	0	35
30-Sep-91	05:40:00	05:25:00	5.417	253.998	2	37
01-Oct-91	08:17:58	08:02:58	8.049	262.048	2	39
02-Oct-91	04:05:00	03:50:00	3.833	265.881	1	40
04-Oct-91	05:11:00	04:56:00	4.933	270.814	1	41
08-Oct-91	04:08:00	03:53:00	3.883	274.698	1	42
09-Oct-91	07:10:00	06:55:00	6.917	281.614	4	46
14-Oct-91	06:49:00	06:34:00	6.567	288.181	4	50
16-Oct-91	06:17:00	06:02:00	6.033	294.214	1	51
18-Oct-91	05:05:00	04:50:00	4.833	299.048	1	52
21-Oct-91	03:03:58	02:48:58	2.816	301.864	2	54
22-Oct-91	06:31:02	06:16:02	6.267	308.131	0	54

Table A-2 (Page 2 of 2). Flight Log - European Area 2.

Date	Flt Dur (H/M)	AOCP Dur	AOCP (H)	Flt Hrs (Cum)	SEU	SEU (Cum)
24-Oct-91	03:02:00	02:47:00	2.783	310.914	1	55
30-Oct-91	02:41:00	02:26:00	2.433	313.348	0	55
07-Nov-91	08:54:00	08:39:00	8.650	321.998	0	55
08-Nov-91	05:57:00	05:42:00	5.700	327.698	2	57
13-Nov-91	08:22:00	08:07:00	8.117	335.814	1	58
14-Nov-91	01:03:00	00:48:00	0.800	336.614	0	58
15-Nov-91	07:16:00	07:01:00	7.017	343.631	1	59
19-Nov-91	06:54:00	06:39:00	6.650	350.281	1	60
21-Nov-91	05:50:00	05:35:00	5.583	355.864	1	61
22-Nov-91	04:10:09	03:55:09	3.919	359.783	0	61
26-Nov-91	08:56:00	08:41:00	8.683	368.467	0	61
27-Nov-91	07:20:00	07:05:00	7.083	375.550	0	61
03-Dec-91	04:15:00	04:00:00	4.000	379.550	1	62
04-Dec-91		07:15:00	7.250	386.800	0	62
10-Dec-91		08:55:00	8.917	395.717	0	62
12-Dec-91		06:49:00	6.817	402.533	0	62
17-Dec-91		08:35:00	8.583	411.117	3	65
18-Dec-91		08:23:00	8.383	419.500	0	65
07-Jan-92		06:06:00	6.100	425.600	1	66
09-Jan-92		07:19:00	7.317	432.917	0	66
16-Jan-92		05:49:00	5.817	438.733	0	66
21-Jan-92		07:46:00	7.767	446.500	1	67
22-Jan-92		07:30:00	7.500	454.000	1	68
28-Jan-92		05:52:00	5.867	459.867	0	68
30-Jan-92		08:30:00	8.500	468.367	1	69
03-Feb-92		05:39:00	5.650	474.017	1	70
04-Feb-92		07:53:00	7.883	481.900	0	70
09-Feb-92		08:15:00	8.250	490.150	1	71
10-Feb-92		04:23:00	4.383	494.533	2	73
11-Feb-92		07:14:00	7.233	501.767	2	75
12-Feb-92		04:45:00	4.750	506.517	1	76
18-Feb-92		07:45:00	7.750	514.267	0	76
19-Feb-92		06:25:00	6.417	520.683	2	78
21-Feb-92		05:36:00	5.600	526.283	2	80
24-Feb-92		06:22:00	6.367	532.650	1	81
26-Feb-92		05:42:00	5.700	538.350	2	83
03-Mar-92		04:00:00	4.000	542.350	0	83

Bibliography

1. T. Armstrong, K. Chandler, and J. Barish, "Calculation of Neutron Flux Spectra Induced in the Earth's Atmosphere by Galactic Cosmic Rays," Journal of Geophysical Research, Vol. 78, No. 16, June 1, 1973.
2. G. Eichhorn and R. Piercey, "Techniques to Maximize Software Reliability in Radiation Fields," IEEE Trans. Nucl. Sci., NS-33, No. 4, Dec. 1986.
3. B. Johnson, "Design and Analysis of Fault-Tolerant Digital Systems," Addison-Wesley, ISBN 0-201-07570-9, 1989.
4. A.H. Taber, "Flight Upset Experiment," IBM IR&D Brochure, Project 9A18, March 30, 1989.
5. J.C. Ritter, "Space Systems Survivability, Historical Overview and Technical Background," Tutorial Short Course Presented at the 1989 Nuclear and Space Radiation Effects Conference, Marco Island, FL, July 1989.
6. D.W. Richards and J.A. Collins, "Intelligent Built-In Test and Stress Management," AUTOTESTCON '89 Conference Record, 261, Philadelphia, PA, Sept. 1989
7. R.E. Morgan, "Neutron Induced Upset in the TMS 32020 & 320C25 Microprocessors," paper presented at the Seventh Single Event Effects Symposium, Los Angeles, CA, April 1990.
8. A.H. Taber, A.V. Gillow, and R.E. Dickinson, "Space Shuttle General Purpose Computer Radiation Effects Study - 1991 Update," IBM TR 91-L75-001, February 26, 1991.

List of Abbreviations

A

AOCP. Airborne Operational Control Program.

AWACS. Airborne Warning and Command System.

B

BGR. Burst Generation Rate

Bit. One memory cell

BPSRC. Boeing Physical Sciences Research Center

C

CMOS. Complementary Metal Oxide Semiconductor

CPU. Central Processing Unit

CRUX. Cosmic Ray Upset Experiment

D

DC. Digital Computer

DNA. Defense Nuclear Agency

DoD. Department of Defense

DRAM. Dynamic Random Access Memory

DUT. Device Under Test

E

ECC. Error Correction Coding

EDAC. Error Detection and Correction

EEPROM. Electrically Erasable Programmable Read Only Memory

EMI. Electromagnetic Interference

ENDF. Evaluated Neutron Data File

eV. Electron Volt

F

f/bd. Fails per bit per day

FET. Field Effect Transistor

FLUX. Flight Upset Experiment

FSC. Federal Sector Company

G

GFE. Government Furnished Equipment

GSFC. Goddard Space Flight Center

H

Hz. Hertz

I

IBM. International Business Machines

IEEE. Institute of Electrical and Electronics Engineers

I/O. Input/Output

IR&D. Independent Research and Development

J

JSC. Johnson Space Center

K

keV. Kiloelectron volts

kHz. Kilohertz

L

LAMPF. Los Alamos Meson Production Facility

LET. Linear Energy Transfer (units of $MeVcm^2/mg$)

LiF. Lithium Fluoride

M

MeV. Million Electron Volts

MHz. Megahertz

MIL-STD. Military Standard

MOS. Metal Oxide Semiconductor

MOSFET. Metal Oxide Semiconductor Field Effect Transistor

MMU. Monolithic Memory Unit

MTTF. Mean Time to Failure. The expected time that a system will operate before the first failure occurs.

N

NASA. National Aeronautics and Space Administration

NCS. Neutron Cross Section

NMOS. N-Channel Metal Oxide Semiconductor

NSEU. Neutron-induced Single Event Upset

P

PC. Personal Computer

R

RAM. Random Access Memory

RF. Radio Frequency

RPI. Rensselaer Polytechnic Institute

S

SEB. Single Event Burnout

SEC-DED. Single Error Correction-Double Error Detection

SEE. Single Event Effect

SEL. Single Event Latchup

SEM. Secondary Emission Monitor

SER. Soft Error Rate

SEU. Single Event Upset

SOW. Statement of Work

SRAM. Static Random Access Memory

T

TLD. Thermal Luminescent Dosimeter

TMR. Triple Modular Redundancy

Trans.. Transactions

U

UCD. University of California at Davis

μP. Microprocessor

UVEPROM. Ultraviolet Erasable Programmable Read Only Memory.

V

VLSI. Very Large Scale Integration

DISTRIBUTION LIST

DNA-TR-94-123

DEPARTMENT OF DEFENSE

ASSISTANT TO THE SECRETARY OF DEFENSE
ATTN: EXECUTIVE ASSISTANT

DEFENSE ELECTRONIC SUPPLY CENTER
ATTN: DESC-E

DEFENSE INTELLIGENCE AGENCY
ATTN: DT-1B
ATTN: PGI-4

DEFENSE NUCLEAR AGENCY
2 CY ATTN: IMTS
ATTN: RAES

DEFENSE TECHNICAL INFORMATION CENTER
2 CY ATTN: DTIC/OC

FIELD COMMAND DEFENSE NUCLEAR AGENCY
ATTN: FCINI
ATTN: FCTO
ATTN: FCTT DR BALADI

TECHNICAL RESOURCES CENTER
ATTN: JNGO

DEPARTMENT OF THE ARMY

ADVANCED RESEARCH PROJECT AGENCY
ATTN: ASST DIR ELECTRONIC SCIENCES DIV
ATTN: R REYNOLDS

ARMY RESEARCH LABORATORIES
ATTN: AMSRL-WT-NG
ATTN: AMSRL-WT-NJ
ATTN: DR TIM OLDHAM

PED MISSILE DEFENSE SFAE-MD-TSD
ATTN: CSSD-SL

U S ARMY COMM R&D COMMAND DEFENSE CMD
ATTN: CSSD-SA-E
ATTN: CSSD-SD-A

U S ARMY MISSILE COMMAND
ATTN: AMCPM-HA-SE-MS

U S ARMY NUCLEAR & CHEMICAL AGENCY
ATTN: MONA-NU DR D BASH

U S ARMY RESEARCH OFFICE
ATTN: R GRIFFITH

U S MILITARY ACADEMY
ATTN: LTC AL COSTANTINE

USAISC
ATTN: ASOP-DO-TL

DEPARTMENT OF THE NAVY

DEPARTMENT OF THE NAVY
ATTN: CODE H21 F WARNOCK

NAVAL COMMAND, CONTROL & OCEAN SURVEILLANCE CTR
ATTN: CODE 250

NAVAL RESEARCH LABORATORY
ATTN: CODE 4600 D NAGEL
ATTN: CODE 4682 D BROWN
ATTN: CODE 6613 A B CAMPBELL
ATTN: CODE 6813 N SAKS
ATTN: CODE 6816 H HUGHES

NAVAL SURFACE WARFARE CENTER
ATTN: CODE H-21

NAVAL TECHNICAL INTELLIGENCE CTR
ATTN: LIBRARY

NAVAL WEAPONS SUPPORT CENTER
ATTN: CODE 6054 D PLATTETER

NAWCWPNSDIV DETACHMENT
ATTN: CLASSIFIED LIBRARY

PROGRAM EXECUTIVE OFFICE
ATTN: AIR-536T

STRATEGIC SYSTEMS PROGRAM
ATTN: JIM HOWARD SP-23

DEPARTMENT OF THE AIR FORCE

AIR FORCE CTR FOR STUDIES & ANALYSIS
ATTN: AFSAA/SAI

AIR UNIVERSITY LIBRARY
ATTN: AUL-LSE

PHILLIPS LABORATORY
ATTN: CAPT CHARLES BROTHERS
ATTN: PL/VTE
ATTN: PL/VTEE S SAMPSON

ROME LABORATORY/CC
ATTN: ESR

USAF ROME LABORATORY TECH LIBRARY FL2810
ATTN: RBR

WL/ELE BLDG 620
ATTN: WL/ELE
ATTN: WRDC/MTE

DEPARTMENT OF ENERGY

DEPARTMENT OF ENERGY
ALBUQUERQUE OPERATIONS OFFICE
ATTN: NESD

LAWRENCE LIVERMORE NATIONAL LAB
ATTN: L-156 J YEE
ATTN: L-82 G POMYKAL
ATTN: W ORVIS

LOS ALAMOS NATIONAL LABORATORY
ATTN: E LEONARD

SANDIA NATIONAL LABORATORIES
ATTN: DEPT 1332 F SEXTON
ATTN: L D POSEY DIV 9351
ATTN: P WINOKUR DIV 1332
ATTN: T F WROBEL DIV 9341

OTHER GOVERNMENT

CENTRAL INTELLIGENCE AGENCY
ATTN: OSWR/NED 5S09 NHB
ATTN: OSWR/STD/MTB 5S09 NHB

NASA
ATTN: CODE 900 E STASSINOPOULOS

NATIONAL INSTITUTE OF
STANDARDS & TECHNOLOGY
ATTN: P ROITMAN

DEPARTMENT OF DEFENSE CONTRACTORS

ADVANCED RESEARCH & APPLICATIONS CORP
ATTN: R ARMISTEAD

AEROSPACE CORP
ATTN: C RICE
ATTN: D SCHMUNK
ATTN: G CUEVAS
ATTN: K G HOLDEN
ATTN: LEE MENDOSA
ATTN: N SRAMEK
ATTN: R KOGA
ATTN: S MCGREGOR

ALLIED-SIGNAL, INC
ATTN: DOCUMENT CONTROL

ANALYTIC SERVICES, INC (ANSER)
ATTN: A HERNDON
ATTN: A SHOSTAK

BOEING CO
ATTN: D KINGSBURY
ATTN: D EGELKROUT
ATTN: ROS WOOD

BOEING TECHNICAL & MANAGEMENT SVCS, INC
2 CY ATTN: E NORMAND
ATTN: P R MEASEL
ATTN: W C BOWMAN
ATTN: W G BARTHOLET

BOOZ ALLEN & HAMILTON INC
ATTN: D VINCENT
ATTN: L ALBRIGHT

CALIFORNIA INSTITUTE OF TECHNOLOGY
ATTN: C BARNES

CHARLES STARK DRAPER LAB, INC
ATTN: J BOYLE

CLEMSON UNIVERSITY
ATTN: P J MCNULTY

COMPUTER PRODUCTS A DIVISION OF AMPEX
ATTN: B RICKARD
ATTN: K WRIGHT

DAVID SARNOFF RESEARCH CENTER, INC
ATTN: R SMELTZER

E-SYSTEMS, INC
ATTN: MAIN LIBRARY

EATON CORP
ATTN: R BRYANT

ELECTRONIC INDUSTRIES ASSOCIATION
ATTN: J KINN

GENERAL ELECTRIC CO (ASD)
ATTN: D SWANT
ATTN: D TASCA
ATTN: H O'DONNELL
ATTN: J ANDREWS
ATTN: J LINNEN
ATTN: J LOMAN

GENERAL ELECTRIC CO
ATTN: B FLAHERTY
ATTN: L HAUGE

GEORGE WASHINGTON UNIVERSITY
ATTN: A FRIEDMAN

HARRIS CORPORATION
ATTN: E YOST
ATTN: W ABARE

HONEYWELL INC
ATTN: C SANDSTROM

HONEYWELL, INC
ATTN: MS 725-5

HUGHES AIRCRAFT COMPANY
ATTN: E KUBO

IBM CORP
ATTN: A SADANA

IBM FEDERAL SYSTEMS CO
2 CY ATTN: A H TABER

INSTITUTE FOR DEFENSE ANALYSES
ATTN: TECH INFO SERVICES

JAYCOR
ATTN: D WALTERS

JAYCOR
ATTN: CYRUS P KNOWLES
ATTN: R SULLIVAN

JAYCOR
ATTN: R POLL
ATTN: S ROGERS

JOHNS HOPKINS UNIVERSITY
ATTN: R MAURER

KAMAN SCIENCES CORP
ATTN: DASIAC

KAMAN SCIENCES CORPORATION
ATTN: DASIAC
ATTN: R RUTHERFORD

KEARFOTT GUIDANCE AND NAVIGATION CORP
ATTN: J D BRINKMAN

LITTON SYSTEMS INC
ATTN: F MOTTER

LOCKHEED MISSILES & SPACE CO, INC
ATTN: TECHNICAL INFO CENTER

LOCKHEED MISSILES & SPACE CO, INC
ATTN: G LUM
ATTN: J CAYOT
ATTN: L ROSSI
ATTN: P BENE

LOCKHEED SANDERS, INC
ATTN: BRIAN G CARRIGG

LOGICON R & D ASSOCIATES
ATTN: D CARLSON

LORAL AERONUTRONIC
ATTN: TECHNICAL LIBRARY

LORAL FEDERAL SYSTEMS - OWEGO
ATTN: DEPT L75

LORAL FEDERAL SYSTEMS-MANASSAS
ATTN: N HADDAD

LORAL VOUTHG SYSTEMS CORP
2 CY ATTN: LIBRARY EM-08

MARTIN MARIETTA
ATTN: J MILLER

MARTIN MARIETTA DENVER AEROSPACE
ATTN: RESEARCH LIBRARY

MARTIN MARIETTA TECHNOLOGIES, INC
ATTN: H SCHISLER

MARYLAND, UNIVERSITY OF
ATTN: H C LIN

MAXWELL LABORATORIES INC
ATTN: J M WILKENFELD

MISSION RESEARCH CORP
ATTN: D ALEXANDER

MISSION RESEARCH CORP
ATTN: J LUBELL
ATTN: W WARE

MITRE CORPORATION
ATTN: J R SPURRIER
ATTN: M FITZGERALD

NORTHROP GRUMMAN CORPORATION
ATTN: J R SROUR

PACIFIC-SIERRA RESEARCH CORP
ATTN: H BRODE

PHYSITRON INC
ATTN: MARK CHRISTOPHER

PHYSITRON INC
ATTN: MARION ROSE

RAYTHEON CO
ATTN: D D LEE
ATTN: JOSEPH SURRO

RESEARCH TRIANGLE INSTITUTE
ATTN: M SIMONS

ROCKWELL INTERNATIONAL CORP
ATTN: V DE MARTINO

SCIENCE APPLICATIONS INTL CORP
ATTN: D MILLWARD
ATTN: DAVID LONG

SCIENCE APPLICATIONS INTL CORP
ATTN: W CHADSEY

SCIENCE APPLICATIONS INTL CORP
ATTN: P ZIELIE

SCIENTIFIC RESEARCH ASSOC, INC
ATTN: H GRUBIN

SUNDSTRAND CORP
ATTN: C WHITE

SYSTRON-DONNER CORP
ATTN: SECURITY OFFICER

TECHNOLOGY DEVELOPMENT ASSOCIATES
ATTN: R V BENEDICT

TELEDYNE BROWN ENGINEERING
ATTN: G R EZELL
ATTN: G R EZELL
ATTN: LEWIS T SMITH
ATTN: M P FRENCH

THE RAND CORPORATION
ATTN: C CRAIN

TRW
ATTN: M J TAYLOR

TRW INC
ATTN: TIC

TRW S. I. G.
ATTN: C BLASNEK

TRW SPACE & DEFENSE SECTOR
ATTN: D M LAYTON

UNISYS CORPORATION-DEFENSE SYSTEMS
ATTN: P MARROFFINO

VISIDYNE, INC
ATTN: C H HUMPHREY
ATTN: W P REIDY